# Magnetic anisotropy transfer from mono- to poly-metallic complexes

Marion Poncet, Ang Li, Geoffrey Gontard, Lise-Marie Chamoreau, Yanling Li, Laurent Lisnard, Jurgen von Bardeleben, Sourav Dey, Gopalan Rajaraman, Yves Journaux

# Magnetic anisotropy transfer from mono- to poly-metallic complexes

**Marion Poncet,[a] Ang Li,[a] Geoffrey Gontard,[a] Lise-Marie Chamoreau,[a] Yanling Li,[a] Laurent Lisnard,[a] Jurgen Von Bardeleben[b], Sourav Dey[c] , Gopalan Rajaraman[c] and Yves Journaux*[a]**

[a] Dr M. Poncet, Dr A. Li, G. Gontard, L.-M. Chamoreau, Dr. Y. Li, Dr. L. Lisnard, Dr. Y. Journaux
Sorbonne Université, CNRS,
Institut Parisien de Chimie Moléculaire, IPCM
4 place Jussieu, 75005, Paris, France
Fax: (+) 33 1 44 27 38 81
E-mail: yves.journaux@sorbonne-universite.fr
http://www.ipcm.fr/article241.html

[b] Dr J. Van Bardeleben
Institut des Nanosciences de Paris, UMR 7588
4 place Jussieu, 75005, Paris, France

[c] Pr G. Rajaraman, Dr. S. Dey
Department of Chemistry, Indian Institute of Technology Bombay
Powai, Mumbai - 400 076, India

**Abstract:** The reaction of multi-bidentate oxamate-based copper(II) complexes with the [Ni($^{i}$Prtacn)$Cl_2$] complex ($^{i}$Prtacn:1,4,7-triisopropyl-1,4,7-triazacyclononane) has been investigated. X-ray diffraction studies reveal that for all compounds the oxamato κO,κO' bidentate coordination site replaces the two chloride ions in [Ni(iPrtacn)$Cl_2$] to form trimetallic {$CuNi_2$} (**1**-**3),** hexametallic {$Cu_2Ni_4$} (**4**) and enneametallic {$Cu_3Ni_6$} (**5**) complexes. The investigation of the magnetic properties shows that Cu-Ni interactions through the oxamato bridge are in the expected range (-111 $cm^{-1}$, -68 $cm^{-1}$). For **1**-**3,** both the sign and strength of the magnetic couplings are computed independently from DFT calculations, and these estimates broadly agree with the experiments. The magnetization measurements and EPR studies reveal that **1**-**3** are anisotropic: a significant portion of the large anisotropy of the [Ni($^{i}$Prtacn)$Cl_2$] complex is retained, resulting in a *D* value for the *S*=3/2 ground state of 5 $cm^{-1}$ on average. This is no longer the case for **4** and **5** where the anisotropy of the Ni(II) complexes is diluted due to the high nuclearity of the final edifices. These results show that it is possible to obtain trimetallic complexes with a high anisotropy and a high spin value for the ground state by a judicious choice of the interacting metal ions.

## Introduction

Since the discovery of single-molecule magnets (SMM) twenty years ago,[1] one of the main challenge is to increase the height of the anisotropy energy barrier, $\Delta$, in order to obtain memory effects at temperatures compatible with technological applications. At first sight, the strategy to obtain high energy barriers looks simple since $\Delta$ is equal to $|D|.S^2$ for integer spin value or $|D|(S^2\text{-}1/4)$ for half-integer spin value and it should be sufficient to synthesize high-spin molecules to get high energy barriers. Driven by this hypothesis that the height of the barrier is a quadratic function of the spin value, a lot of efforts have been devoted to the synthesis of high-spin polymetallic complexes comprised of anisotropic metal ions. As it was highlighted by several authors however,[2–4] while single ions anisotropy can be as large as several wavenumbers, the zero-field splitting (ZFS) in polymetallic complexes is generally less than one wavenumber. For instance, the ZFS value in the archetype $\{Mn_{12}Ac\}$ SMM complex is only $D$=-0.51 $cm^{-1}$.[5] There are at least three reasons to explain this observation. The first one is known since the eighties by EPR spectroscopists involved in the study of polymetallic complexes. In the strong exchange limit, the ZFS value of spin states $S$ in a polymetallic complex is given by a linear combination of the ZFS of the single ions and a generally smaller contribution due to anisotropic exchange[6–8] $D_S = \sum_i d_i^S D_i + \sum_{i<j} d_{i,j}^S D_{i,j}$. In almost every case, there is a dilution of the anisotropy in polymetallic complexes and these dilution coefficients $d_i$ are significantly lower than one, leading to small ZFS values for the spin states of the polymetallic complexes. The second reason is related to the relative orientations of the local ZFS tensors. The equation giving the ZFS of a spin state is a tensorial relationship and this can lead to mutual cancellation of the local anisotropy when local tensors have different orientations. This situation is well illustrated by the existence of the so-called "Jahn Teller isomerism" in the $\{Mn_{12}O_{12}\}$ coordination clusters family. In this family, some samples show two different relaxation processes and this is interpreted by the presence of two kinds of molecules within the crystal. For the molecules with the rapid relaxation process, one of the six Mn(III) ions has its Jahn Teller axis almost perpendicular to the others leading to the decrease of the anisotropy energy barrier from 66 K to 32 K[9,10]. Finally, the last reason is even more fundamental and is related to the dependence of single ion $D_i$ parameters with the spin value. Neese and Solomon[2,11] have shown that this parameter is approximately a function of $1/S^2$ leading to a height of the energy barrier independent of the spin value. Overall, these three factors contribute to the decrease of $D_S$ values in polymetallic complexes. Of course, it is unrealistic to fight against quantum mechanics and this is the reason why research has turned to other strategies to obtain SMM[12] and lot of work has been done on monometallic complexes with very anisotropic magnetic ions such as lanthanide[3,13–19], actinide[16,20,21] or transition metal ions with low coordination number. This later approach is original and leads to an exciting and unusual coordination chemistry and can lead to orbitally degenerate ground state.[22–28]. A very large energy barrier has been observed in a linear Fe(I) complex [29] or in linear Co(II) complexes[30,31]. Another original way to obtain SMMs has been explored by Andruh, Totti, Vaz et al[32–34] with the synthesis of 2p-3d-4f complexes. In this article, we present an alternative approach which consist of using very anisotropic 3d metal complexes with $D$ values larger than ten wavenumbers as building units to synthesize polymetallic complexes. This strategy is also being explored by Pichon and Sutter using pentagonal bipyramid complexes as building blocks.[35,36] The reduction of the $D$ values for the spin states in the resulting polymetallic complexes will be operative but high local single-ion anisotropy values should lead to $D$ values of the order of a few wavenumbers for the ground state. If this expectation is true, this is one order of magnitude greater than the values generally observed in polymetallic complexes. To test our approach, we have first synthesized simple linear {NiCuNi} trimetallic complexes with a $S$=3/2 ground state. Our anisotropic 3d complex is the five-coordinate Ni(II) complex of formula $[Ni(iPrtacn)Cl_2]$ in which the Ni(II) ion is chelated by the tridentate macrocyclic ligand 1,4,7-triisopropyl-1,4,7-triazacyclononane (iPrtacn). The $D$ value in this complex is equal to 14 $cm^{-1}$ [37]. We have used the complex-as-ligand strategy with three different oxamato copper complexes $[Cu(pma)_2]^{2-}$, $[Cu(Me_3pma)_2]^{2-}$ and $[Cu(opba)]^{2-}$ (pma = N-phenyloxamato, $Me_3$pma = N-2,4,6-trimethylphenyloxamato and opba = o-phenylenebis-(oxamato) to form the targeted trimetallic complexes of formula $[Cu(pma)_2Cl\{Ni(^{i}Prtacn)\}_2]Cl\cdot 10H_2O$ (**1**), $[Cu(Me_3pma)_2(NO_3)_{0.6}\{Ni(^{i}Prtacn)\}_2]Cl_{0.4}(NO_3)\cdot 9H_2O$ (**2**) and $[Cu(opba)Cl\{Ni(^{i}Prtacn)(H_2O)\}\{Ni(^{i}Prtacn)\}]Cl\cdot 12H_2O$ (**3**). In a second step, we have tried to increase the spin values of our complexes by assembling these trimetallic subunits with meta substituted phenyl rings (mpba= N ,N ′ -1,4-phenylenebis- (oxamato), T-triox= N,N′,N″-1,3,5-benzenetriyltris- (oxamato)), and we have prepared the hexametallic complex $[Cu_2(mpba)_2Cl_2\{Ni(iPrtacn)\}_4](NO_3)_2\cdot 16H_2O$ (4), and the enneametallic one $[Cu_3(T\text{-}Triox)_2(NO_3)_{1,5}(H_2O)_{1,5}\{Ni(^{i}Prtacn)(H_2O)\}_{1,5}\{Ni(^{i}Prtacn)\}_{4,5}](NO_3)_{4,5}\cdot 37H_2O$ (**5**). Indeed, it is well established that meta-substituted aromatic rings are good ferromagnetic coupling unit with the occurrence of a spin polarization mechanism.[4,38–41] Therefore, hexametallic and enneametallic complexes with ground state spin-values of 3 and 9/2 are expected.

## Results and Discussion

### Synthesis:

Compounds **1**-**5** have been obtained following a "complex as ligand" strategy based on the reaction of oxamate-based metalloligand with the anisotropic complex bearing labile positions $[Ni(^{i}Prtacn)Cl_2]$. The oxamato groups being bis-chelating ligands, taking advantage of the copper ions binding affinity for the κO,κO' chelating site of the oxamato group the coordination of copper ion through one nitrogen atom and one oxygen atom leaves two uncoordinated carbonyl groups, that is one free chelating position. Therefore, the stoichiometric reaction of copper(II) ions with the mono-, bis- or tris-oxamate ligands $(pma)^{2-}$, $(Me_3pma)^{2-}$, $(opba)^{4-}$, $(mpba)^{4-}$ or $(T\text{-}Triox)^{4-}$ in water leads to the in situ formation of the monometallic complexes $[Cu(pma)_2]^{2-}$, $[Cu(Me_3pma)_2]^{2-}$, and $[Cu(opba)]^{2-}$,[42] the dimetallic complex $[Cu_2(mpba)_2]^{4-}$ [40] and the trimetallic complex $[Cu_3(T\text{-}Triox)_2]^{6-}$,[39] which are bis-bidentate, tetra-bidentate and hexa-bidentate metalloligands, respectively. Reacting stoichiometric amounts of the nickel(II) starting material leads then to the targeted anisotropic tri-, hexa- and ennea-metallic compounds displaying one, two or three $\{CuNi_2\}$ motifs (see Scheme 1). All the compounds have been characterized structurally with single-crystal X-ray diffraction (see Table 1 and the experimental section for details).

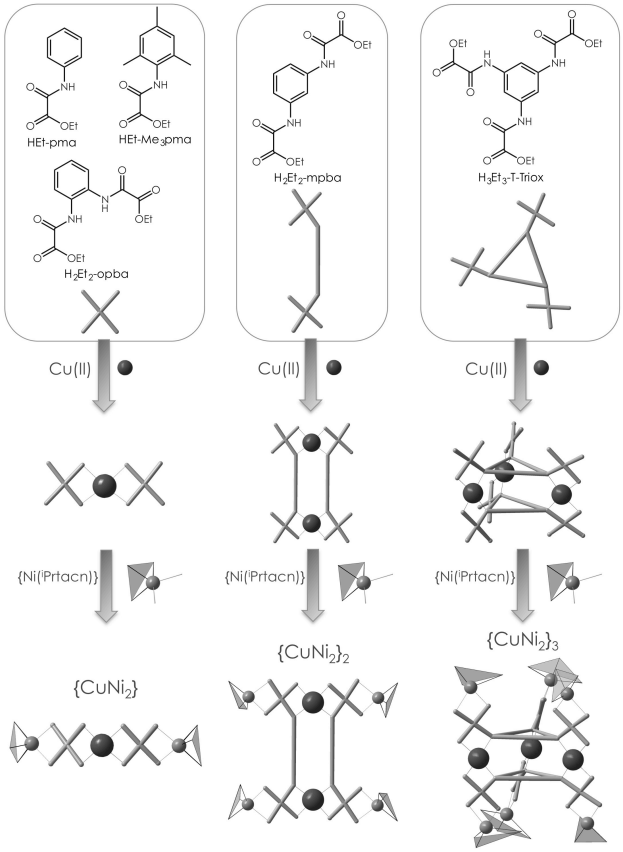


Scheme 1. Synthetic strategy employed for the preparation of anisotropic polymetallic complexes.

**Structural descriptions:**

The trimetallic complex **1** crystallizes in the *P-1* triclinic space group. The asymmetric unit is made of three crystallographically non-equivalent yet chemically and structurally similar complexes. Each complex is built on a central $[Cu(pma)_2]^{2-}$ bis-bidentate metalloligand completed by two $[Ni(iPrtacn)]^{2+}$ complexes (Figure 1a). In the copper(II) building block two $(pma)^{2-}$ ligands bind the metallic center in a *trans* fashion, each via one nitrogen and one oxygen atom of the oxamato group, and the copper ion's coordination sphere is completed by a chloride anion. The two remaining carbonyl groups of each oxamate ligand coordinate a $[Ni(iPrtacn)]^{2+}$ complex resulting in a trimetallic species where nickel ions are five-coordinate. Stereochemical analysis indicate strongly distorted environments nearing a trigonal bipyramid geometry for the copper centre and square pyramidal geometries for the nickel ions.[43,44] These distortions result in a non-linear arrangement of the metallic atoms with an average Ni–Cu–Ni angle of 146.1° [143.9°-148.6°] (see Table 2). The bond length distances are however homogenous (see Table 3) and the average Cu–Ni distance is of 5.31 Å. In the solid there are, besides H-bonds involving solvent molecules, no obvious supramolecular interactions between the complexes (see Figure S1 of the supporting information), which are well separated from each other, the shortest intermolecular metal-metal distance being of 6.536(1) Å.

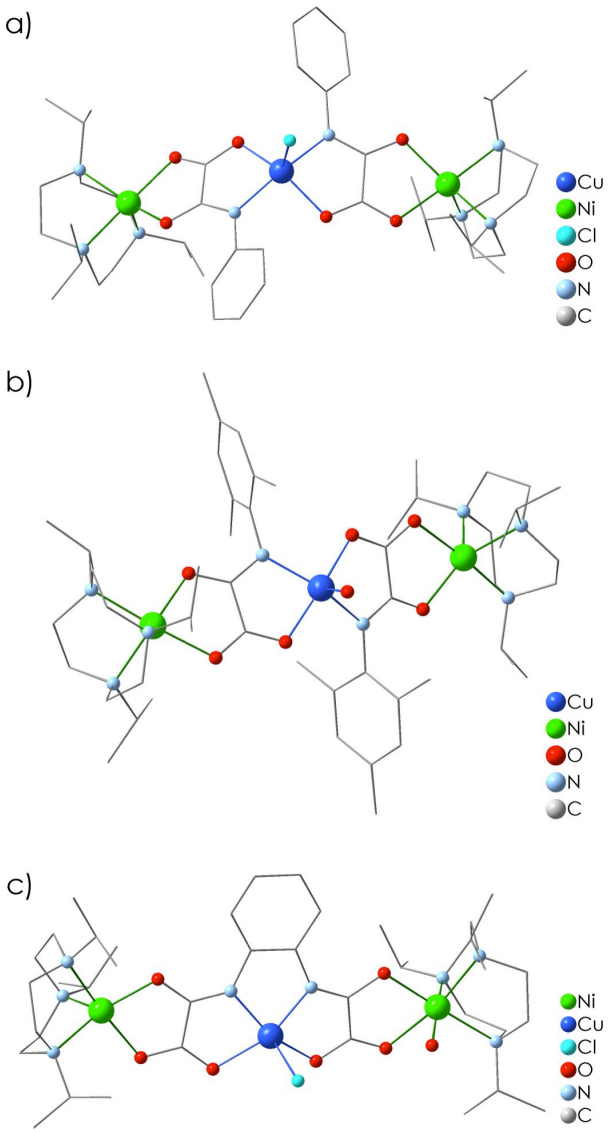


Figure 1. Structures representation of **1** (a), **2** (b) and **3** (c). H atoms have been omitted for clarity.

Complexes **2** and **3** both present a topology similar to that of **1** with one central copper(II) metalloligand coordinating two $[Ni(^{i}Prtacn)]^{2+}$ complexes via oxamate bridges, yielding trimetallic compounds as well (Figures 1b and 1c). In **2**, all the metal ions are five-coordinate. The $(Me_3pma)^{2-}$ oxamate ligands define the base of the square planar or square pyramidal geometries adopted by the copper centre, the latter occurring when a nitrate anion in partial occupancy (50 %) binds the metal ion. The two nickel ions show distorted geometries, one is found in a square pyramidal environment, the other in a trigonal bipyramidal geometry.[45–47] The metallic arrangement is more linear than that of **1**, with a Ni–Cu–Ni angle of 161.3°, the two Cu–Ni distances are fairly similar: 5.275(1) and 5.284(1) Å (see Table 2). As in **2** the metallic arrangement in **3** is closer to linearity with a nearly equal Ni–Cu–Ni angle (161.8°) and comparable Cu–Ni distances (5.306(1) and 5.333(1) Å). In **3**, the copper ion adopts a square pyramidal geometry with a base defined by the chelating bis-oxamate ligand $(opba)^{2-}$ and an apical chloride anion. The nickel ions' environments are strongly distorted, one ion is five-coordinate in a square pyramidal geometry when the other binds an additional water molecule resulting in a distorted octahedral surrounding. As in **1**, the bond length distances for compounds **2** and **3** are quite homogenous (see Table 3). Besides H-bonds with solvent molecules there are no obvious supramolecular interactions in the solid (see Figure S2 and S3 for **2** and **3**, respectively, in the supporting information) and the shortest intermolecular metal-metal distances are found at 6.606(1) Å for **2** and 7.078(2) Å for **3**. Complex **1** is the first example of a coordination compound based on the $(pma)^{2-}$ ligand and **2** is the first example of a molecular polymetallic complex based on the $(Me_3pma)^{2-}$ ligand, only the metalloligand $[Cu(Me_3pma)_2]^{2-}$ and its one-dimensional adduct with cobalt(II), $[CuCo(Me_3pma)_2]_n$, had been characterized so far.[48,49] With regard to **3**, the use of a bis-oxamate copper-based metalloligand has yielded several examples of $\{CuNi_2\}$ trimetallic complexes. However, the use of $(opba)^{2-}$ has only been reported once[50] all the other known structures are based on copper(II)-propylenebisoxamate with one example where the $^{i}$Prtacn blocking ligand has been used for the nickel(II) complex,[51–53] or on a different choice of metal ions.[54–58] These previously reported trimetallic $\{CuNi_2\}$ complexes reveal less distortion that compounds **1**-**3**, with an average Ni–Cu–Ni angle of 173.1° [165.9-178.4°], the most distorted ones being the $\{Ni(^{i}Prtacn)\}$- and the {Cu(opba)}-based complexes (169.2° and 165.9°, respectively; see Table 2).[50,53]

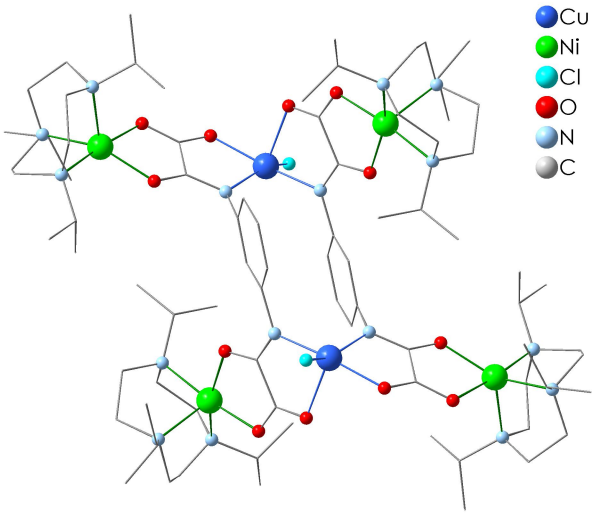


Figure 2. Structure representation of compound **4**. H atoms have been omitted for clarity.

The centrosymmetric hexametallic complex **4** is built on the dimetallic tetra-bidendate $[Cu_2(mpba)_2]^{4-}$ metalloligand. Two $(mpba)^{4-}$ bis-oxamate ligands bind two copper(II) cations, leaving four oxamate groups that chelate each a $[Ni(^{i}Prtacn)]^{2+}$ unit via two carbonyl groups (Figure 2). A chloride anion complete the coordination sphere of the copper(II) ions. All the metal ions are five-coordinate, and stereochemical analyses indicate distorted square pyramidal geometries for the nickel ions and an intermediate square pyramidal/trigonal bipyramid geometry for the copper(II) ion.[45,46,59] The Ni–N/O bond lengths are homogenous and match the values observed for compounds **1**-**3** (see Table 3), while the Cu–N/O distances reflect the distorted coordination sphere of the ion with elongated distances. In the $\{CuNi_2\}$ sub-unit the metal-metal distances compare well with compounds **1**-**3** –5.304(1) and 5.374(1) Å. The metallic arrangement however differs. The metallic triad is strongly bent with a Ni–Cu–Ni angle of 112.8°. This can be explained by the peculiar coordination mode of the penylenebisoxamate ligands, possibly occurring to arrange the bulky $^{i}$Prtacn ligands. Indeed the conformation differs from that of the structures reported for the metalloligand $Na_4[Cu_2(mpba)_2]$ and the two known complexes based on it, the homometallic hexametallic $[Cu_2(mpba)_2F(H_2O)\{Cu(Me_5dien)\}_4](PF_6)_3$ complex and the heterometallic pentametallic complex $[Ni(cyclam)][Cu_2(mpba)_2\{Ni(cyclam)_3\}](ClO_4)_4$.[40,60] In these compounds the two phenyl rings are located on the same side of the plan defined by the oxamate groups nitrogen atoms, facing each other (Figure 3a), and the dihedral angles between the oxamate functions and the phenyl rings are similar within a ligand (Figure 3c), and tend toward orthogonally (72.2° [65.6-87.9°]). In **4**, the phenyl rings of the $(mpba)^{4-}$ ligands are located on each side of the plane defined by the four oxamate nitrogen atoms and the dihedral angles between the oxamate groups and the phenyl ring are 70.2 and 30.7° (Figure 3b and 3d). As a result, the atypical conformation observed in **4** leads to a slightly elongated Cu–Cu distance within the complex (see Table 2). The metal-metal distances within the oxamate-bridged triads seem however comparable, the most striking structural consequence of the coordination mode observed in **4** is the bending of the {Ni–Cu–Ni} triads, which, as mentioned above, assuredly helps accommodating the coordination of four $\{Ni(^{i}Prtacn)\}$ sub-units, resulting in the desired hexametallic complex that could not have been achieved using $[Ni(cyclam)]^{2+}$. The crystal packing of **4** does not show any particular supramolecular interactions and the complexes are relatively well separated from each other (see Figure S4 of the supplementary materials).

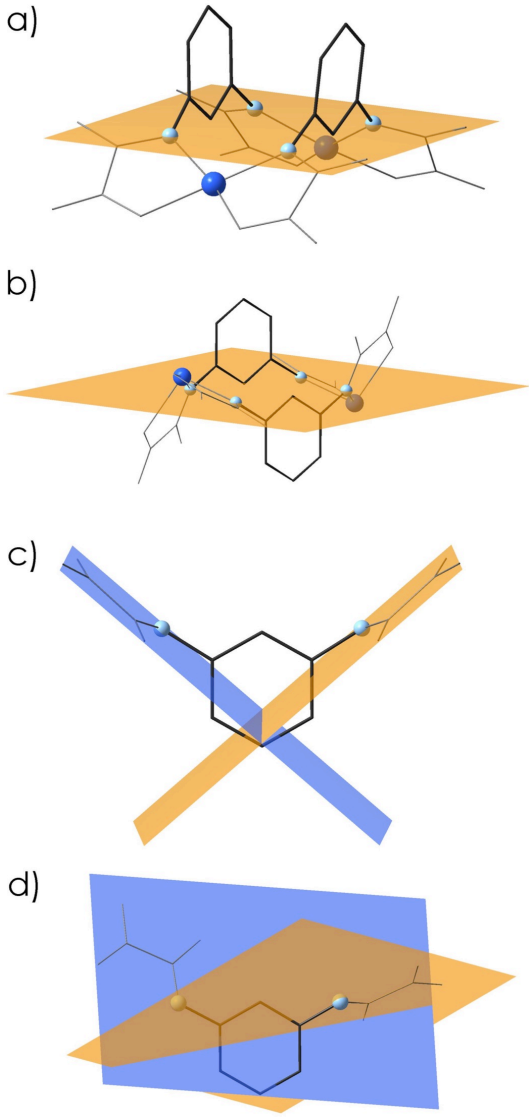


Figure 3. Schematic view of the structural differences between compound **4** and the $[Cu_2(mpba)_2]^{4-}$ complex (see text for details and references).

The asymmetric unit of compound **5** is composed of two pseudo-stereoisomers of the enneametallic complexe that also differs by the number of terminal water molecules or nitrate anions coordinated to the metal ions; the full formula would be: $[Cu_3(T\text{-}Triox)_2(NO_3)_2(H_2O)\{Ni(^{i}Prtacn)\}_6]$-$[Cu_3(T\text{-}Triox)_2(H_2O)_2\{Ni(^{i}Prtacn)(H_2O)\}_2\{Ni(^{i}Prtacn)\}_4](NO_3)_{10}$. The enneametallic species is made of two $(T\text{-}Triox)^{6-}$ ligands – facing each other with non fully eclipsed phenyl rings (-26.1 and 25.2°) – that sandwich three copper ions, leaving six chelating positions where the carbonyl groups of the oxamate functions bind six {Ni(iPrtacn)]} fragments (Figure 4). In each of the two pseudo-conformers, the copper centres are all but one five-coordinate, each chelated by two oxamato groups and either nitrate anions or water molecules completing the coordination spheres. Stereochemical analysis of the metal ions coordination spheres indicates strongly distorted surroundings with intermediate geometries between that of a square pyramid and that of a trigonal bipyramid.[45–47] The sixth copper ion adopts a distorted square-planar geometry defined by its two chelated oxamato groups. An oxygen atom from a nitrate anion is positioned in what would be the apical position of a square-based pyramid. However the distance is rather long (2.6 Å).

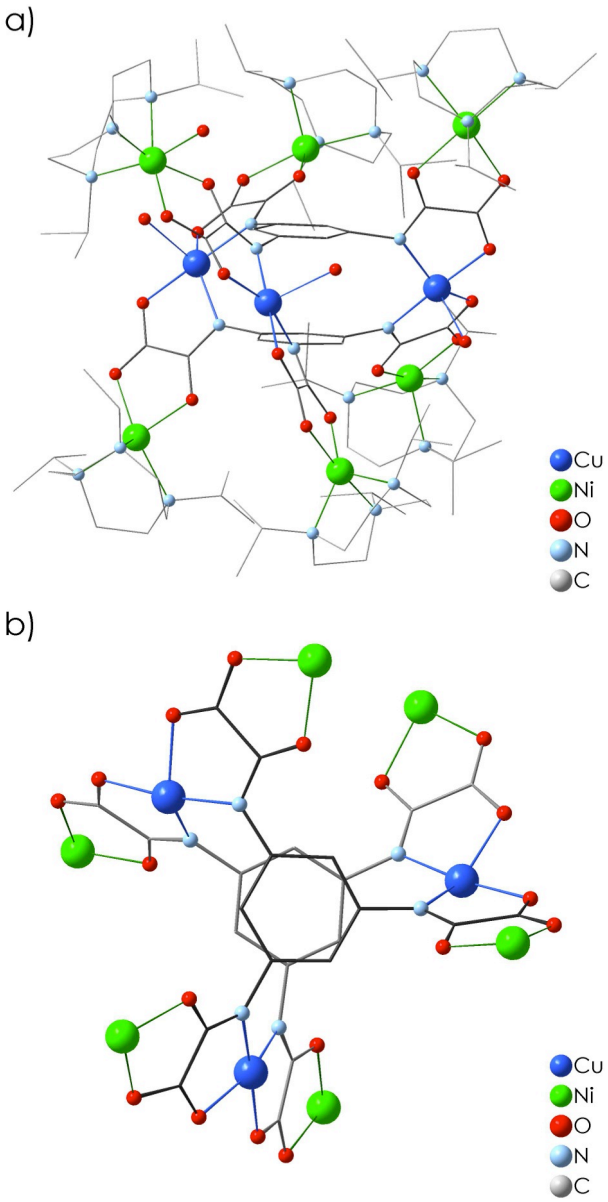


Figure 4. Structure representation of compound **5** (a) and highlight of the metallic core (b). H atoms have been omitted for clarity.

The coordination of the nickel ions also differs from one enneametallic fragment to the other, with either none or two octahedral nickel ions present in the complex. All the other nickel ions are however five-coordinate and adopt a distorted square pyramidal geometry.[45–47] As illustrated in Table 3 the metal–N/O bond lengths are homogeneous. Within the $\{CuNi_2\}$ triads, the metal ions are not aligned, the average Ni–Cu–Ni angle is of 154° (see Table 2). These distortions are also evidenced with the relatively large range of values found for the dihedral angles between the phenyl rings and the planes of the oxamato groups (from 37.6 to 70.6°, see Table 2). As observed in **4**, such distortions may occur to arrange the blocking ligands of the nickel ions. In comparison, the other two known polymetallic complexes based on the $[Cu_3(T\text{-}Triox)_2]^{6-}$ metalloligand and featuring {Cu(pmdien)} peripheral complexes – $[Cu_3(T\text{-}Triox)_2(H_2O)_3\{Cu(pmdien)\}_6](ClO_4)_6$ and $[Cu_2Ni(T\text{-}Triox)_2(H_2O)_4\{Cu(pmdien)\}_6](ClO_4)_6$ – are less distorted.[61,62] The triads are far less bent (> 170°, see Table 2), the average dihedral angles close to 70° and the phenyl rings facing each other are closer to the eclipsed conformation (torsion angles between 12 and 15°). In the unconstrained $K_6[Cu_3(T\text{-}Triox)_2(H_2O)]$ complex, the ligands are eclipsed and the dihedral angles average 84°. In spite of these conformational differences, the intermolecular metal-metal distances are similar throughout the whole series of $\{Cu_3(T\text{-}Triox)_2\}$-based complexes. In the solid, the shortest metal-metal distances (≥ 6.58 Å) actually compares well with the shortest intramolecular distances for non-oxamato-bridged metal-metal pairs (≥ 7.35 Å). There are however no sign of supramolecular interactions in the crystal packing of **5**, besides H-bonds through anions and solvent molecules (see Figure S5 of the supplementary materials).

Table 1. Crystallographic details for compounds **1**-**5**.

| | **1** | **2** | **3** | **4** | **5** |
|---|---|---|---|---|---|
| Formula[a] | $C_{46}H_{84.9}Cl_2CuN_8Ni_2O_{10.45}$ | $C_{52}H_{100}Cl_{1.5}CuN_{8.5}Ni_2O_{13.5}$ | $C_{40}H_{91}Cl_2CuN_8Ni_2O_{16.5}$ | | $C_{228}H_{408}Cu_6N_{52}Ni_{12}O_{56}$ |
| $M_r$ [g mol$^{-1}$] | 1169.17 | 1294.53 | 1200.06 | | 5859.8 |
| Crystal system | Triclinic | Triclinic | Monoclinic | Monoclinic | Monoclinic |
| Space group | *P-1* | *P-1* | *C 2/c* | *C 2/c* | *C 2* |
| *a* [Å] | 15.0298(6) | 11.9500(3) | 62.1543(15) | 25.9581(9) | 53.7256(12) |
| *b* [Å] | 19.4514(8) | 15.3578(3) | 10.6755(3) | 27.5456(10) | 21.1119(5) |
| *c* [Å] | 30.7714(12) | 18.9604(4) | 17.4521(4) | 18.1562(7) | 33.9318(8) |
| $\alpha$ [°] | 75.614(2) | 71.910(2) | 90 | 90 | 90 |
| $\beta$ [°] | 79.512(2) | 86.422(2) | 105.040(2) | 121.2760(10) | 106.113(2) |
| $\gamma$ [°] | 70.839(2) | 77.860(2) | 90 | 90 | 90 |
| *V* [Å$^3$] | 8181.4(6) | 3233.73(13) | 11183.3(5) | 11095.6(7) | 36975.2(15) |
| *Z* | 6 | 2 | 8 | 4 | 4 |
| *T* [K] | 200(2) | 200(2) | 200(2) | 200(2) | 200(2) |
| $\lambda$ [Å] | 1.54178 | 0.71073 | 1.54178 | 1.54178 | 1.54178 |
| $\rho_{calc}$ [g cm$^{-3}$] | 1.424 | 1.330 | 1.426 | 1.415 | 1.053 |
| $\mu$ [mm$^{-1}$] | 2.656 ($Cu_{K\alpha}$) | 1.027 ($Mo_{K\alpha}$) | 2.684 ($Cu_{K\alpha}$) | 2.279 ($Cu_{K\alpha}$) | 1.479 |
| Measured reflections | 67320 | 66233 | 47499 | 36429 | 84884 |
| Unique reflections | 28201 | 18989 | 9895 | 9900 | 37431 |
| $R_{int}$ | 0.0375 | 0.0493 | 0.0502 | 0.0216 | 0.0354 |
| Reflections I>2σ(I) | 21759 | 11145 | 8815 | 9250 | 31179 |
| Parameters | 1891 | 742 | 620 | 635 | 3196 |
| Restraints | 0 | 22 | 0 | 6 | 3535 |
| $R_1$[b] [I>2σ(I)] | 0.0401 | 0.0611 | 0.0428 | 0.0538 | 0.0535 |
| $wR_2$[c] [I>2σ(I)] | 0.1005 | 0.1727 | 0.1200 | 0.1680 | 0.1448 |
| GOF | 1.016 | 1.023 | 1.036 | 1.033 | 1.031 |
| Largest residuals [eÅ$^3$] | 0.379 and -0.595 | 1.405 and -0.963 | 1.079 and -0.570 | 1.613 and -0 .743 | 0.617 and -0.350 |

[a] Including solvate molecules [b] $R_1 = \sum \left| |F_o| - |F_c| \right| / \sum |F_o|$ [c] $\omega R_2 = \left[ \sum \left( w \left( F_o^2 - F_c^2 \right)^2 \right) / \sum \left( w \left( F_o^2 \right)^2 \right) \right]^{1/2}$

Table 2. Selected distances (Å) and angles (°) for compounds **1**-**5** and for relevant oxamate-based complexes reported in the literature.

| | M—Cu—M[a] | Cu–M[a] | Cu–Cu[b] | Dihedral angle[c] | O/N—Cu—O/N[d] |
|---|---|---|---|---|---|
| **1** | 146.1 [143.9-148.6] | 5.316 [5.297(1)-5.339(1)] | n.a. | n.a. | 8.7 [82.1 – 115.7] |
| **2** | 161.3 | 5.275(1) and 5.284(1) | n.a. | n.a. | 9.6 [79.8 – 106.9] |
| **3** | 161.8 | 5.306(1) and 5.333(1) | n.a. | n.a. | 10.7 [81.6 – 110.7] |
| $[Cu(pba)\{Ni(bapa)(H_2O)\}_2](ClO_4)_2$.[51] | 174.9 | 5.305 and 5.326 | n.a. | n.a. | 6.1 [83.1 – 97.7] |
| $[Cu(pba)\{Ni(bispictn)\}_2](ClO_4)_2$.[52] | 175.4 | 5.296 | n.a. | n.a. | 5.4 [84.3 – 96.6] |
| $[Cu(pba)\{Ni(cth)\}_2](ClO_4)_2$.[52] | 178.4 | 5.291 and 5.312 | n.a. | n.a. | 5.0 [84.4 – 96.8] |
| $[Cu(opba)\{Ni(dpt)(H_2O)\}_2](ClO_4)_2$.[50] | 165.9 | 5.327 and 5.347 | n.a. | n.a. | 6.2 [83.3 – 108.5] |
| $[Cu(pba)\{Ni(tacn)(H_2O)\}_2](ClO_4)_2$.[63] | 175.1 | 5.345 and 5.311 | n.a. | n.a. | 5.4 [83.7 – 103.1] |
| $[Cu(pba)\{Ni(iPrtacn)\}_2](BPh_4)$.[53] | 169.2 | 5.234 | n.a. | n.a. | 3.8 [85.8 – 96.4] |
| $[Cu(opba)\{Co^{II}(PyPz_3)\}_2][ClO_4]_2$[64] | 159.7 | 5.329 and 5.362 | n.a. | n.a. | 9.2 [82.7 – 108.3] |
| **4** | 112.8 | 5.304(1) and 5.374(1) | 7.373(1) | 30.7 and 70.2 | 7.7 [80.8 – 109.9] |
| $Na_4[Cu_2(mpba)_2]$.[40] | n.a. | n.a. | 6.822 | 79.9 [73.1-87.9] | 7.8 [82.5 – 107.3] |
| $[Cu_2(mpba)_2F(H_2O)\{Cu(Me_5dien)\}_4](PF_6)_3$.[60] | 155.5 and 162.1 | 5.308 [5.286-5.348] | 6.636 | 76.5 [69.7-80.8] | 6.8 [82.4 – 105.2] |
| $[Ni(cyclam)][Cu_2(mpba)_2\{Ni(cyclam)_3\}](ClO_4)_4$.[60] | 146.9 | 5.318 [5.284-5.347] | 6.930 | 69.2 [65.6-72.6] | 6.8 [83.6 – 104.7] |
| **5** | 154.0 [145.6-170.4] | 5.297 [5.252(3)-5.339(2)] | 6.835 [6.659(2)-7.154(2)] | 55.0 [37.6-70.6] | 8.5 [79.8 – 133.9] |
| $K_6[Cu_3(T\text{-}Triox)_2(H_2O)]$.[39] | n.a. | n.a. | 6.993 [6.898-7.064] | 83.8 [74.4-89.9] | 7.0 [82.7 – 105.7] |
| $[Cu_3(T\text{-}Triox)_2(H_2O)_3\{Cu(pmdien)\}_6](ClO_4)_6$.[65] | 171.0 [165.7-173.4] | 5.334 [5.248-5.404] | 6.917 [6.836-7.051] | 67.9 [59.3-81.2] | 6.6 [80.9 – 105.7] |
| $[Cu_2Ni(T\text{-}Triox)_2(H_2O)_4\{Cu(pmdien)\}_6](ClO_4)_6$.[66] | 173.6 and 179.8 | 5.368 [5.310-5.447] | 6.752 and 6.961 | 67.3 [62.5-73.9] | 7.1 [79.2 – 106.5] |

[a]: through oxamate bridges; [b]: intramolecular though phenylenebisoxamate bridges; [c]: between oxamate groups and phenyl rings, intraligand; [d] averaged deviation from orthogonality and coordination polyherda angles'range

Table 3. Selected bond length (Å) for compounds **1**-**5**.

| | **1** | **2** | **3** | **4** | **5** |
|---|---|---|---|---|---|
| Cu—O/N[a] | 2.012 [1.997(2)-2.040(2)] | 1.987 [1.980(3)-1.998(3)] | 1.999 [1.939(2)-2.061(2)] | 2.050 [1.987(2)-2.213(3)] | 1.984 [1.947(8)-2.057(6)] |
| Ni—O/N[b] | 2.057 [1.987(2)-2.092(3)] | 2.051 [1.977(2)-2.089(4)] | 2.090 [1.989(2)-2.147(2)] | 2.049 [1.991(2)-2.085(3)] | 2.053 [1.971(7)-2.182(9)] |
| Cu—X[c] | 2.479 [2.444(1)-2.525(1)] | 2.048(10) | 2.461(10) | 2.278(1) | 2.269 [2.170(9)-2.409(10)] |
| Ni—X[c] | n.a. | n.a. | 2.144(1) | n.a. | 2.092(8) & 2.226(16) |

[a]: O/N atoms from oxamate ligands; [b]: O/N atoms from oxamate and $^i$Prtacn ligands; [c]: coordinated anions or water molecules

**Magnetic properties:**

DC magnetic susceptibility measurements were performed for **1** to **5** at 1 kOe in the 2-300 K temperature range. (Figure 5)

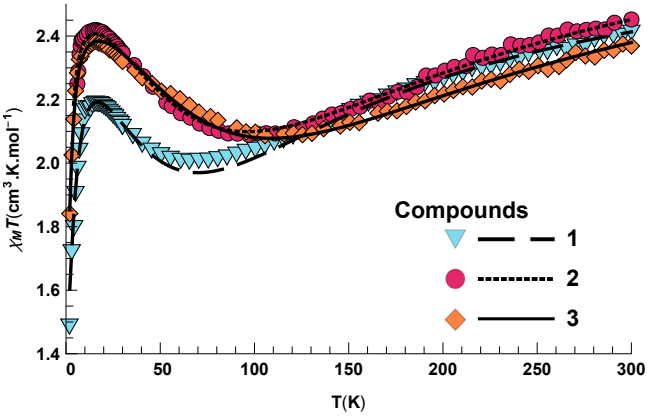


Figure 5 : Plots of $\chi_M T$ *vs.* *T* measured from 300 to 2 K for **1** (△), **2** (●) and **3**(◆);the solid and dashed black lines are the best-fit curves

All the curves are typical examples of ferrimagnetic behaviour with a minimum in the $\chi_M T$ versus T curves. This is a clear signature of a strong antiferromagnetic interaction (AF) between the Cu(II) and Ni(II) ions through the oxamato bridge. At 300 K, for **1-3**, the $\chi_M T$ values are in the 2.41-2.45 $cm^3.K.mol^{-1}$ range. These values are lower than expected for two Ni(II) and one Cu(II) uncoupled ions ($\chi_M T$=3.03 $cm^3.K.mol^{-1}$ with *g*=2.1) confirming the antiferromagnetic interaction between the Ni(II) and Cu(II) ions. Upon cooling, all $\chi_M T$ curves decrease to reach minima around 100K for **2** and **3** and 71 K for **1**. The shift of the minimum to a lower temperature in **1** shows that the AF interaction is weaker than in **2** and **3**, which was foreseeable due to its distorted structure. Upon further cooling the $\chi_M T$ values increase to reach a maximum at 16 K for all three compounds of $\chi_M T_{max}$=2.19 $cm^3.K.mol^{-1}$ for **1**, $\chi_M T_{max}$=2.42 $cm^3.K.mol^{-1}$ for **2** and $\chi_M T_{max}$=2.38 $cm^3.K.mol^{-1}$ for **3**. Below 16 K the $\chi_M T$ values decrease and there is no evidence of a plateau expected for an S=3/2 ground state. The lack of plateau and the drop of cMT at low temperature are related either to intermolecular interactions or to magnetic anisotropy of in the molecules. However, given the relatively large intermolecular distances in this familly of compounds the drop of $\chi_M T$ is likely related to the magnetic anisotropy of the *S*=3/2 ground state. Moreover, this interpretation is supported by magnetisation studies versus field and temperature between 2 T and 7 T and 2 K and 10 K. At these temperatures where only the ground state *S*=3/2 is populated, the spreading of the isofield curves for **1-3** indicates the presence of zero field splitting (Figure 6 (b) for **1** and Figure S6 for **2** and **3**).

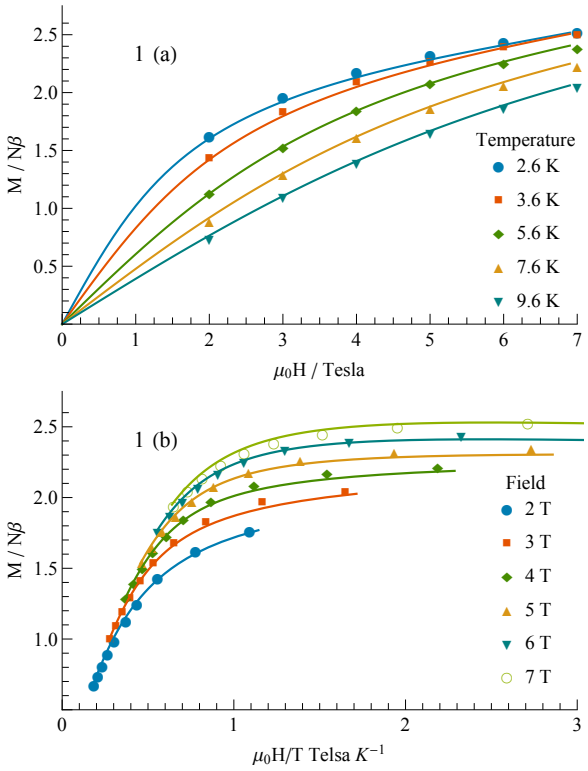


Figure 6 : Magnetization *vs* $\mu_0 H$ (a) and isofield curves *vs* $\mu_0 H/T$ (b) for **1** the solid lines are the best-fit curves

To interpret the magnetic data of **1-3**, the following Hamiltonian has been used (Equation 1)

$$\mathcal{H} = -J\left(\hat{S}_{Cu}.\hat{S}_{Ni1} + \hat{S}_{Cu}.\hat{S}_{Ni2}\right)$$
$$+D_{Ni}\left(\hat{S}^2_{z_{Ni1}} - \frac{\hat{S}^2_{Ni1}}{3} + \hat{S}^2_{z_{Ni2}} - \frac{\hat{S}^2_{Ni2}}{3}\right) - E_{Ni}\left(\hat{S}^2_{x_{Ni1}} - \hat{S}^2_{y_{Ni1}} + \hat{S}^2_{x_{Ni2}} - \hat{S}^2_{y_{Ni2}}\right)$$
$$+g_{v_{Ni}}\beta H\left(\hat{S}_{v_{Ni1}} + \hat{S}_{i_{Ni2}}\right) + g_{v_{Cu}}\beta H_v\hat{S}_{v_{Cu}} \qquad [1]$$

with v=x,y or z

In this Hamiltonian we have idealized the geometries of the complexes and we have only considered one Cu-Ni interaction and one ZFS parameter in spite of the two different coordination geometries for the two Ni(II) ions in complexes **2** and **3**. This approximation is particularly crude for **3** where one of the two Ni(II) ions is hexacoordinated. In a first attempt, to get an order of magnitude for the Cu-Ni interaction, we have modeled high temperature data neglecting the ZFS of Ni(II) ions. *J* values of -72 $cm^{-1}$, -100 $cm^{-1}$ and -111 $cm^{-1}$ have been found for **1**, **2** and **3** respectively, showing that the Cu-Ni interaction through the oxamato bridge is quite strong which in turn means that only the *S*=3/2 ground state is populated below 10K. To obtain reliable values for the anisotropy parameters for **1**, we have performed a simultaneous fit of $\chi_M T$ and magnetization data and we have minimized the following expression. (Equation 2)

$$G = w_\chi \sum_i \left(\chi_M.T_i^{exp} - \chi_M.T_i^{calc}\right)^2 + w_M \sum_j \left(M_j^{exp} - M_j^{calc}\right)^2 \qquad [2]$$

with $w_\chi$=$w_M$=1. Considering the large interaction between the Cu(II) and Ni(II) ions, we have only taken into account the *S*=3/2 ground state of the complexes to fit the magnetization curves. To perform these fits we have taken into account the tensorial relation between the postulated coaxial local parameters ($D_{Ni}$, $E_{Ni}$, $g_{Ni}$ and $g_{Cu}$) and the parameters of the *S*=3/2 ground state for a linear trimetallic complexe (see SI). (Equation 3)

$$D_{|^3/_2>} = {}^{7D_{Ni1}}/_{30} + {}^{7D_{Ni2}}/_{30} \approx {}^{14D_{Ni}}/_{30}$$
$$E_{|^3/_2>} = {}^{7E_{Ni1}}/_{30} + {}^{7E_{Ni2}}/_{30} \approx {}^{14E_{Ni}}/_{30} \quad \text{and}$$
$$g_{|\frac{3}{2}>} = \frac{3g_{Ni1} + 3g_{Ni2} - g_{Cu}}{5} \approx \frac{6g_{Ni} - g_{Cu}}{5}. \qquad [3]$$

The calculated $\chi_M T$ and *M* values are obtained by full diagonalization of the Hamiltonian matrices. The fitting were done using Mathematica software and Nelder-Mead Algorithm. To avoid overparametrization we have taken an isotropic $g_{Ni}$ Landé factor, an axial $g_{Cu}$ landé factor with $g_{Cu//}$=$g_{Cu\perp}$ +0.2 and we set $E_{Ni}$=|$D_{Ni}$|/3 which is the ratio giving the best simulation of the EPR spectrum (see EPR part). To obtain reliable values and not local minima, we have performed for each compounds at least 20 fits with different sets of starting parameters. The least square fit of the magnetic data gives $J_{CuNi}$=-72 $cm^{-1}$, $g_{Cu}$=2.03, $g_{Ni}$=2.18 and $D_{Ni}$=±9.9 $cm^{-1}$. The quality of the fit is insensitive to the sign of the $D_{Ni}$ parameter. The function *G* is equal to 5.6 $10^{-2}$ which corresponds to the following agreement factors $F\chi_T$=6.1 $10^{-5}$ and $F_M$=7.8 $10^{-4}$ with $\left(F_A = \frac{\sum_j \left(A_j^{exp} - A_j^{calc}\right)^2}{\sum_j \left(A_j^{exp}\right)^2}\right)$ *A*=$\chi_M T$ or *M*. The $D_{Ni}$ value corresponds to $D_{3/2}$=4.62 $cm^{-1}$ and $E_{3/2}$= 1.54 $cm^{-1}$ and that gives an energy barrier Δ=2 $D_{3/2}$=9.24 $cm^{-1}$.

For **2** and **3**, simultaneous fit of $\chi_M T$ and magnetization does not lead to good modeling. In particular, the isofield curves are poorly modeled. This is probably related to the large difference in geometry between the two Ni(II) ions within the trimetallic units in **2** and **3**. For these two complexes it is probably necessary to take into account the fact that local ZFS values are different for the two ions but also the respective orientations of the local $D_{Ni}$ tensors. However, it seems unreasonable to model $\chi_M T$ and magnetization curves with too many parameters. Hence for **2** and **3** we modeled $\chi_M T$ and magnetization data separately. The least square fit of the magnetic $\chi_M T$ data gave

$J_{CuNi}$=-98 $cm^{-1}$, $g_{Cu}$=2.09, $g_{Ni}$=2.25 $D_{Ni}$=±5.5 $cm^{-1}$ and $E_{Ni}$=1.83 $cm^{-1}$ and $J_{CuNi}$=-110 $cm^{-1}$, $g_{Cu}$=2.09, $g_{Ni}$=2.24, $D_{Ni}$=±5.98 $cm^{-1}$ and $E_{Ni}$= 1.99 $cm^{-1}$ for **2** and **3** respectively.

The classical agreement factors $\left(F = \frac{\sum_j \left(\chi_M.T_j^{exp} - \chi_M.T_j^{calc}\right)^2}{\sum_j \left(\chi_M.T_j^{exp}\right)^2}\right)$ are equal to $F\chi_T$ =3.8 $10^{-7}$ and 4.3 $10^{-7}$ for **2** and **3** respectively. The $D_{Ni}$ values correspond to $D_{3/2}$=2.56 $cm^{-1}$, $E_{3/2}$= 0.86 $cm^{-1}$ and $D_{3/2}$=2.79 $cm^{-1}$, $E_{3/2}$= 0.93 $cm^{-1}$ for **2** and **3** respectively. (Table 4)

For the fit of the magnetization curves the *E/D* ratio has been set to the one giving the best simulations of the EPR spectra, *E/D*=0.296 and *E/D*=0.280 for **2** and **3** respectively. The least square fit of magnetization data for the 3/2 ground state for **2** and **3** gave $g_x$=2.67, $g_y$=2.50, $g_z$=2.1, $D_{3/2}$=4.97 $cm^{-1}$, $E_{3/2}$=1.47 and *gx=2.30, gy*= 2.48, *gz*=2.00, $D_{3/2}$=4.08 $cm^{-1}$, $E_{3/2}$=1.14 $cm^{-1}$with agreement factors equal to 1.9 $10^{-4}$ and 9. $10^{-5}$ for **2** and **3** respectively. These $D_{3/2}$ values of the S=3/2 ground states corresponds to average local $D_{Ni}$ values of 10.7 $cm^{-1}$ and 8.7 $cm^{-1}$ respectively. The smallest $D_{Ni}$ value for **3** is coherent with the presence of one octahedral Ni(II) ions. For **2** and **3** the $D_{3/2}$ values obtained from the fit of the magnetization data are larger than the ones determined by the modelization of $\chi_M T$ but are probably more accurate because magnetization at low temperature is more sensitive to anisotropy parameters than measurements of the product $\chi_M T$. These values leads to energy barriers of Δ=12.0 $cm^{-1}$ and Δ=8.2 $cm^{-1}$ for **2** and **3** respectively.

Table 4 : Best parameters obtained for modeling the $\chi_M T$ product and magnetization measurements

| | | | | | $\chi_M T$ =f(T) fit | | M= G(T,H) fit | |
|---|---|---|---|---|---|---|---|---|
| | $J_{CuNi}$/$cm^{-1}$ | $J_{CuCu}$ / $cm^{-1}$ | $g_{Cu}$ | $g_{Ni}$ | $D_{3/2}$ / $cm^{-1}$ | $E_{3/2}$ / $cm^{-1}$ | $D_{3/2}$ / $cm^{-1}$ | $E_{3/2}$ / $cm^{-1}$ |
| **1** | -72. | | 2.03 | 2.18 | 4.62 | 1.54 | 4.62 | 1.54 |
| **2** | -98. | | 2.09 | 2.25 | 2.56 | 0.86 | 4.97 | 1.47 |
| **3** | -110. | | 2.09 | 2.24 | 2.79 | 0.93 | 4.08 | 1.14 |
| **4** | -91.8<br>-68.8 | 0 or 5 (EPR) | 2.12 | 2.19 | 2.79 | 0 | 3.5 | 0 |
| **5** | -90.4 | 9.8 or 29 (M) | 2.20 | 2.33 | 0 | 0 | 3.9 | 0 |

The $\chi_M T$ versus temperature curve for **4** is also typical of a ferrimagnetic behavior with a minimum at 78K (Figure 7 a). At 250K the value of $\chi_M T$=*4.69* cm$^3$.K.mol$^{-1}$ is lower than the expected one for four Ni(II) and two Cu(II) uncoupled ions ($\chi_M T$=5.67 cm$^3$.K.mol$^{-1}$ with $g_{Cu}$=2.1 and $g_{Ni}$=2.2). This a clear signature of an antiferromagnetic interaction between the Ni(II) and Cu(II) ions. At low temperature a maximum, $\chi_M T_{max}$= 4.47 cm$^3$.K.mol$^{-1}$, is observed around 14K and is close to the expected value for two uncoupled *S*=3/2 states ($\chi_M T$=4.33 cm$^3$.K.mol$^{-1}$ with $g_{3/2}$=2.15). Below 14 K $\chi_M T$ values decrease to reach a value of 3.77 cm$^3$.K.mol$^{-1}$ at 1.9 K. There is no evidence of ferromagnetic coupling between the *S*=3/2 ground states of the two {NiCuNi} subunits by spin polarization mechanism through the phenyl rings.

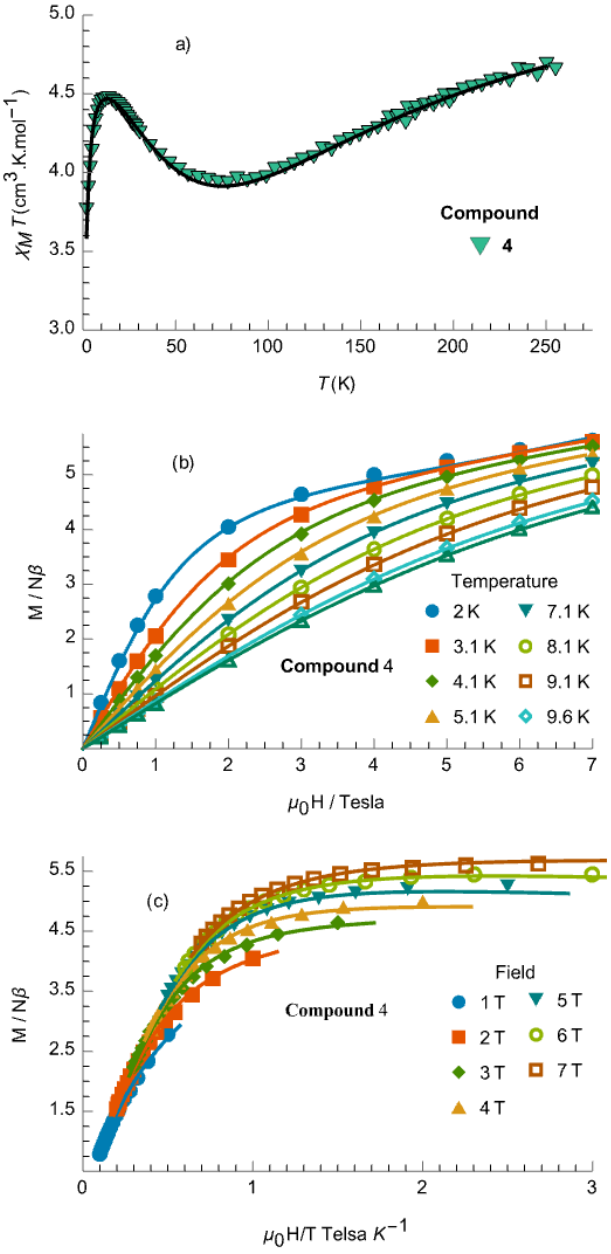


Figure 7 : (a) Plots of $\chi_M T$ *vs. T* measured from 300 to 2 K for **4** (▽) the solid black line is the best-fit curve. Magnetization *vs* $\mu_0$H (b) and isofield curves *vs* $\mu_0$H/T (c) for **4** the solid lines are the best-fit curves

The magnetization versus field curve and temperature between 2 T and 7 T and 2 K and 10 K. and the isofield versus $\mu_0$H/T are shown in Figure 7b, c. As for samples **1-3** the decrease of $\chi_M T$ at low temperature and the spreading the isofield curves (Figure 7c) are likely related to the magnetic anisotropy of **4** but the existence of populated excited levels of different spin values coming from the weak coupling through the aromatic rings is also possible.

Modeling the magnetic properties of **4** is complicated by the presence of three different exchange interactions pathways and two different Ni(II) ions leading to 16 independents parameters. Taking into account the molecular structure it is possible to simplify the model and reduce the number of parameters. The copper ions present an intermediate geometry between 3+2 (BTP) and 4+1 (SQ) coordination modes with a long Cu-O bond (2.213(3) Å). This leads to a smaller (3+2) or almost zero (4+1) spin delocalization of the *S*=1/2 spin of the copper ion onto this oxygen atom. This situation is known in the litterature[67,68] and leads to a reduced exchange

interaction through the oxamato bridge. In the BPT (SQ) arrangement the foreseen interaction is roughly ¾ (¼) the one observed in the situation where all the short chemical bonds are coplanar with the oxamato bridge as it is the case for the interaction between the Cu center and the Ni1 atom (see SI). As the geometry of the Cu ions are closer to BTP we have set $J_{CuNi2}$= $3J_{CuNi1}/4$ and used the following Hamiltonian. (Equation 4)

$$\mathcal{H} = -J_{CuNi}\sum_{n=1}^{2}\left(\hat{S}_{Cu}^{n}.\hat{S}_{Ni1}^{n}+\frac{3}{4}\hat{S}_{Cu}^{n}.\hat{S}_{Ni2}^{n}\right)- J_{CuCu}\hat{S}_{Cu}^{1}.\hat{S}_{Cu}^{2}$$
$$+ D_{Ni}\sum_{n=1}^{2}\left(\hat{S}_{z_{Ni1}}^{n\,2}-\frac{\hat{S}_{Ni1}^{n\,2}}{3}+\hat{S}_{z_{Ni2}}^{n\,2}-\frac{\hat{S}_{Ni2}^{n\,2}}{3}\right)$$
$$+ E_{Ni}\sum_{n=1}^{2}\left(\hat{S}_{x_{Ni1}}^{n\,2}-\hat{S}_{y_{Ni1}}^{n\,2}+\hat{S}_{x_{Ni2}}^{n\,2}-\hat{S}_{y_{Ni2}}^{n\,2}\right)$$
$$+ \sum_{n=1}^{2}\left[g_{Ni}\left(\hat{S}_{vNi1}^{n}+\hat{S}_{vNi2}^{n}\right)+g_{Cu}\hat{S}_{vCu}^{n}\right]\beta H_{v} \qquad [4]$$

with v= x,y,z

Due to the particular orientation of phenyl groups with respect to the magnetic orbital of copper ions with one of the two dihedral angles at only 35° (Cu-N1-C9, phenyl), the interaction between copper ions must be low and probably not detectable because masked by the effect of ZFS at low temperature. Indeed, this geometrical arrangement considerably reduces the interaction between the π orbitals of the phenyl rings and SOMOs of the copper ions responsible for the spin polarization mechanism. Therefore we modeled the magnetic data as two uncoupled trimetallic subunits. The least square fit of the magnetic data gave $J_{CuNi1}$=-91.8 cm$^{-1}$, $g_{Cu}$=2.12, $g_{Ni}$=2.19 $D_{Ni}$=5.98 cm$^{-1}$ and $E$=0 with an agreement factors equal to 5. 10$^{-5}$. (Table 4) Nevertheless, we have checked that taking into account the interaction between copper ions does not significantly improve the quality of the fit. The value of $J_{CuNi1}$ corresponds to a $J_{CuNi2}$=-68.8 cm$^{-1}$ and with these two large values for the interaction only the S=3/2 ground states of the trimetallic subunits are populated at low temperature. It is thus possible to model the magnetization data as two weakly interacting $S$=3/2 spin state using the following Hamiltonian. (Equation 5)

$$\mathcal{H} = -J_{F}\hat{S}^{1}.\hat{S}^{2}+ D_{3/2}\sum_{n=1}^{2}\left(\hat{S}_{z}^{n\,2}-\frac{\hat{S}^{n\,2}}{3}\right)$$
$$+E_{3/2}\sum_{n=1}^{2}\left(\hat{S}_{x}^{n\,2}-\hat{S}_{y}^{n\,2}\right)$$
$$+g_{v_{3/2}}\beta H_{v}\left(\hat{S}_{v}^{1}+\hat{S}_{v}^{2}\right) \qquad [5]$$

with $S^{1}$=$S^{2}$=3/2 and $v$=$x$,$y$ or $z$

The introduction of a coupling constant between the two S=3/2 states does not improve the quality of the fit and good agreement between the experimental data and theoretical curves is obtained setting $J_F$=0. The least square fit of the magnetization data gave $J_F$=0, $D_{3/2}$=3.5 cm$^{-1}$, $g_x$=$g_y$=2.25, $g_z$=2.08 with an agreement factor equal to 1.2 10$^{-5}$. In fact, the interaction between the two $S$=3/2 spin state, if it exists, is too weak to be detectable by magnetic measurements. The $D_{3/2}$ value of 3.5 cm$^{-1}$ corresponds to an average local $D_{Ni}$ value of $D_{Ni}$=30$D_{3/2}$/7=15 cm$^{-1}$ in the expected range for a pentacoordinated Ni(II) ions coordinated by $^{i}$Prtacn ligand[37]. A $g_z$ value lower than $g_x$ and $g_y$ is also not surprising. As $g_{zCu}$ > $g_{xCu,}$ $g_{yCu}$ this leads to $g_{z3/2}$ lower than $g_{x3/2}$ and $g_{y3/2}$ since $g_{|\frac{3}{2}>}=\frac{6g_{Ni}-g_{Cu}}{5}$ and $g_{Ni}$ of [Ni(iPrtacn)X$_2$] are almost isotropic.[37]

The $\chi_M T$ versus temperature curve for **5** is also typical of a ferrimagnetic behavior (Figure 8a). At 300K, the $\chi_M T$ value is equal to 8 cm$^3$.K.mol$^{-1}$. This is lower than the expected one for six Ni(II) and three Cu(II) uncoupled ions ($\chi_M T$=8.51 cm$^3$.K.mol$^{-1}$ with $g_{Cu}$=2.1 and $g_{Ni}$=2.2). This a clear signature of an antiferromagnetic interaction between the Ni(II) and Cu(II) ions. The $\chi_M T$ product steadily decreases when lowering the temperature, reaches a minimum of 6.71 cm$^3$.K.mol$^{-1}$ at *ca.* 90 K, and then increases to a maximum of 10.1 cm$^3$Kmol$^{-1}$ at 3 K. In contrast to **4**, the experimental points at low temperature are above the expected limit for 3 non-interacting {NiCuNi} subunits delimited by the gray curve in Figure 8a. This is a clear evidence of ferromagnetic coupling between the $S$=3/2 ground states of the three {NiCuNi} subunits by a spin polarization mechanism through the phenyl rings.

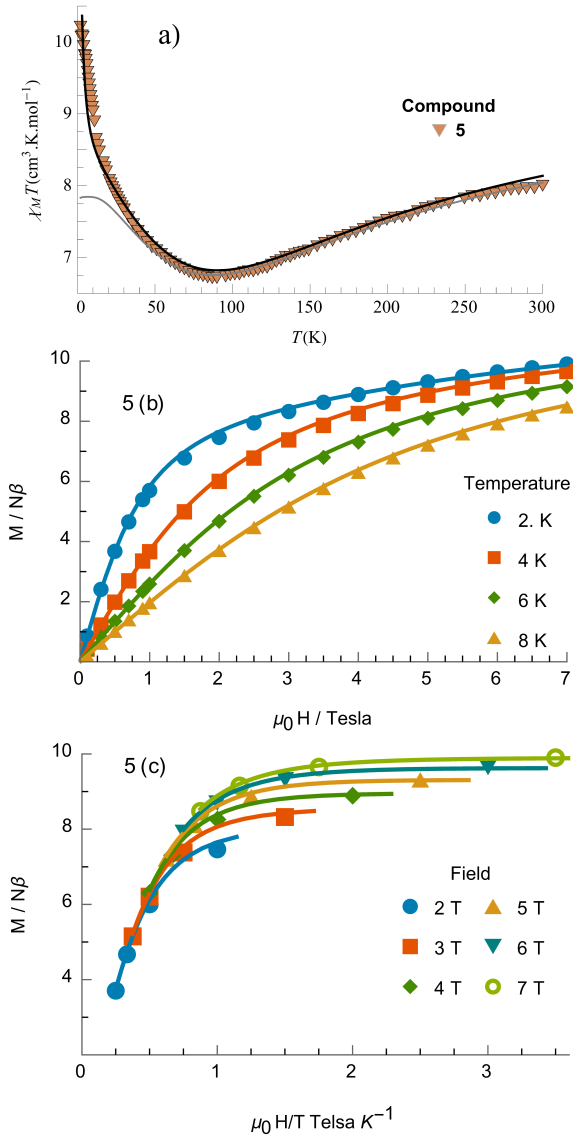


Figure 8: (a) Plots of $\chi_M T$ *vs.* *T* measured from 300 to 2 K for **5** (▽) the solid black line is the best-fit curve, the solid gray line is the best fit of the high temperature data for 3 independent {NiCuNi} subunits, (b) Magnetization *vs* $\mu_0$H , (c) isofield curves *vs* $\mu_0$H/T for **5** the solid lines are the best-fit curves

The lack of decrease for $\chi_M T$ at low temperature shows that the anisotropy is weak in **5**. The spreading of the isofield curves is in this case mainly related to the presence of a series of 12 spin levels coming from the ferromagnetic coupling between the three S=3/2 trimetallic subunits without, however, excluding some anisotropy. (Figure 8c).

As there is no evidence of anisotropy for **5**, we have modelled the $\chi_M T$ experimental data using the following Hamiltonian: (Equation 6)

$$\mathcal{H} = -J_{CuNi}\sum_{n=1}^{3}\left(\hat{S}_{Cu}^{n}.\hat{S}_{Ni1}^{n} + \hat{S}_{Cu}^{n}.\hat{S}_{Ni2}^{n}\right)$$
$$- J_{CuCu}\left(\hat{S}_{Cu}^{1}.\hat{S}_{Cu}^{2} + \hat{S}_{Cu}^{1}.\hat{S}_{Cu}^{3} + \hat{S}_{Cu}^{2}.\hat{S}_{Cu}^{3}\right) + \sum_{n=1}^{3}\left[g_{Ni}\left(\hat{S}_{Ni1}^{n} + \hat{S}_{Ni2}^{n}\right) + g_{Cu}\hat{S}_{Cu}^{n}\right]\beta H$$

[6]

In a first step, to avoid a multi-parameters time-consuming optimization, we have modelled the high temperature data without taking into account the ferromagnetic interaction between the {NiCuNi} subunits since it is not operative at high temperature. In a second step, we have modeled the data in the whole temperature range using the $J_{CuNi}$ value found in the first step. The least square fit of the magnetic data gave $J_{CuNi}$=-90.4 cm$^{-1}$, $J_{CuCu}$=9.8 cm$^{-1}$, $g_{Cu}$=2.20 and $g_{Ni}$=2.33 with an agreement factors equal to 9.6 10$^{-4}$. The interaction between the copper and nickel ions is large with $J_{CuNi}$=-90.4 cm$^{-1}$ (Table 4). Consequently, at low temperature only the *S*=3/2 ground state of the trimetallic subunits are populated. The ferromagnetic coupling between the Cu ions leads to a weakly stabilized S=9/2 ground state for compound **5**. The first excited state is at less than 2 cm$^{-1}$. The magnetization curves have been modeled using an isoceles triangle of *S*=3/2 spins. In contrast to the modeling of $\chi_M T$ it is impossible to obtain a good agreement between experimental curves and theoretical ones without the introduction of axial anisotropy on the *S*=3/2 states. The following Hamiltonian has therefore been used: (Equation 7)

$$\mathcal{H} = -J_{eff}\left(\hat{S}^{1}.\hat{S}^{2} + \hat{S}^{2}.\hat{S}^{3} + \hat{S}^{1}.\hat{S}^{3}\right) + \sum_{n=1}^{3}\hat{S}^{n}D^{n}\hat{S}^{n} + \sum_{n=1}^{3} g_{\upsilon\frac{3}{2}}\hat{S}_{\upsilon}^{n}\ \beta H_{\upsilon} \qquad [7]$$

In Hamiltonian [6], the three $D^n$ tensors are related to each other by a 120° rotation to take into account the presence in **5** of a pseudo $C_3$ symmetry axis. The least square simultaneous fit of magnetization and low temperature $\chi_M T$ data gave $J_{eff}$ = 0.13 $cm^{-1}$, $3D_{zz}/2$=3.9 $cm^{-1}$, $g_{x3/2}$=2.96, $g_{y3/2}$=1.80 and $g_{z3/2}$=2.38 with an agreement factor equal to 1.4 $10^{-4}$ for the magnetization data and 5.8 $10^{-3}$ for $\chi_M T$ data (Figure S7). The relation between the $J_{eff}$ value to the real $J_{CuCu}$ interaction is equal to $J_{CuCu}$=225$J_{eff}$ =29 $cm^{-1}$ (see SI) and $D_{Ni}$ = 7$D_{zz}$/10 =1.8 $cm^{-1}$. The $J_{CuCu}$ value obtained by the modeling of the magnetization data seems very large when compared to the one observed in the parent trimetallic $[Cu_3(T\text{-}Triox)_2]^{6-}$ compound where $J_{CuCu}$=+16.5 $cm^{-1}$.[39] This is probably due to the over-simplified model taking into account only three spins. However, it is almost impossible to model magnetization data for the enneametallic system in a reasonable amount of time. Nevertheless, the modeling clearly indicates that there is still some anisotropy in **5** even if it is not visible on the $\chi_M T$ curve. The reduced anisotropy probably comes from the combination of the three local $S$=3/2 anisotropy tensors with different orientations.

None of the compounds studied in this article shows SMM behavior. Even in the presence of a static DC field they did not show any AC frequency-dependent signal suggesting slow relaxation of the magnetization. In the trimetallic complexes **1**-**3**, the spin value of the ground state $S$=3/2 and the $D_{3/2}$ value are too small to lead to high energy barrier. Furthermore, the magnetization cleary indicate a positive $D$ value in **2**, which is not the ideal situation to observe slow relaxation of the magnetization, even if reports show slow relaxation with positive D value [25,69,70]. In **4** the coupling between the trimetallic subunits is too small to stabilize a high-spin ground state and **5** does not show enough anisotropy which excludes SMM behavior.

To confirm the magnetic studies we have carried out theoretical calculations and EPR studies in X-band. The theoretical calculations were only made on compounds **1** to **3** in order to calculate the exchange coupling constants and the expected anisotropy of the $S$=3/2 ground state taking explicity into account the actual geometry

**Theoretical calculations**

To get a deeper understanding of the nature and magnitude of the exchange coupling obtained above, we have performed BS-DFT calculations on complexes **1**-**3** (see computational details).[71] There are three types of magnetic exchanges operational in complexes **1**-**3** which are found to take place between (i) Cu and Ni1 centres ($J_1$), (ii) Cu and Ni2 centres ($J_2$), (iii) Ni1 and Ni2 centres ($J_3$). In the experimental simulation $J_1 \approx J_2$ scenario was assumed. The calculated exchange coupling constants are given in Table 5. Apart from complex **2**, the values are in the same range as those estimated from the fitting of the magnetic properties and unambiguously confirm that the oxamate bridge is very efficient in transmitting the electronic interaction between two metal ions separated by around 5.2 Å. The DFT computed magnetic exchange in **2** is underestimated compared to the experiment, this may be due to the fact that for this complex the approximation of $J_1 \approx J_2$ is not strictly valid as the two computed $Js$ differ by ~20 $cm^{-1}$. However, the calculated values for the interaction between the two nickel ions are very weak, which validates our approach for modelling the magnetic properties where we have neglected this interaction. Furthermore, to find out the origin of this antiferromagnetic exchange, we have calculated the overlap integral between each metal centre's SOMO (singly occupied molecular orbital). The overlap integral between the SOMOs of Cu and Ni centres is found to be largest in **3**; then, it decreases in **1** and **2,** respectively (Tables S2-4 and Figures S7-S9). The larger overlap integral leads to the large antiferromagnetic exchange, which corroborates the experimental data. These large values of the interaction lead to well stabilized $S$=3/2 ground states, the first excited $S$=1/2 state being at least 36 $cm^{-1}$ above the ground state. Compounds **1**-**3** are in the so-called strong exchange limit at low temperatures.[8]

Furthermore, to probe the origin of g and ZFS parameters of the metal centres, detailed *ab initio* CASSCF/NEVPT2 calculations were performed on complexes **1**-**3**. To mention, this methodology has been proven to yield good numerical estimates for various examples studied by us and others.[72–76] The zero-field splitting (ZFS) parameters of the Ni centres were determined from the following spin-Hamiltonian,[74] (Equation 8)

$$\widehat{H}_{ZFS} = D\left[\hat{S}_Z^2 - \frac{S(S+1)}{3}\right] + E(\hat{S}_x^2 - \hat{S}_y^2) \qquad [8]$$

The components of axial ZFS parameters (D) are derived from the second-order perturbation theory as follows,[28](Equation 9)

$$D_{ij} = -\frac{\square^2}{4S^2}\sum_{a,b}\frac{\langle\square_a|l_i|\square_b\rangle\langle\square_b|l_j|\square_a\rangle}{\varepsilon_b-\varepsilon_a} - \frac{\square^2}{4S^2}\sum_{c,d}\frac{\langle\square_c|l_i|\square_d\rangle\langle\square_d|l_j|\square_c\rangle}{\varepsilon_d-\varepsilon_c} \qquad [9]$$

where $\square$ is the effective spin-orbit coupling constant, $\varepsilon_a$, $\varepsilon_c$ and $\varepsilon_b$, $\varepsilon_d$ corresponds to the energy of ground and excited states, respectively. Further, $l_i$ and $l_j$ denotes the x, y and z components of the total angular momentum $L$. The first term in equation (8) corresponds to the spin allowed $\beta\rightarrow\beta$ transition from $\square_a$ to $\square_b$ MO and the second term correspond to the spin allowed $\alpha\rightarrow\alpha$ transition from $\square_c$ to $\square_d$ MO. The value of $D_{Ni}$ becomes positive when $D_{xx}$ and $D_{yy}$ terms are larger than the $D_{zz}$ and it becomes negative for vice versa from equation (8). The $D_{xx}$ and $D_{yy}$ terms become dominant when an electronic transition occurs between different $m_l$ levels, and $D_{zz}$ term becomes dominant when the electronic transition occurs between the same $m_l$ levels.

The principal values and orientation of the local tensors calculated using the diamagnetic substitution method (see computational details section) are shown in Figures S10-15 and Tables 6 and S6. The $g$ and $D_{Ni}$ anisotropy axis is found to be oriented along the highest order symmetry axis. The computed $g_z$ values become larger compared to $g_x$, and $g_y$ implies significant magnetic anisotropy of the Cu centres in all the complexes (Table S5). Further, the computed $D_{Ni}$ values are similar in all the complexes, which range from 16-19 $cm^{-1}$ except for the Ni1 centre of complexes **3** where the $D_{Ni}$ value is found to be -5 $cm^{-1}$. This can be ascribed due to the difference in the coordination geometry of the metal centres. A close look at complexes **1**-**3** reveals that the Ni1 centre in **3** lies in an octahedral environment while all other metal centres in complexes **1**-**3** reside in the square pyramidal geometry. However, the computed $D_{Ni}$ and $E/D$ values are consistent with the experimental one (from X-band EPR), giving confidence to our methodology to estimate these parameters.

To explain the nature of the $D_{Ni}$ values, we have shown the AILFT (ab initio ligand field theory) eigen value plot of the 3d orbitals of the Ni centres in Figures 9 and S24-26. The ground state of the Ni centre in **1**-**3** (except for the Ni1 centre in complex **3**) is multiconfigurational in nature with the dominant electronic configuration of $d_{xz}^2 d_{yz}^2 d_{xy}^2 d_z^{21} d_{x^2-y^2}^{21}$ (Tables S6-9). The positive $D_{Ni}$ values of the Ni centres can be explained by the coupling of the ground state with two close-lying triplet excited states with a dominant electronic

configuration of $d_{xz}^2 d_{yz}^1 d_{xy}^2 d_z^{22} d_{x^2-y^2}^{21}$ (or $d_{xz}^1 d_{yz}^2 d_{xy}^2 d_z^{22} d_{x^2-y^2}^{21}$ in **2** and **3**) and $d_{xz}^1 d_{yz}^2 d_{xy}^2 d_z^{21} d_{x^2-y^2}^{22}$ respectively (Figures 9 and S16-18). As coupling between these states related to the electronic transitions from $d_{xz}$ to $d_{x^2-y^2}$ (or $d_{xz}$ to $d_z^2$ in **2** and **3**) and $d_{yz}$ to $d_z^2$ orbitals which corresponds to the different $m_l$ levels, it contributes to the positive $D$ value according to equation (8). Further, as the energy gap between these orbitals is more than 6500 $cm^{-1}$, a quite small $D_{Ni}$ value is observed for the Ni centre in all the complexes. It is important to mention that the other electronic transitions with the same $m_l$ levels contribute to the negative $D_{Ni}$ value, but those are higher-lying (>12500 $cm^{-1}$) in energy.

For the Ni1 centre of complex **3**, the ground state is also found to be multiconfigurational in nature, with a dominant electronic configuration of $d_{xy}^2 d_{yz}^2 d_{xz}^2 d_{x^2-y^2}^{21} d_z^{21}$ (44%). The negative $D_{Ni}$ value of this complex originates from the coupling of the ground state with the first excited state $d_{xy}^1 d_{yz}^2 d_{xz}^2 d_{x^2-y^2}^{22} d_z^{21}$ (49%) at ca. 9800 $cm^{-1}$ (Table S9). This coupling involves electronic transitions from the $d_{xy}$ to $d_{x^2-y^2}$ orbital with the same $m_l$ levels, contributing to the negative $D_{Ni}$ value.

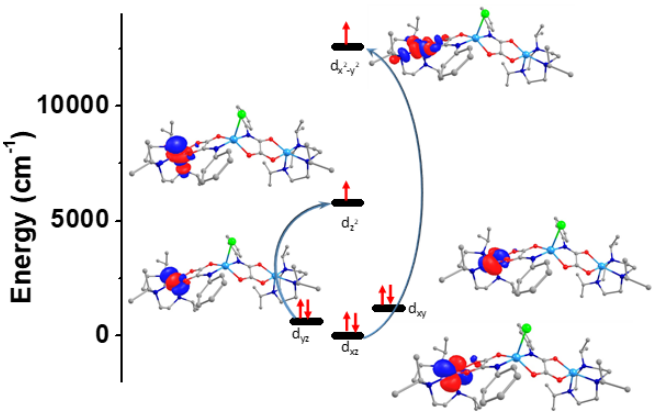


Figure 9: NEVPT2-AILFT computed d orbital energies of Ni1 centre of **1** and the most important electronic transitions contributing to the total $D$ value. Colour code: Ni-blue violet, Cu-sky blue, Cl-green, O-red, N-blue and C-grey. Hydrogens are omitted for clarity.

Table 5: BS-DFT exchange coupling constants for compounds **1**-**3.** The $J$ values are given in $cm^{-1}$

| | Cu-Ni$_1$ ($J_1$) | Cu-Ni$_2$($J_2$) | Ni$_1$-Ni$_2$ |
|---|---|---|---|
| **1** | -90.8 | -92.0 | -0.2 |
| **2** | -78.9 | -61.2 | -0.2 |
| **3** | -117.9 | -116.3 | -0.4 |

Table 6: The CASSCF/NEVPT2 computed D and E/D parameters of Ni1 and Ni2 centre of complexes **1**-**3**.

| | $D_{Ni}$ ($cm^{-1}$) | | | $E/D$ | | |
|---|---|---|---|---|---|---|
| | **1** | **2** | **3** | **1** | **2** | **3** |
| Ni1 | 18.6 | 17.0 | -5.0 | 0.19 | 0.21 | 0.27 |
| Ni2 | 17.2 | 21.5 | 18.2 | 0.25 | 0.33 | 0.23 |

Table 7: Calculated principal values and orientations of the $g$ and $D$ tensors of the $S$=3/2 ground state using tensorial equation [2]. The Euler's angles are calculated with respect to the g tensor of the $S$=3/2 ground state. $D$ and $E$ values are given in $cm^{-1}$

| | | Principal values | | | Euler's angles | | |
|---|---|---|---|---|---|---|---|
| | | x | y | z | α | β | γ |
| **1** pma | $g_{3/2}$ | 2.381 | 2.273 | 2.123 | 0° | 0° | 0° |
| | $D_{3/2}$ | -3.250 | -1.134 | 4.384 | -177.5° | 38.5° | 118.5° |
| | | $D$=6.58, $E$=1.01 | | | | | |
| **2** $Me_3$pma | $g_{3/2}$ | 2.372 | 2.278 | 2.151 | 0° | 0° | 0° |
| | $D_{3/2}$ | -14.33 | -0.01 | 14.34 | -7.70° | -116.4° | -173.3° |
| | | $D$=6.89, $E$=2.31 | | | | | |
| **3** opba | $g_{3/2}$ | 2.318 | 2.265 | 2.157 | 0° | 0° | 0° |
| | $D_{3/2}$ | -2.431 | -0.418 | 2.849 | -22.2° | -31.1° | 81.1° |
| | | $D$=4.27, $E$= 1.00 | | | | | |

From the $D_{3/2}$ values in Table 7, it is possible to calculate the energy barrier $\Delta=D_{3/2}$ ($S^2$-1/4)=2 $D_{3/2}$, giving $\Delta$=13.19 $cm^{-1}$, 13.78 $cm^{-1}$ and 8.54 $cm^{-1}$ for **1**, **2** and **3** respectively.

In a nutshell, the calculated exchange coupling and anisotropy parameters values are in the same range of magnitude as the ones determined experimentally. In particular, the anisotropy parameters of the $S$=3/2 ground state are, as expected, reduced when compared to one of the anisotropic starting complex [Ni(iPrtacn)$Cl_2$] due to the dilution factor $d^{S}_{i}$ in polymetallic complexes and misalignment of local tensors but are still high. These results confirm that using very anisotropic 3d metal complexes as building units is a very interesting approach to explore.

## X Band EPR

We used EasySpin toolbox[77] to simulate the EPR spectra. For compounds **1**-**3**, the ground state $S$=3/2 is sufficiently stabilized with respect to the first excited state to consider only this state in the simulation. A priori, the simulation is delicate because of the probable disorientation of the $g$ and $D$ tensors. Moreover, for powder spectra of $S$=3/2 states, transitions appear for others orientation that x, y and z[78] making difficult the estimation of the parameters. Faced with this difficulty, we used as starting parameters in our simulation the values determined by the magnetic measurements or those calculated from the theoretical calculations. Magnetic measurements and theoretical calculations indicate that the $D$ values are well above the X band quantum of energy ($h\nu \approx 0.32$ $cm^{-1}$). In this case, the spectrum no longer depends on the $D$ value. Only the $E/D$ ratio can be determined by simulating the spectrum.

The spectrum of compound **1** shows three main transitions at 1130, 2400 and 3666 Oe. The presence of additional small signals is probably due to the existence of three different {NiCuNi} entities in the crystal lattice. All three main signals are at relatively small magnetic fields, indicating large $g$-factor values which is consistent with the expected $g$-factor values for a {NiCuNi} entity $g_{3/2} \approx (6g_{Ni} - g_{Cu})/5$. The spectrum of **1** is typical of a rhombic $S$=3/2 state with a large positive $D$ value. To simulate the spectrum, we have taken the value of $D_{3/2}$=4.62 $cm^{-1}$ obtained by the simulation of the magnetic measurements and determined the optimal value of the $E/D$ ratio by the fit. An acceptable simulation is obtained for $E/D$ equal to 1/3 and the following $g$ values $g_x$=2.75 $g_y$=2.48 and $g_z$=2.12. These values correctly reproduce the two low field transitions but not the one located at 3666 Oe which is moved to 4280 Oe (see Figure S20). No improvement of the simulation is obtained by misaligning the $g$ and $D$ tensors using the values of the Euler angles obtained by the theoretical calculations (Table 7).

The spectrum of compound **2** shows five extrema at 760, 1360, 2180 and 3200 Oe and three shoulders at 520, 3700 and 4700 Oe. The simulation for compound **2** only allows a reproduction the general shape of the spectrum except for the two low field peaks at 730 Oe and 1370 Oe which are replaced by two peaks at 1030 Oe and 1320 (see Figure S22). As for compound **1** the simulation was carried out using the value of $D_{3/2}$ =5.98 $cm^{-1}$ determined by the magnetic properties modelisation. The $E/D$ ratio is equal to 0.295 and the $g$ values are equal to $g_x$= 2.48, $g_y$=1.93 and $g_z$= 2.43. Again, no improvement of the simulation is obtained by misaligning the $g$ and $D$ tensors.

The spectrum of compound **3** shows five extrema at 1120, 1920, 2800, 3450 and 4310 Oe. For this compound, the simulation manages to reproduce all the features of the spectrum but not the intensity of the central peak. The simulation was carried out using the value of $D_{3/2}$=4.08 $cm^{-1}$ determined by the magnetic properties modelisation. The $E/D$ ratio is found equal to 0.29 and the $g$ values are equal to $g_x$=2.43, $g_y$=1.99 and $g_z$=2.36. As for **1** and **2**, no improvement of the simulation is obtained by misaligning the $g$ and $D$ tensors. (see Figure S24)

The spectrum of compound **4** depicted in Figure 10 shows an intense low-field line at 780 Oe, lines at 2400 Oe and 3300 Oe and two higher-field shoulders at 4310 Oe and 6370 Oe. The spectrum is no longer typical of an isolated $S$=3/2 and indicates that there is a small interaction between the two trimetallic halves. The spectrum was simulated with two interacting $S$=3/2 spins. The simulation was performed using the value of $D_{3/2}$ =3.5 $cm^{-1}$ for the two $S$=3/2 subunits, a value determined by modelling the magnetic properties. The simulation is not excellent but leads to the following parameters $E/D$=0.290, $g_x$=2.48, $g_y$=1.82 and $g_z$=2.38 and a value of the interaction between the two $S$=3/2 subnuits of $J_{eff}$ =0.20 $cm^{-1}$. This value of $J_{eff}$ found for the effective interaction between the two trimetallic subunits corresponds to a value $J_{CuCu}$=5 $cm^{-1}$ ($J_{CuCu}$= 25$J_{eff}$ see SI). This small value found for the interaction between the two Cu ions is effectively undetectable with magnetic measurements due to the large value of the anisotropy.

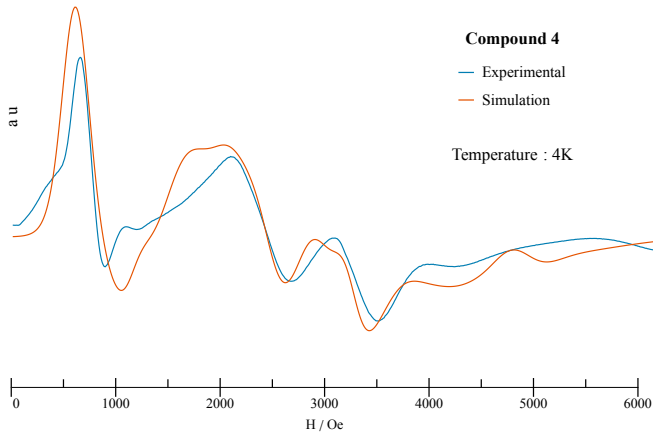


Figure 10: EPR spectrum of **4** at 4K in blue and best simulation in red using two interacting S=3/2 state

The EPR spectrum of compound **5**, with a single broad line centred at 990 Oe, contains too little information to extract relevant parameters (see Figure S14)

The best parameters obtained from the simulations are given in Table 8 and Table S1.

Table 8 : Best parameters from the simulation of EPR spectra

| | *D*/ $cm^{-1}$ *fixed* | E/ *D* | $g_x$ | $g_y$ | $g_z$ | |
|---|---|---|---|---|---|---|
| **1** pma | 4.62 | 1/3 | 2.75 | 2.48 | 2.12 | |
| **2** Me3pma | 5.98 | 0.296 | 2.53 | 2.03 | 2.33 | |
| **3** opba | 4.08 | 0.28 | 2.48 | 1.99 | 2.38 | |
| | | | | | | $J_{eff}$ |
| **4** mpba | 3.5 | 0.29 | 2.48 | 1.82 | 2.38 | 0.2 |

## Discussion :

Our results highlight a synthetic strategy that targets SMM behavior in polymetallic complexes of transition elements using highly anisotropic synthons. As the energy barrier $\Delta$ is equal to $|D|.S^2$ or $|D|(S^2\text{-}1/4)$, the goal is to find a compromise between the necessity of having a high spin value for the ground state which implies the synthesis of polymetallic complexes and the intrinsic dilution coefficient of the anisotropy $d_i$ in such polymetallic complexes[6–8]. The best compromise may not be obtained for a 3d single ion complex where the highest value for an anisotropic spin is $S$=2 leading to an energy barrier of $\Delta = 4D_i$ where $D_i$ is the local anisotropy parameter. On the other hand, the dilution coefficient of the anisotropy in polymetallic complexes is a clear drawback to obtain high energy barrier. Several years ago, Waldmann published a very interesting paper on the variation of this dilution coefficient $d_i$ with the spin value of polymetallic complexes.[79] He showed that the highest value for the energy barrier is obtained for the ferromagnetic spin state and that the $d_i$ coefficient is equal to $S_i(2\,S_i - 1)/S(2\,S - 1)$ for this state. For an homometallic system this formula becomes $d_i = (2\,S_i - 1)/n(2\,nS_i - 1)$ where n is the nuclearity of the complex. The upper limit for $d_i$ is in this case equal to ¼. It is obtained for n=2 and infinite spin value for $S_i$, meaning that there is at least a dilution of the local anisotropy by a factor 4 in homopolymetallic complexes. As it is ilustrated in Figure 10 the dilution coefficient $d_i$ decreases rapidly with the nuclearity and very slightly increases with the local spin value.

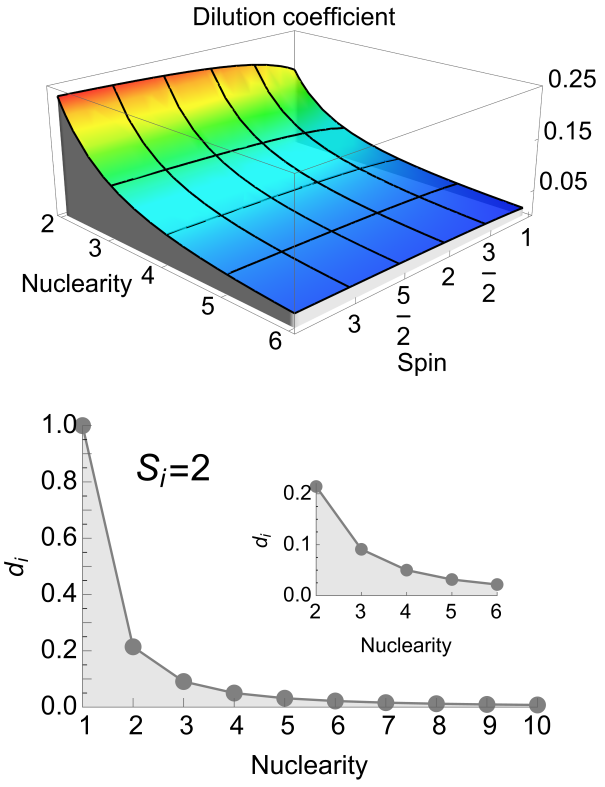


Figure 11 : (a) dilution coefficient $d_i$ for the anisotropy in a homometallic ferromagnetically coupled polymetallic complex versus spin and nuclearity; (b) variation of the dilution coefficient $d_i$ versus nucléarity for a spin $S_i$=2, insert : magnification of the 2-6 nuclearity range.

From Figure 11 it seems obvious that the optimal situation is probably obtained for low nuclearity complexes with the highest possible local spin value. This means that one need a controlled synthetic strategy to fulfil this goal and this is not the least of paradoxes to note that the best *polymetallic* SMMs published in the literature have been obtained by serendipity approach where there is no control of nuclearity. By contrast, a step by step approach using the complex-as-ligand strategy allowed us to control the nuclearity of the complexes from trimetallic to enneametallic polymetallic units. To mitigate the problem of the dilution coefficient $d_i$, the

best targets for very anisotropic systems are the trimetallic complexes **1**-**3**. Actually, these complexes built from anisotropic [Ni(iPrtacn)$Cl_2$] complexes present noticeable anisotropy for their *S*=3/2 ground state: in the 3-6 $cm^{-1}$ range. Taking into account the dilution coefficient $d_i$ of 7/30, this is just slightly smaller than the expected value, showing the validity of our approach. With these almost linear species, there is only weak reduction of the anisotropy related to the disorientation of the local $D_{Ni}$ tensors. Nevertheless, we are far from obtaining SMM due to the combination of two competiting factors. First, the anisotropy of the starting complex, [Ni(iPrtacn)$Cl_2$], is not so large and furthermore positive with $D_{Ni}$=14 $cm^{-1}$. However complexes of pentacoordinated Ni(II) ions with D value as high as -180 $cm^{-1}$ have been published recently in the literature[26]. Using such building units would lead to $D_{3/2}$ values around -80 $cm^{-1}$ for a {NiCuNi} units comparable to the highest energy barrier observed for *S*=3/2 complexes.[80] Second, the spin of Ni(II) ions is only *S*=1 leading to a small spin value for the ground state of the {NiCuNi} units (*S*=3/2). Using anisotropic Co(II) or Fe(II) complexes as building blocks would lead to ground state spin values of *S*=5/2 and 7/2 for the {CoCuCo} and {FeCuFe} units respectively. The corresponding dilution coefficients are equal to $d_i$=9/35 and $d_i$=11/42 meaning that the gain would be effective on both factors with greater spin value for the ground state and less dilution of the local anisotropy. It is also worthy of note that the dilution of the local anisotropy in these heterometallic complexes is slightly smaller than the upper limit of homodimetallic entities with values of 3.89 and 3.82 instead of 4. Some complexes with five coordinate Co(II) or Fe(II) ions also present very large anisotropy.[81] Recently Zhang et al showed that this strategy is effective with the synthesis of the [Cu(opba){$Co^{II}(PyPz_3)$}$_2$][$ClO_4$]$_2$ complex where the Co(II) ions show a trigonal prismatic coordination. This complex is an SMM even though the energy barrier of 35 $cm^{-1}$ is low due to tunneling effects.[64]

By contrast with these encouraging results obtained with {NiCuNi} units, the results obtained with the hexa and ennea polymetallic complexes are not surprising but nevertheless disappointing. Several reasons can explain the failure of our strategy to increase the spin value of the ground state while retaining a significant anisotropy. The most obvious one is the value of the dilution coefficients $d_i$ in the hexa and ennea complexes which are equal 7/150 and 7/360 for the *S*=3 and *S*=9/2 ground-states respectively (see SI). In these high-nuclearity units the dilution of the local anisotropy is therefore huge with values of more than 21 and 51 for the hexa and ennea entities respectively. But it is probably not the only reason for our unsatisfactory results. In **4**, we are facing the limit of the complex-as-ligand strategy, in spite of the step by step synthesis, the final entity is not quite the expected one. **4** is an hexametallic complex but it presents large distortions which preclude strong ferromagnetic interaction by spin polarization mechanism and, actually, this complex almost behaves like two independent trimetallic units without any stabilization of a higher spin ground state. This shows that a total control of the synthesis is just illusory and this was already illustrated with **3** where one of the Ni(II) ions is hexacoordinated while the pentacoordination is needed to achieve high anisotropy. For **5** the geometry of the $[Cu_3(T\text{-}triox)_2]^{6-}$ subunit shows some distortions when compared to the geometry of the original complex $K_6$[Cu3(T-triox)$_2$].8.5$H_2O$[39] but its geometry is still effective to promote ferromagnetic coupling between the Cu(II) ions by spin polarization mechanism and the high-spin *S*=9/2 ground state is stabilized by 1.8 $cm^{-1}$ from the first excited state. The magnetic studies show that the anisotropy in **5** is small. In addition to the high dilution factor in an enneametallic species, the small anisotropy in **5** is likely related to the relative orientations of the local $D_{3/2}$ tensors of the {NiCuNi} subunits and actually indicates that the principal axis of anisotropy of the local $D_{3/2}$ tensors probably lie almost parallel to the aromatic rings plane and point toward the center of the ring (see SI). Nevertheless, if one is interested in SMM behavior, the synthesis of polymetallic complexes with a $C_3$ symmetry axis is a good strategy to minimize the quantum tunneling (QTM) which is the limiting factor for the relaxation time of the magnetization. Whatever the symmetry of the local tensors their combination by a $C_3$ axis leads to an axial tensor removing all the rhombic component which is one of the main mechanism responsible of quantum tunnelling [4].

## Conclusion

Our results show that it is possible to obtain highly anisotropic polymetallic complexes using very anisotropic single-ion complex as building blocks. The best target for nuclearity is probably bi or trimetallic complexes and possibly tetrametallic complexes to partially avoid the intrinsic dilution of the anisotropy in polymetallic systems. Our linear heterotrimetallic {M-Cu-M} are probably close to the optimum situation. Indeed, by contrast to dimetallic systems where ferromagnetic interaction is compulsory, it is possible to obtain high-spin ground state for {M-Cu-M} complexes using antiferromagnetic (AF) interaction which leads in the {M-Cu-M} unit to the parallel alignement of the two external spins of the M ions by the small spin ½ of the Cu(II) ion. As it is well known the AF interaction is the most common interaction and the easiest to obtain[82]. Furthermore it is also well established that AF interaction is usually considerably larger than the ferromagnetic one[82,83] and high-spin ground state obtained by AF interaction involving no frustrated triangle are likely well separated from the first excited state. This situation avoids the *S* mixing with excited states which increases QTM and decreases the effective energy barrier $U_{eff}$.[84,85] It is also worthy of note that depending on the nature of M, the dilution factor for this {M-Cu-M} unit could be close to 4 which is the upper limit for a homodimetallic complex. Finally, the linear arrangement of the {M-Cu-M} unit prevents excessive disorientation of local M tensors that could drastically reduce the anisotropy of the spin states of the polymetallic complex. In our opinion, all these properties make {M-Cu-M} units particularly attractive targets to obtain high-energy barrier SMMs. The next step is now to obtain trimetallic {M-Cu-M} using Co(II), Fe(II) or Mn(III) building blocks complexes presenting very high anisotropy and possessing two *cis* labile position able to coordinate to the oxamate ligand.

### Experimental Section

**Materials:** All reagents were used as purchased with no further purification.

The $^{i}$Prtacn ligand was prepared as described in the literature in 23% yield from N,N',N''-tritosyldiethylenetriamine disodium salt.[86,87] $^1$H NMR (300 MHz, $CDCl_3$): δ (ppm) 2.85 (hept, J = 6.6 Hz, 3H), 2.62 (s, 12H), 0.95 (d, J = 6.6 Hz, 18 H).

The [Ni($^i$Prtacn)$Cl_2$] complex was prepared according to the literature procedure.[37] Yield: 62 % (based on Ni). Elemental analysis (%) calculated for $C_{15}H_{33}Cl_2N_3Ni$ ($M_r$ = 385.04 g mol$^{-1}$): C 46.79, H 8.64, N 10.91. Found: C 46.22, H 8.28, N 10.81.

The HEt-pma (ethyl ester of N phenyl oxamic acid), HEt-Me3pma (ethyl ester of N (2,4,6 trimethylphenyl) oxamic acid), H2Et2-opba (diethyl ester of the o-phenylenebis(oxamic acid)), H2Et2-mpba (diethyl ester of the m-phenylenebis(oxamic acid)) and H3Et3-T-Triox (triethyl ester of benzene-1,3,5-tris(oxamic acid)) pro-ligands were prepared following the literature procedure in 78, 76, 85, 82 and 57% yields, respectively[39,40,42,48,88]

HEt-pma. $^1$H NMR (400 MHz, DMSO) δ (ppm): 10.75 (s, 1H, N–H), 7.73 (d, *J* = 7.6 Hz, 2H, $H_{ar}$), 7.36 (dd, *J* = 8.4, 7.6 Hz, 2H, $H_{ar}$), 7.15 (t, *J* = 7.4 Hz, 1H, $H_{ar}$), 4.31 (q, *J* = 7.1 Hz, 2H, O–$CH_2$), 1.32 (t, *J* = 7.1 Hz, 3H, $CH_3$); $^{13}$C NMR (101 MHz, DMSO) δ (ppm): 160.68, 155.55, 137.44, 128.74, 124.71, 120.46, 62.36, 13.84.

HEt-$Me_3$pma. $^1$H NMR (400 MHz, DMSO) δ (ppm): 10.19 (s, 1H, N–H), 6.91 (s, 3H, $H_{ar}$), 4.30 (t, *J* = 7.1 Hz, 2H, O–$CH_2$), 2.09 (s, 9H, *Ph*–$CH_3$), 1.32 (t, *J* = 7.1 Hz, 3H, $CH_3$); $^{13}$C NMR (101 MHz, DMSO) δ (ppm): 160.88, 155.85, 136.20, 134.72, 130.96, 128.35, 62.17, 20.46, 17.79, 13.84.

$H_2Et_2$-opba. $^1$H NMR (400 MHz, DMSO) δ (ppm): 10.39 (s, 2H, N–H), 7.59 (d, *J* = 9.6 Hz, 2H, $H_{ar}$), 7.31 (d, *J* = 9.6 Hz, 2H, $H_{ar}$), 4.32 (q, *J* = 7.1 Hz, 4H, O–$CH_2$), 1.32 (t, *J* = 7.1 Hz, 6H, $CH_3$); $^{13}$C NMR (101 MHz, DMSO) δ (ppm): 160.24, 155.52, 129.64, 126.33, 125.62, 62.54, 13.80.

$H_2Et_2$-mpba. $^1$H NMR (400 MHz, DMSO) δ (ppm): 10.82 (s, 2H, N–H), 8.19 (s, 1H, $H_{ar}$), 7.48 (d, *J* = 8.0 Hz, 2H, $H_{ar}$), 7.33 (t, 1H, $H_{ar}$), 4.31 (q, *J* = 7.1 Hz, 4H, O–$CH_2$), 1.32 (t, *J* = 7.1 Hz, 6H, $CH_3$); $^{13}$C NMR (101 MHz, DMSO) δ (ppm): 160.65, 155.77, 137.70, 128.97, 117.08, 112.88, 62.34, 13.83.

$H_3Et_3$-T-Triox. $^1$H NMR (400 MHz, DMSO) δ (ppm): 10.89 (s, 3H, N–H), 7.91 (s, 3H, $H_{ar}$), 4.31 (q, *J* = 7.1 Hz, 6H, O–$CH_2$), 1.32 (t, *J* = 7.1 Hz, 9H, $CH_3$); $^{13}$C NMR (101 MHz, DMSO) δ (ppm): 160.64, 156.05, 137.78, 109.72, 62.35, 13.84.

**[Cu(pma)$_2$Cl{Ni($^i$Prtacn)}$_2$]Cl·10$H_2O$ (1):** A suspension of HEt-pma (0.019 g, 0.1 mmol) in water (5 mL) was treated with 2 mL of KOH 0.1 M, stirred at room temperature until complete dissolution of the ligand and filtered. An aqueous solution of $Cu(NO_3)_2.3H_2O$ (0.025 M, 2 mL, 0.05 mmol ) was then added dropwise to the oxamate solution resulting in a deep green solution of the copper complex that was stirred for 10 min at room temperature, filtered and then added to a 2 mL aqueous solution of the [Ni($^i$Prtacn)$Cl_2$] complex (0.038 g, 0.1 mmol). The resulting green solution was further stirred for 12 hours, filtered and left to slowly evaporate at room temperature. After several weeks green crystals of **1** were collected by filtration and dried in air. Yield: 0.024 g (37 % based on Cu). Elemental analysis (%) calculated for $C_{46}H_{87}Cl_2CuN_8Ni_2O_{16}$ ($M_r$ = 1266.9 g mol$^{-1}$): C, 43.57; H, 7.58; N, 8.84. Found: C, 43.25; H, 7.82; N, 8.66. ATR/FT-IR (cm$^{-1}$): 214(w), 296(w), 403(w), 482(w), 516(w), 581(w), 695(m), 722(m), 753, 799(m), 845(w), 868(m), 901(m), 1013(w), 1049(m), 1065(m), 1129(m), 1146(m), 1167(w), 1293(m), 1328(s), 1393(m), 1429(m), 1490(m), 1584(m), 1602(s), 2974(m), 3387(m).

**[Cu($Me_3$pma)$_2$($NO_3$)$_{0,6}$\{Ni($^i$Prtacn)$_2$\}]$Cl_{0.4}$($NO_3$)·9$H_2O$ (2):** A suspension of HEt$Me_3$-pma (0.023 g, 0.1 mmol) in water (5 mL) was treated with 0.2 mL of KOH 1 M, stirred at room temperature until complete dissolution of the ligand and filtered. An aqueous solution of $Cu(NO_3)_2.3H_2O$ (0.025 M, 2 mL, 0.05 mmol) was then added dropwise to the oxamate solution resulting in a deep green solution of the copper complex that was stirred for 10 min at room temperature, filtered and then added to a 2 mL aqueous solution of the [Ni($^i$Prtacn)$Cl_2$] complex (0.038 g, 0.1 mmol). The resulting green solution was further stirred for 12 hours, filtered and left to slowly evaporate at room temperature. After several weeks yellow-green crystals of **2** were collected by filtration and dried in air. Yield: 0.029 g (42 % based on Cu). Elemental analysis (%) calculated for $C_{52}H_{106}Cl_{0.4}CuN_{9.6}Ni_2O_{19.8}$ ($M_r$ = 1377.74 g mol$^{-1}$): C, 45.33; H, 7.75; N, 9.75. Found: C, 45.12; H, 7.14; N, 9.45. ATR/FT-IR (cm$^{-1}$): 292(w), 323(w), 484(w), 522(w), 603(w), 723(m), 778(m), 829(w), 867(m), 962(m), 1012(w), 1065(m), 1145(m), 1166(w), 1206(w), 1318(s), 1370(m), 1353(m), 1596(s), 2974 (m), 3407(m).

**[Cu(opba)Cl{Ni($^i$Prtacn)($H_2O$)}{Ni($^i$Prtacn)}]Cl·12$H_2O$ (3):** A suspension of $H_2Et_2$-opba (0.015 g, 0.05 mmol) in water (5 mL) was treated with 2 mL of LiOH 0.1 M, stirred at room temperature until complete dissolution of the ligand and filtered. An aqueous solution of $CuCl_2.2H_2O$ (0.025 M, 2 mL, 0.05 mmol) was then added dropwise to the oxamate solution resulting in a deep green solution of the copper complex that was stirred for 10 min at room temperature, filtered and then added to a 2 mL aqueous solution of the [Ni($^i$Prtacn)$Cl_2$] complex (0.038 g, 0.1 mmol). The resulting green solution was stirred for 30 min, filtered to remove a purple precipitate that has formed, further stirred overnight, and left to slowly evaporate at room temperature. After 10 days green crystals of **3** were collected by filtration and dried in air. Yield: 0.043 g (35 % based on Cu). Elemental analysis (%) calculated for $C_{40}H_{96}Cl_2CuN_8Ni_2O_{19}$ ($M_r$ = 1245.1 g mol$^{-1}$): C, 38.58; H, 7.77; N, 8.99. Found: C, 38.21; H, 6.69; N, 8.86. ATR/FT-IR (cm$^{-1}$): 290(w), 338(w), 487(w), 618(w), 722(w), 773(w), 869(w), 958(w), 1060(s), 1284(w), 1356(w), 1429(w), 1601(s), 2974(m), 3541(sh).

**[$Cu_2$(mpba)$_2$$Cl_2$\{Ni($^i$Prtacn)\}$_4$]($NO_3$)$_2$.16$H_2O$, (4):** A suspension of $H_2Et_2$-mpba (0.031 g, 0.1 mmol) in water (5 mL) was treated with 2 mL of LiOH 0.2 M, stirred at room temperature until complete dissolution of the ligand and filtered. An aqueous solution of $Cu(NO_3)_2.3H_2O$ (0.024 g, 0.1 mmol, 2.5 mL) was then added dropwise to the oxamate solution resulting in a deep green solution of the copper complex that was stirred for 10 min at room temperature, filtered and then added to a 1 mL aqueous solution of the [Ni($^i$Prtacn)$Cl_2$] complex (0.077 g, 0.2 mmol). The resulting green solution was further stirred overnight, filtered and left to slowly evaporate at room temperature. After 10 days green crystals of **4** were collected by filtration and dried in air. Yield: xxx g (71% based on Cu). Elemental analysis (%) calculated for $C_{80}H_{172}Cl_2Cu_2N_{18}Ni_4O_{34}$ ($M_r$ = 2363.1 g mol$^{-1}$): C, 40.66; H, 7.33; N, 10.67. Found: C, 40.60; H, 6.72; N, 10.63. ATR/FT-IR (cm$^{-1}$): 335(w), 383(w), 488(w), 690(w), 723(w), 776(w), 819(w), 846(w), 876(w), 962(m), 1004(w), 1065(m), 1146(m), 1167(w), 1294(w), 1342(m), 1417(w), 1456(w), 1599(s), 2976(m), 3377(sh).

**[$Cu_3$(T-Triox)$_2$($NO_3$)($H_2O$)$_{1,5}$\{Ni($^i$Prtacn)($H_2O$)\}\{Ni($^i$Prtacn)\}$_5$]($NO_3$)$_5$·38$H_2O$ (5):** A suspension of $H_3Et_3$-T-Triox (0.042 g, 0.1 mmol) in water (5 mL) was treated with 3 mL of KOH 0.2 M, stirred at room temperature until complete dissolution of the ligand and filtered. An aqueous solution of $Cu(NO_3)_2.3H_2O$ (0.036 g, 0.15 mmol, 2.5 mL) was then added dropwise to the oxamate solution resulting in a deep green solution of the copper complex that was stirred for 10 min at room temperature, filtered and then added to a 1.5 mL aqueous solution of the [Ni($^i$Prtacn)$Cl_2$] complex (0.115 g, 0.3 mmol). The resulting green solution was further stirred for 12 hrs, filtered and left to slowly evaporate at room temperature. After 2 weeks green crystals of **5** were collected by filtration and dried in air. Yield: 0.061 g (32% based on Cu). Elemental analysis (%) calculated for $C_{114}H_{285}Cu_3N_{30}Ni_6O_{76.5}$ ($M_r$ = 3834.43 g mol$^{-1}$): C, 35.62; H, 7.46; N, 10.93. Found: C, 36.23; H, 6.68; N, 10.41. ATR/FT-IR (cm$^{-1}$): 320(w), 365(w), 483(w), 574(w), 722(w), 775(w), 825(m), 962(m), 1011(w), 1048(w), 1064(w), 1145(m), 1164(w), 1294(w), 1335(m), 1435(w), 1494(w), 1602(s), 2975(m), 3384(sh).

**Physical measurements:** Crystallographic data were collected on a Bruker Kappa-APEX II CCD diffractometer for **1-5** (**2**: $Mo_{K\alpha}$, λ = 0.71069 Å, **1** and **3-5**: $Cu_{K\alpha}$, λ = 1.54178). Crystals were mounted on a Hamilton cryoloop using Paratone-N oil and placed in the cold flow produced with an Oxford Cryocooling device. Partial hemispheres of data –preselected with the APEX II software[89]– were collected using φ and ω scans. Integrated intensities were obtained with SAINT+ and were corrected for absorption with SADABS;[89,90] structure solution and refinement was performed with the SHELXTL-package.[91] The structures were solved by direct methods and completed by iterative cycles of Δ*F* syntheses and full-matrix least-squares refinement against $F^2$. Crystallographic data and refinements parameters for **1**-**5** are given in Table 1. Crystallographic

details are available in CIF format, free of charge via www.ccdc.cam.ac.uk/conts/retrieving.html (or from the Cambridge Crystallographic Data Centre, 12, Union Road, Cambridge CB2 1EZ, UK; fax: (+44) 1223-336-033; or deposit@ccdc.cam.ac.uk). CCDC numbers 2216053-2216057.

Magnetic measurements in dc and ac modes were performed on Quantum Design MPMS SQUID and PPMS on crushed crystalline powder restrained in a plastic film, drops of Paratone-N oil was added to prevent crystallite torqueing. Data were corrected for the diamagnetism contributions of the samples using Pascal constants. The sample holder and Paratone-N oil diamagnetism were measured and subtracted from the raw data. To model the magnetic properties we used homemade Mathematica codes which establishes the hamiltonian matrix and calculates the partition function allowing the derivation of the physical properties. The best parameters were found using the Neldear-Mead algorithm. For double checked, we also used Phi free software to model the magnetic data[92]

The EPR spectra were measured at X-band (9.34 GHz) with a Bruker ER200 instrument equipped with a liquid helium cryostat from Oxford, Inc. To simulate and fit the EPR spectra we used EasySpin MATLAB toolbox[77]

$^{1}$H and $^{13}$C NMR spectra were collected on a 300 MHz Bruker Avance spectrometer at 298 K in the "Plateforme RMN Moléculaire / IPCM-Sorbonne Université".

ATR/FT-IR spectra were collected on a Bruker TENSOR 27 equipped with a simple reflexion ATR diamond plate of the Harrick MPV2 series.

**Computational Details:** All the DFT calculations for complexes **1**-**3** have been performed with hybrid B3LYP functional in the Gaussian09 programme package[93]. We have used Ahlrichs TZVP (triple-ζ valence polarization) basis set for Ni, Cu, O and N atoms and Ahlrichs SVP (split valence plus polarization) basis set for C and H atoms. The quadratic convergence method was used to get the most stable wave function. The magnetic exchange coupling in all the complexes has been estimated with a broken symmetry approach using the linear equation proposed[94] with one high spin (Ni1↑-Cu↑-Ni2↑) and three broken symmetry configurations (Ni1↑-Cu↑-Ni2↓, Ni1↓-Cu↑-Ni2↑ and Ni1↑-Cu↓-Ni2↑). We have considered the following Heisenberg Hamiltonian to model the magnetic exchange.

$$H = -J_1\hat{S}_{Cu}\hat{S}_{Ni1} - J_2\hat{S}_{Cu}\hat{S}_{Ni2} - J_3\hat{S}_{Ni1}\hat{S}_{Ni2} \quad (1)$$

where, $J_1$, $J_2$ and $J_3$ denotes the exchange coupling between Cu and Ni1, Cu and Ni2, and Ni1 and Ni2 centres, respectively.

The ab initio CASSCF calculations have been performed on the X-ray crystal structure of complexes 1-3 using the ORCA 4.0.1 programme package. We have used the diamagnetic substitution method to estimate the magnetic anisotropy of each metal centre in all the complexes. The relativistic effect in our calculations was taken into account by Douglas-Kroll-Hess (DKH) Hamiltonian. We have employed DKH contracted basis set during our calculations: DKH-def2-TZVP for Ni, Cu, Zn and Cl, DKH-def2-TZVP(-f) basis set for O and N, DKH-def2-SVP basis set for rest of the atoms. Furthermore, RI (resolution of identity) approximation along with def2-TZVP/C (def2-SVP/C for C and H) auxiliary basis set was used to speed up the calculations. The state average complete active space self-consistent field calculations were performed with eight metal electrons in five metal d-orbitals for Ni(II) and nine metal electrons in five metal d-orbitals for Cu(II). Using this active space, we have computed the energy of the ten triplets and fifteen singlets for Ni(II) and five doublets for Cu(II) metal centres. The dynamic electron correlation in our calculations has been taken into account by second-order N-electron valence perturbation theory (NEVPT2) on top of the SA-CASSCF wave function. The def2-TZVP/C auxiliary basis set was used with trafostep RIMO approximation for all the atoms except C and H, for which the def2-SVP/C auxiliary basis set was used. The spin-orbit interaction between the spin-free states was accounted for with quasi degenerate perturbation theory (QDPT) with the spin-orbit mean-field (SOMF) operator. The zero-field splitting parameters (D and E) and g tensors of the metal centres were estimated from the effective Hamiltonian approach (EHA). Finally, accurate d orbital energies of complexes **1**-**3** have been obtained from ab initio ligand field theory (AILFT) analysis,

## Supporting Information

The authors have cited additional references within the Supporting Information.[8,95]

## Acknowledgements

This work was supported by the Ministère de l'Enseignement Supérieur, de la Recherche et de l'Innovation (MESRI), the Centre National de la Recherche Scientifique (CNRS) and the China Scholarship Council (CSC) in the form of M. Ang Li's PhD fellowship.. The authors would like to thank Dr. Michael Baker of the School of Chemistry of the University of Manchester for his assistance in modelling EPR spectra. GR would like to thank SERB (DST/CSA-03/2018-10; SB/SJF/2019-20/12) for funding. We thank the staff of the low temperature physical measurement MPBT technical platform in Sorbonne Université.

**Keywords:** Heteropolymetallic complex • Magnetic anisotropy • Magnetic properties • Oxamate • Self-Assembly

[1] A. Caneschi, D. Gatteschi, R. Sessoli, M. A. Novak, *Nature* **1993**, *365*, 141.
[2] F. Neese, D. A. Pantazis, *Faraday Discuss.* **2011**, *148*, 229–238.
[3] D. N. Woodruff, R. E. P. Winpenny, R. A. Layfield, *Chem. Rev.* **2013**, *113*, 5110–5148.
[4] T. Glaser, *Chem. Commun.* **2011**, *47*, 116–130.
[5] R. Sessoli, H.-L. Tsai, A. R. Schake, S. Wang, J. B. Vincent, K. Folting, D. Gatteschi, G. Christou, D. N. Hendrickson, *J. Am. Chem. Soc.* **1993**, *115*, 1804–1816.
[6] R. P. Scaringe, D. J. Hodgson, W. E. Hatfield, *Mol. Phys.* **1978**, *35*, 701–713.
[7] E. Buluggiu, *J. Phys. Chem. Solids* **1982**, *43*, 997–1001.
[8] A. Bencini, D. Gatteschi, *EPR of Exchange Coupled Systems*, Springer-Verlag, Berlin Heidelberg, **1990**.
[9] Z. Sun, D. Ruiz, D. N. Hendrickson, N. R. Dilley, M. B. Maple, M. Soler, K. Folting, G. Christou, J. Ribas, *Chem. Commun.* **1999**, 1973–1974.
[10] K. Awaga, Y. Suzuki, H. Hachisuka, K. Takeda, *J. Mater. Chem.* **2006**, *16*, 2516–2521.
[11] F. Neese, E. I. Solomon, *Inorg. Chem.* **1998**, *37*, 6568–6582.
[12] A. Zabala-Lekuona, J. M. Seco, E. Colacio, *Coord. Chem. Rev.* **2021**, *441*, 213984.
[13] N. Ishikawa, M. Sugita, T. Ishikawa, S. Koshihara, Y. Kaizu, *J. Am. Chem. Soc.* **2003**, *125*, 8694–8695.
[14] A. Watanabe, A. Yamashita, M. Nakano, T. Yamamura, T. Kajiwara, *Chem. Eur. J.* **2011**, *17*, 7428–7432.
[15] J. D. Rinehart, J. R. Long, *Chem. Sci.* **2011**, *2*, 2078–2085.
[16] S. G. McAdams, A.-M. Ariciu, A. K. Kostopoulos, J. P. S. Walsh, F. Tuna, *Coord. Chem. Rev.* **2017**, *346*, 216–239.
[17] A. H. Vincent, Y. L. Whyatt, N. F. Chilton, J. R. Long, *J. Am. Chem. Soc.* **2023**, *145*, 1572–1579.

[18] F.-S. Guo, B. M. Day, Y.-C. Chen, M.-L. Tong, A. Mansikkamäki, R. A. Layfield, *Science* **2018**, *362*, 1400–1403.
[19] C. A. P. Goodwin, F. Ortu, D. Reta, N. F. Chilton, D. P. Mills, *Nature* **2017**, *548*, 439–442.
[20] J. D. Rinehart, K. R. Meihaus, J. R. Long, *J. Am. Chem. Soc.* **2010**, *132*, 7572–7573.
[21] M. A. Antunes, L. C. J. Pereira, I. C. Santos, M. Mazzanti, J. Marçalo, M. Almeida, *Inorg. Chem.* **2011**, *50*, 9915–9917.
[22] D. E. Freedman, W. H. Harman, T. D. Harris, G. J. Long, C. J. Chang, J. R. Long, *J. Am. Chem. Soc.* **2010**, *132*, 1224–1225.
[23] W. H. Harman, T. D. Harris, D. E. Freedman, H. Fong, A. Chang, J. D. Rinehart, A. Ozarowski, M. T. Sougrati, F. Grandjean, G. J. Long, J. R. Long, C. J. Chang, *J. Am. Chem. Soc.* **2010**, *132*, 18115–18126.
[24] P.-H. Lin, N. C. Smythe, S. I. Gorelsky, S. Maguire, N. J. Henson, I. Korobkov, B. L. Scott, J. C. Gordon, R. T. Baker, M. Murugesu, *J. Am. Chem. Soc.* **2011**, *133*, 15806–15809.
[25] J. M. Zadrozny, J. Liu, N. A. Piro, C. J. Chang, S. Hill, J. R. Long, *Chem. Commun.* **2012**, *48*, 3927–3929.
[26] R. Ruamps, R. Maurice, L. Batchelor, M. Boggio-Pasqua, R. Guillot, A. L. Barra, J. J. Liu, E. Bendeif, S. Pillet, S. Hill, T. Mallah, N. Guihery, *J. Am. Chem. Soc.* **2013**, *135*, 3017–3026.
[27] A. Eichhöfer, Y. Lan, V. Mereacre, T. Bodenstein, F. Weigend, *Inorg. Chem.* **2014**, *53*, 1962–1974.
[28] S. Gómez-Coca, A. Urtizberea, E. Cremades, P. J. Alonso, A. Camón, E. Ruiz, F. Luis, *Nat. Commun.* **2014**, *5*, 4300.
[29] J. M. Zadrozny, D. J. Xiao, M. Atanasov, G. J. Long, F. Grandjean, F. Neese, J. R. Long, *Nat. Chem.* **2013**, *5*, 577–581.
[30] X.-N. Yao, J.-Z. Du, Y.-Q. Zhang, X.-B. Leng, M.-W. Yang, S.-D. Jiang, Z.-X. Wang, Z.-W. Ouyang, L. Deng, B.-W. Wang, S. Gao, *J. Am. Chem. Soc.* **2017**, *139*, 373–380.
[31] P. C. Bunting, M. Atanasov, E. Damgaard-Møller, M. Perfetti, I. Crassee, M. Orlita, J. Overgaard, J. van Slageren, F. Neese, J. R. Long, *Science* **2018**, *362*, eaat7319.
[32] A. A. Patrascu, S. Calancea, M. Briganti, S. Soriano, A. M. Madalan, R. A. A. Cassaro, A. Caneschi, F. Totti, M. G. F. Vaz, M. Andruh, *Chem. Commun.* **2017**, *53*, 6504–6507.
[33] A. A. Patrascu, M. Briganti, S. Soriano, S. Calancea, R. A. Allão Cassaro, F. Totti, M. G. F. Vaz, M. Andruh, *Inorg. Chem.* **2019**, *58*, 13090–13101.
[34] M. Briganti, F. Totti, M. Andruh, *Dalton Trans.* **2021**, *50*, 15961–15972.
[35] A. K. Bar, N. Gogoi, C. Pichon, V. M. L. D. P. Goli, M. Thlijeni, C. Duhayon, N. Suaud, N. Guihéry, A.-L. Barra, S. Ramasesha, J.-P. Sutter, *Chem. Eur. J.* **2017**, *23*, 4380–4396.
[36] C. Pichon, N. Suaud, V. Jubault, C. Duhayon, N. Guihéry, J.-P. Sutter, *Chem. Eur. J.* **2021**, *27*, 15484–15495.
[37] J.-N. Rebilly, G. Charron, E. Rivière, R. Guillot, A.-L. Barra, M. D. Serrano, J. Van Slageren, T. Mallah, *Chem. Eur. J.* **2008**, *14*, 1169–1177.
[38] J. A. McCleverty, M. D. Ward, *Accounts Chem. Res.* **1998**, *31*, 842–851.
[39] M.-C. Dul, X. Ottenwaelder, E. Pardo, R. Lescouëzec, Y. Journaux, L.-M. Chamoreau, R. Ruiz-García, J. Cano, M. Julve, F. Lloret, *Inorg. Chem.* **2009**, *48*, 5244–5249.
[40] I. Fernandez, R. Ruiz, J. Faus, M. Julve, F. Lloret, J. Cano, X. Ottenwaelder, Y. Journaux, M. C. Munoz, *Angew. Chem. Int. Ed.* **2001**, *40*, 3039–3042.
[41] P. Karafiloglou, *J. Chem. Educ.* **1989**, *66*, 816.
[42] H. O. Stumpf, Y. Pei, O. Kahn, J. Sletten, J. P. Renard, *J. Am. Chem. Soc.* **1993**, *115*, 6738–6745.
[43] D. Casanova, J. Cirera, M. Llunell, P. Alemany, D. Avnir, S. Alvarez, *J. Am. Chem. Soc.* **2004**, *126*, 1755–1763.
[44] Llunell, Miquel, Casanova, David, Cirera, Jordi, Alemany, Pere, Alvarez, Santiago, "Electronic Structure Group - Continuous Shape and Symmetry Measures. Applications in Structural Chemistry," can be found under http://www.ee.ub.edu/index.php?option=com_content&view=article&id=72&Itemid=469, **n.d.**
[45] S. Alvarez, M. Llunell, *Dalton Trans.* **2000**, *0*, 3288–3303.
[46] S. Alvarez, D. Avnir, M. Llunell, M. Pinsky, *New J. Chem.* **2002**, *26*, 996–1009.
[47] J. Cirera, P. Alemany, S. Alvarez, *Chem. Eur. J.* **2004**, *10*, 190–207.
[48] E. Pardo, R. Ruiz-García, F. Lloret, J. Faus, M. Julve, Y. Journaux, F. Delgado, C. Ruiz-Pérez, *Adv. Mater.* **2004**, *16*, 1597–1600.
[49] E. Pardo, R. Ruiz-García, F. Lloret, J. Faus, M. Julve, Y. Journaux, M. A. Novak, F. S. Delgado, C. Ruiz-Pérez, *Chem. Eur. J.* **2007**, *13*, 2054–2066.
[50] J. Tercero, C. Diaz, J. Ribas, M. Maestro, J. Mahía, H. Stoeckli-Evans, *Inorg. Chem.* **2003**, *42*, 3366–3373.
[51] J. Ribas, C. Diaz, R. Costa, Y. Journaux, C. Mathoniere, O. Kahn, A. Gleizes, *Inorg. Chem.* **1990**, *29*, 2042–2047.
[52] E.-Q. Gao, J.-K. Tang, D.-Z. Liao, Z.-H. Jiang, S.-P. Yan, G.-L. Wang, *Inorg. Chem.* **2001**, *40*, 3134–3140.
[53] Y. S. Yang, W. Zhang, F. X. Gao, S. P. Yan, *J. Coord. Chem.* **2008**, *61*, 571–578.
[54] J. Tercero, C. Diaz, M. S. El Fallah, J. Ribas, X. Solans, M. A. Maestro, J. Mahía, *Inorg. Chem.* **2001**, *40*, 3077–3083.
[55] E.-Q. Gao, Q.-H. Zhao, J.-K. Tang, D.-Z. Liao, Z.-H. Jiang, S.-P. Yan, *Dalton Trans.* **2001**, *0*, 1537–1540.
[56] T. Rüffer, B. Bräuer, A. K. Powell, I. Hewitt, G. Salvan, *Inorg. Chim. Acta* **2007**, *360*, 3475–3483.
[57] T. R. G. Simões, R. V. Mambrini, D. O. Reis, M. V. Marinho, M. A. Ribeiro, C. B. Pinheiro, J. Ferrando-Soria, M. Déniz, C. Ruiz-Pérez, D. Cangussu, H. O. Stumpf, F. Lloret, M. Julve, *Dalton Trans.* **2013**, *42*, 5778–5795.
[58] W. X. C. Oliveira, M. A. Ribeiro, C. B. Pinheiro, M. M. da Costa, A. P. S. Fontes, W. C. Nunes, D. Cangussu, M. Julve, H. O. Stumpf, C. L. M. Pereira, *Cryst. Growth Des.* **2015**, *15*, 1325–1335.
[59] J. Cirera, E. Ruiz, S. Alvarez, *Chem. Eur. J.* **2006**, *12*, 3162–3167.
[60] E. Pardo, R. Ruiz-García, F. Lloret, M. Julve, J. Cano, J. Pasán, C. Ruiz-Pérez, Y. Filali, L.-M. Chamoreau, Y. Journaux, *Inorg. Chem.* **2007**, *46*, 4504–4514.
[61] X. Ottenwaelder, J. Cano, Y. Journaux, E. Rivière, C. Brennan, M. Nierlich, R. Ruiz-García, *Angew. Chem., Int. Ed.* **2004**, *43*, 850–852.
[62] M.-C. Dul, J. Ferrando-Soria, E. Pardo, R. Lescouëzec, Y. Journaux, R. Ruiz-Garcia, J. Cano, M. Julve, F. Lloret, O. Fabelo, J. Pasan, Catalina. Ruiz-Perez, *Inorg. Chem.* **2010**, *49*, 11264–11266.
[63] Q.-L. Wang, L.-N. Zhu, D.-Z. Liao, S.-P. Yan, Z.-H. Jiang, P. Cheng, G.-M. Yang, *J. Mol. Struct.* **2005**, *754*, 10–15.
[64] B. Yao, F. Lu, D.-X. Gan, S. Liu, Y.-Q. Zhang, Y.-F. Deng, Y.-Z. Zhang, *Inorg. Chem.* **2020**, *59*, 10389–10394.
[65] X. Ottenwaelder, J. Cano, Y. Journaux, E. Rivière, C. Brennan, M. Nierlich, R. Ruiz-García, *Angew Chem Int Edit* **2004**, *43*, 850–852.
[66] M.-C. Dul, J. Ferrando-Soria, E. Pardo, R. Lescouëzec, Y. Journaux, R. Ruiz-García, J. Cano, M. Julve, F. Lloret, O. Fabelo, J. Pasán, C. Ruiz-Pérez, *Inorg. Chem.* **2010**, *49*, 11264–11266.
[67] M. Julve, M. Verdaguer, A. Gleizes, M. Philoche-Levisalles, O. Kahn, *Inorg. Chem.* **1984**, *23*, 3808–3818.
[68] Y. Journaux, J. Sletten, O. Kahn, *Inorg. Chem.* **1985**, *24*, 4063–4069.
[69] X. Feng, J. Liu, T. D. Harris, S. Hill, J. R. Long, *J. Am. Chem. Soc.* **2012**, *134*, 7521–7529.
[70] J. Vallejo, I. Castro, R. Ruiz-García, J. Cano, M. Julve, F. Lloret, G. De Munno, W. Wernsdorfer, E. Pardo, *J. Am. Chem. Soc.* **2012**, *134*, 15704–15707.
[71] E. Ruiz, J. Cano, S. Alvarez, P. Alemany, *J. Comput. Chem.* **1999**, *20*, 1391–1400.
[72] S. K. Singh, T. Gupta, P. Badkur, G. Rajaraman, *Chem. Eur. J.* **2014**, *20*, 10305–10313.
[73] S. Vaidya, A. Upadhyay, S. K. Singh, T. Gupta, S. Tewary, S. K. Langley, J. P. S. Walsh, K. S. Murray, G. Rajaraman, M. Shanmugam, *Chem. Commun.* **2015**, *51*, 3739–3742.
[74] M. Atanasov, D. Aravena, E. Suturina, E. Bill, D. Maganas, F. Neese, *Coord. Chem. Rev.* **2015**, *289–290*, 177–214.

[75] G. A. Craig, A. Sarkar, C. H. Woodall, M. A. Hay, K. E. R. Marriott, K. V. Kamenev, S. A. Moggach, E. K. Brechin, S. Parsons, G. Rajaraman, M. Murrie, *Chem. Sci.* **2018**, *9*, 1551–1559.
[76] A. Sarkar, R. Jose, H. Ghosh, G. Rajaraman, *Inorg. Chem.* **2021**, *60*, 9680–9687.
[77] S. Stoll, A. Schweiger, *J. Magn. Reson.* **2006**, *178*, 42–55.
[78] E. Pedersen, H. Toftlund, *Inorg. Chem.* **1974**, *13*, 1603–1612.
[79] O. Waldmann, *Inorg. Chem.* **2007**, *46*, 10035–10037.
[80] A. K. Bar, C. Pichon, J.-P. Sutter, *Coord. Chem. Rev.* **2016**, *308, Part 2*, 346–380.
[81] T. Jurca, A. Farghal, P.-H. Lin, I. Korobkov, M. Murugesu, D. S. Richeson, *J. Am. Chem. Soc.* **2011**, *133*, 15814–15817.
[82] O. Kahn, *Molecular Magnetism*, VCH Publishers Inc, New York, **1993**.
[83] P. W. Anderson, in *Magnetism*, Academic Press, **1963**.
[84] E. Liviotti, S. Carretta, G. Amoretti, *J. Chem. Phys.* **2002**, *117*, 3361–3368.
[85] S. Hill, S. Datta, J. Liu, R. Inglis, C. J. Milios, P. L. Feng, J. J. Henderson, E. del Barco, E. K. Brechin, D. N. Hendrickson, *Dalton Trans.* **2010**, *39*, 4693–4707.
[86] J. E. Richman, T. J. Atkins, *J. Am. Chem. Soc.* **1974**, *96*, 2268–2270.
[87] G. Haselhorst, S. Stoetzel, A. Strassburger, W. Walz, K. Wieghardt, B. Nuber, *J. Chem. Soc., Dalton Trans.* **1993**, 83–90.
[88] P. Langer, R. Schroeder, *Eur. J. Org. Chem.* **2004**, *2004*, 1025–1032.
[89] *Bruker AXS Inc* **1998**.
[90] R. H. Blessing, *Acta Crystallogr. Sect. A* **1995**, *51*, 33–38.
[91] G. M. Sheldrick, *Acta Crystallogr. Sect. A* **2008**, *64*, 112–122.
[92] N. F. Chilton, R. P. Anderson, L. D. Turner, A. Soncini, K. S. Murray, *J. Comput. Chem.* **2013**, *34*, 1164–1175.
[93] Gaussian 09, Revision A.02, M. J. Frisch, G. W. Trucks, H. B. Schlegel, G. E. Scuseria, M. A. Robb, J. R. Cheeseman, G. Scalmani, V. Barone, B. Mennucci, G. A. Petersson, H. Nakatsuji, M. Caricato, X. Li, H. P. Hratchian, A. F. Izmaylov, J. Bloino, G. Zheng, J. L. Sonnenberg, M. Hada, M. Ehara, K. Toyota, R. Fukuda, J. Hasegawa, M. Ishida, T. Nakajima, Y. Honda, O. Kitao, H. Nakai, T. Vreven, J. A. Montgomery, Jr., J. E. Peralta, F. Ogliaro, M. Bearpark, J. J. Heyd, E. Brothers, K. N. Kudin, V. N. Staroverov, R. Kobayashi, J. Normand, K. Raghavachari, A. Rendell, J. C. Burant, S. S. Iyengar, J. Tomasi, M. Cossi, N. Rega, J. M. Millam, M. Klene, J. E. Knox, J. B. Cross, V. Bakken, C. Adamo, J. Jaramillo, R. Gomperts, R. E. Stratmann, O. Yazyev, A. J. Austin, R. Cammi, C. Pomelli, J. W. Ochterski, R. L. Martin, K. Morokuma, V. G. Zakrzewski, G. A. Voth, P. Salvador, J. J. Dannenberg, S. Dapprich, A. D. Daniels, Ö. Farkas, J. B. Foresman, J. V. Ortiz, J. Cioslowski, D. J. Fox, **2016**.
[94] A. Bencini, F. Totti, *J. Chem. Theory Comput.* **2009**, *5*, 144–154.
[95] R. N. Zare, *Angular Momentum: Understanding Spatial Aspects in Chemistry and Physics*, Wiley, New York, **1988**.
[96] Deposition numbers 2216053 (for **1**), 226054 (for **2**), 226055 (for **3**), 226056 (for **4**), 226057 (for **5**).contain the supplementary crystallographic data for this paper. These data are provided free of charge by the joint Cambridge Crystallographic Data Centre and Fachinformationszentrum Karlsruhe Access Structures service

## I) Crystal packing of compounds **1**-**5**

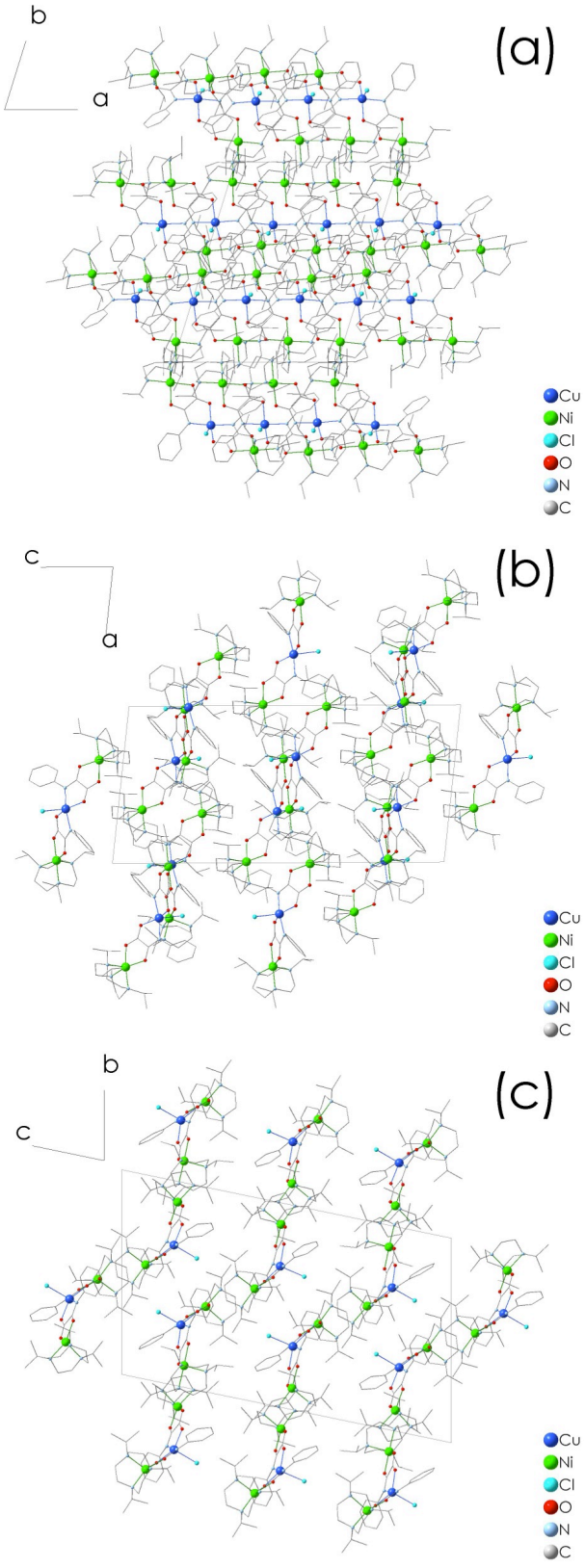


Figure S1. View of the crystal packing in **1**: (a) ab plane, (b) ac plane and (c) bc plane. H atoms and water molecules have been omitted for clarity.

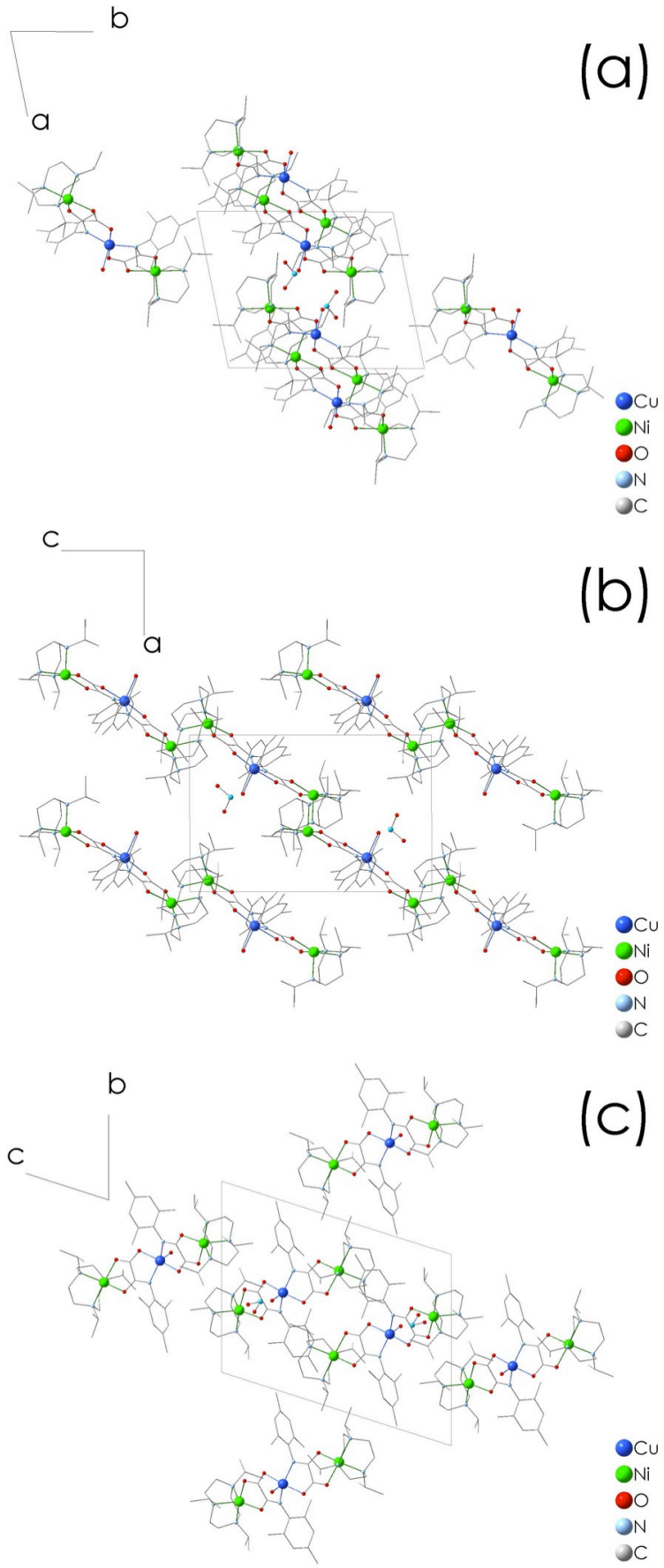


Figure S2. View of the crystal packing in **2**: (a) ab plane, (b) ac plane and (c) bc plane. H atoms and water molecules have been omitted for clarity.

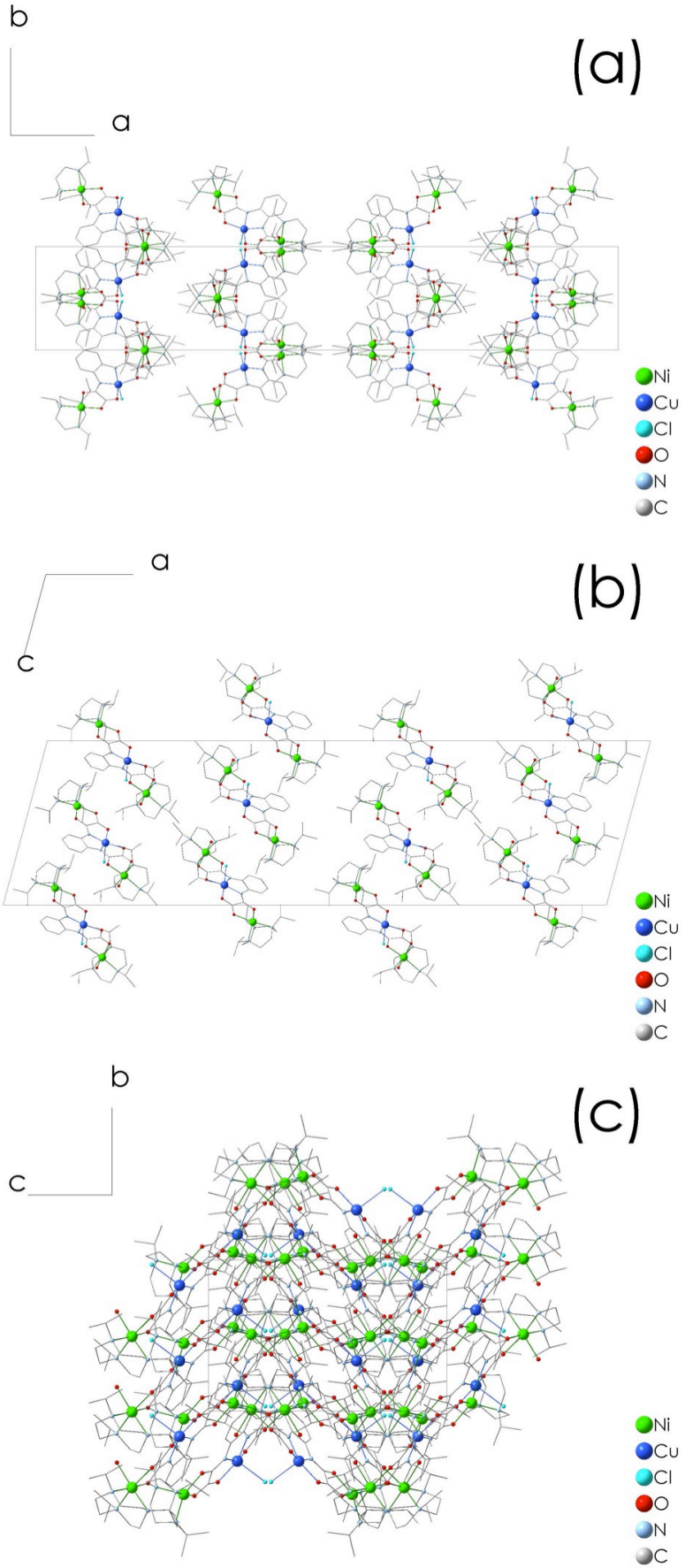


Figure S3. View of the crystal packing in **3**: (a) ab plane, (b) ac plane and (c) bc plane. H atoms and water molecules have been omitted for clarity.

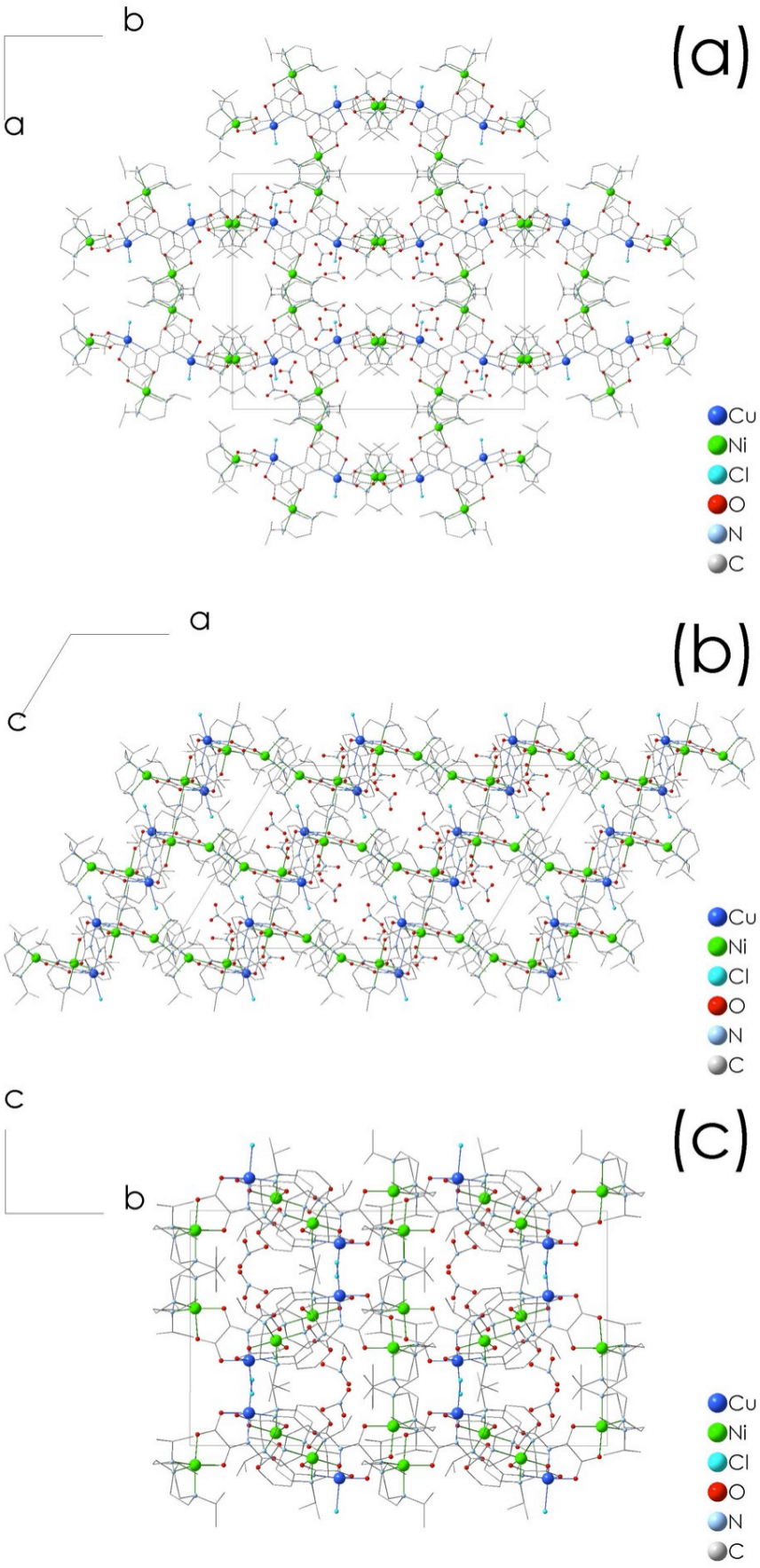


Figure S4. View of the crystal packing in **4**: (a) ab plane, (b) ac plane and (c) bc plane. H atoms and water molecules have been omitted for clarity.

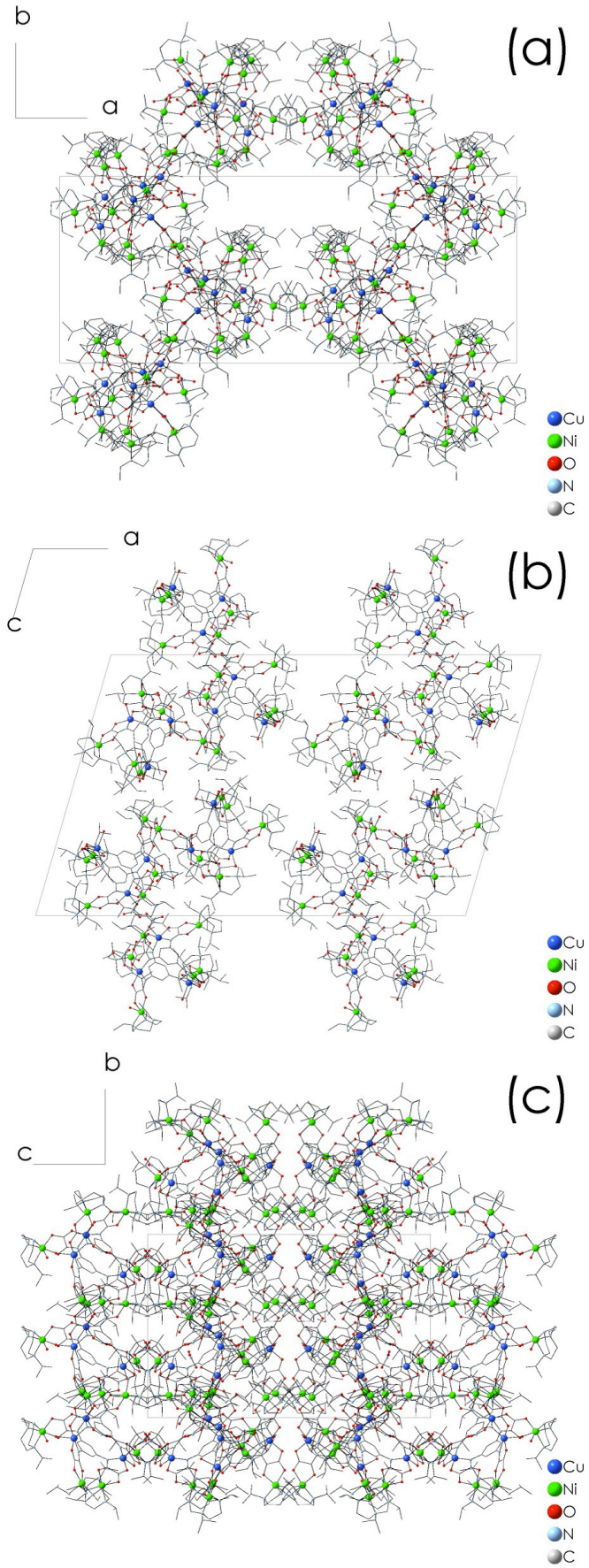


Figure S5. View of the crystal packing in **5**: (a) ab plane, (b) ac plane and (c) bc plane. H atoms and water molecules have been omitted for clarity.

## II) Magnetization versus field and isofield versus H/T curves for compound **1-3**

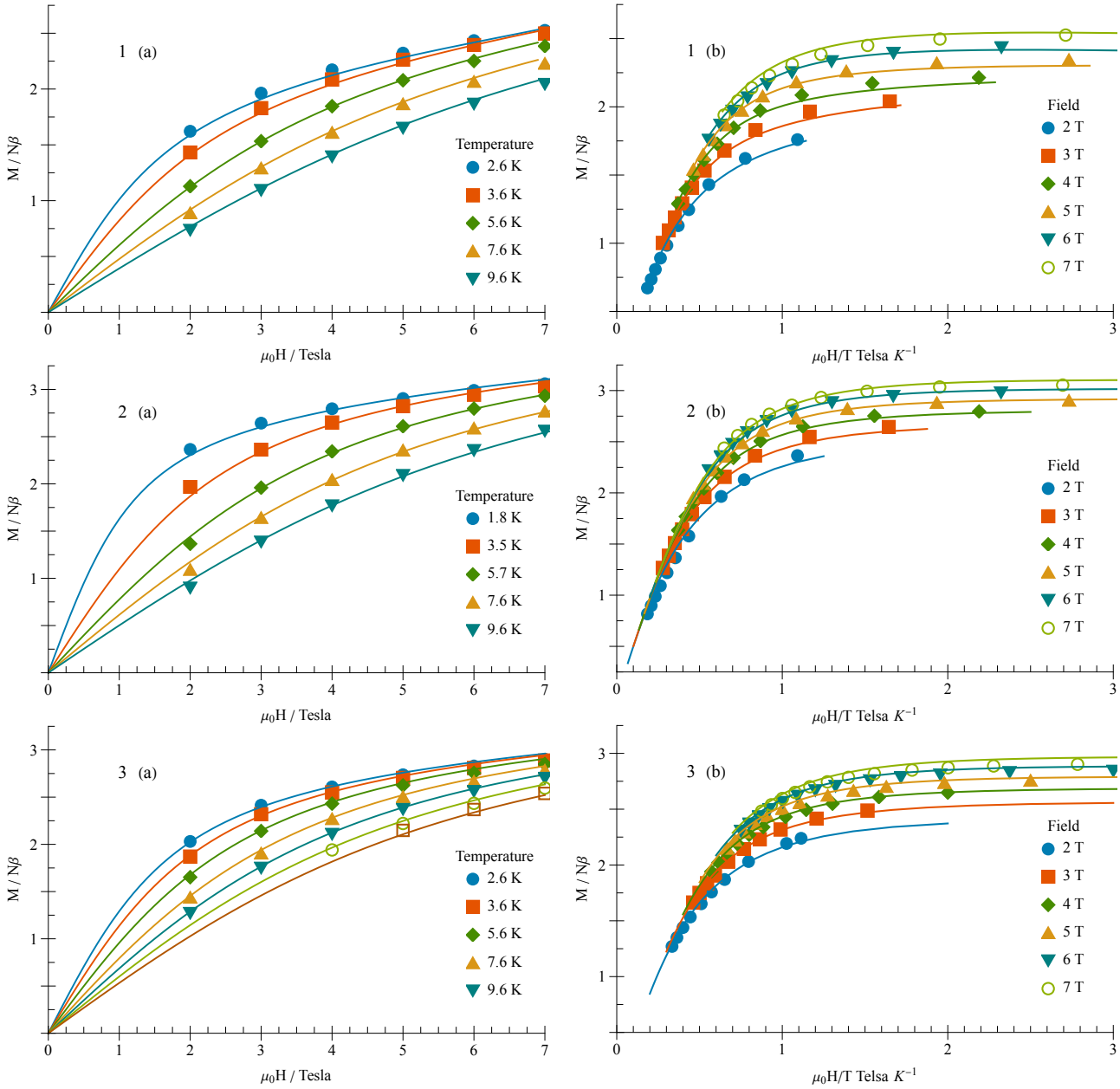


Figure S6 Magnetization *vs* μ0H (a) and isofield curves *vs* μ0H/T (b) for **1** to **3,** the solid lines are the best-fit curves.

## III) Theoretical calculations

Table S1 : Calculated principal values and orientations of hypothetic monometallic complexes $[Cu(pma)_2]^{2-}$, $[Cu(Me_3pma)_2]^{2-}$, $[Cu(opba)]^{2-}$ and [Ni(ⁱPrtacn)ox] with the actual geometry of the Cu and Ni ions in the **1**-**3** . For Ni ions the oxamate bridges were replaced by oxalate dianion. The Euler's angles are calculated with respect to the $g_{Cu}$ tensor principal axis. The local $D$ and $E$ values for Ni(II) ions are calculated according to $D=3D_{zz}/2$ and $E=(D_{xx}-D_{yy})/2$

| | | Principal values in $cm^{-1}$ | | | Euler's angles | | |
|---|---|---|---|---|---|---|---|
| | | x | y | z | α | β | γ |
| **1** pma | $g_{Cu}$ | 2.040 | 2.194 | 2.424 | 0° | 0° | 0° |
| | $g_{Ni1}$ | 2.327 | 2.280 | 2.160 | -14.2° | 84.8° | 119.9° |
| | $g_{Ni2}$ | 2.324 | 2.262 | 2.160 | -19.3° | -71.7° | 63.0° |
| | $D_{Ni1}$ | -2.723 | -9.658 | 12.38 | -15.2° | 84.0° | 63.0° |
| | | $D$=18.6 $E/D$=0.187 | | | | | |
| | $D_{Ni2}$ | -1.500 | -9.959 | 11.459 | -18.6° | -71.6° | -28.6° |
| | | $D$=17.2 $E/D$=0.246 | | | | | |
| **2** $Me_3pma$ | $g_{Cu}$ | 2.071 | 2.117 | 2.419 | 0° | 0° | 0° |
| | $g_{Ni1}$ | 2.319 | 2.265 | 2.156 | 116.4° | -42.2° | 134.2° |
| | $g_{Ni2}$ | 2.379 | 2.263 | 2.156 | 6.48° | 124.2° | -128.3° |
| | $D_{Ni1}$ | -2.079 | -9.223 | 11.30 | 115.6° | -41.1° | 46.7° |
| | | $D$=16.9 $E/D$=0.21 | | | | | |
| | $D_{Ni2}$ | -0.011 | -14.33 | 14.34 | 97.9° | 6.99° | -64.4° |
| | | $D$=21.5 $E/D$=0.332 | | | | | |
| **3** opba | $g_{Cu}$ | 2.091 | 2.103 | 2.447 | 0° | 0° | 0° |
| | $g_{Ni1}$ | 2.200 | 2.223 | 2.248 | 158.3° | 169.0° | -135.3° |
| | $g_{Ni2}$ | 2.336 | 2.277 | 2.163 | -114.4° | -61.5° | -46.0° |
| | $D_{Ni1}$ | 0.305 | 3.031 | -3.337 | 155.5° | 165.4 | -45.7° |
| | | $D$=-5.0 $E/D$=0.272 | | | | | |
| | $D_{Ni2}$ | -1.930 | -10.21 | 12.14 | -114.5 | -60.3° | -134.0° |
| | | $D$=18.2 $E/D$=.227 | | | | | |

Table S2: The overlap integral values between the SOMOs of Cu(II) and Ni(II) ions in **1**.

| Cu→<br>Ni↓ | 260 |
|---|---|
| 244 ($Ni_1$) | -0.236 |
| 245 ($Ni_1$) | -0.107 |
| 246 ($Ni_2$) | 0.417 |
| 247 (Ni2) | -0.196 |

Table S3: The overlap integral values between the SOMOs of Cu(II) and Ni(II) ions in **2**.

| Cu→<br>Ni↓ | 291 |
|---|---|
| 272 ($Ni_1$) | 0.038 |
| 273 ($Ni_1$) | -0.173 |
| 275 ($Ni_2$) | 0.040 |
| 277 (Ni2) | -0.187 |

Table S4: The overlap integral values between the SOMOs of Cu(II) and Ni(II) ions in **3**.

| Cu→<br>Ni↓ | 243 |
|---|---|
| 238 ($Ni_1$) | 0.450 |
| 239 ($Ni_1$) | -0.365 |
| 234 ($Ni_2$) | 0.054 |
| 235 (Ni2) | -0.059 |

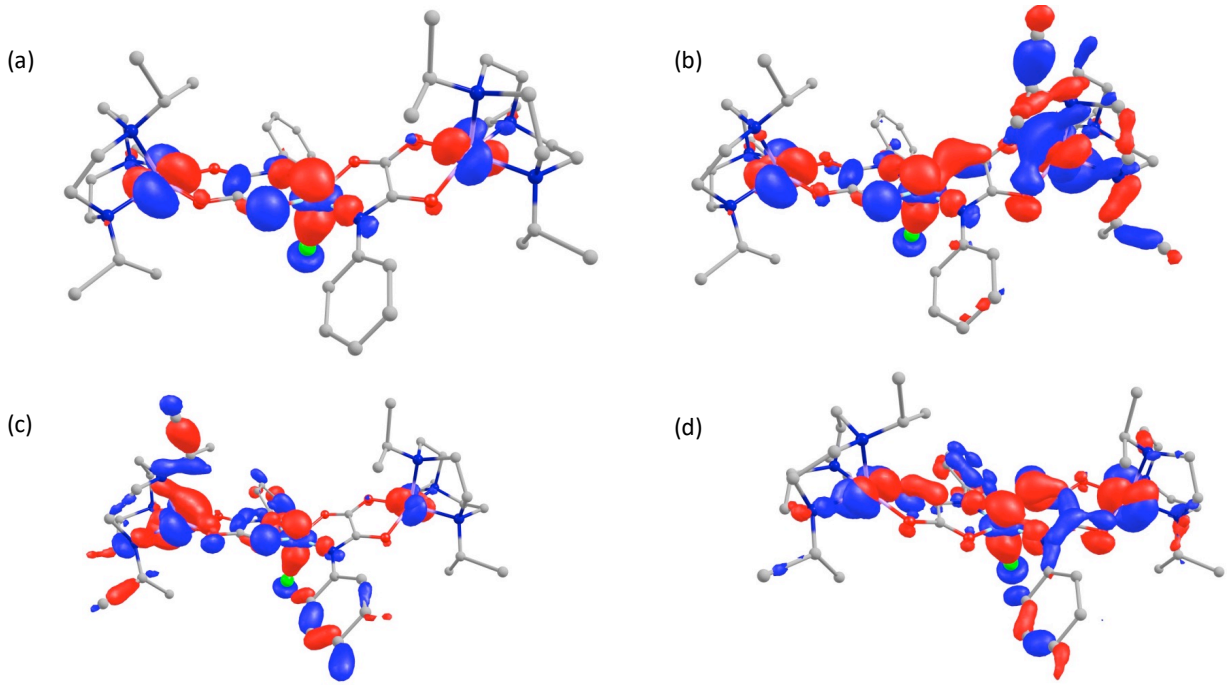


Figure S7: The overlap between (a) 244 and 260 (b) 245 and 260 (c) 246 and 260 (d) 247 and 260 SOMOs of **1**. Colour code: Cu-sky blue, Ni-violet, Cl-green, O-red, N-blue and C-grey. Hydrogens are omitted for clarity.

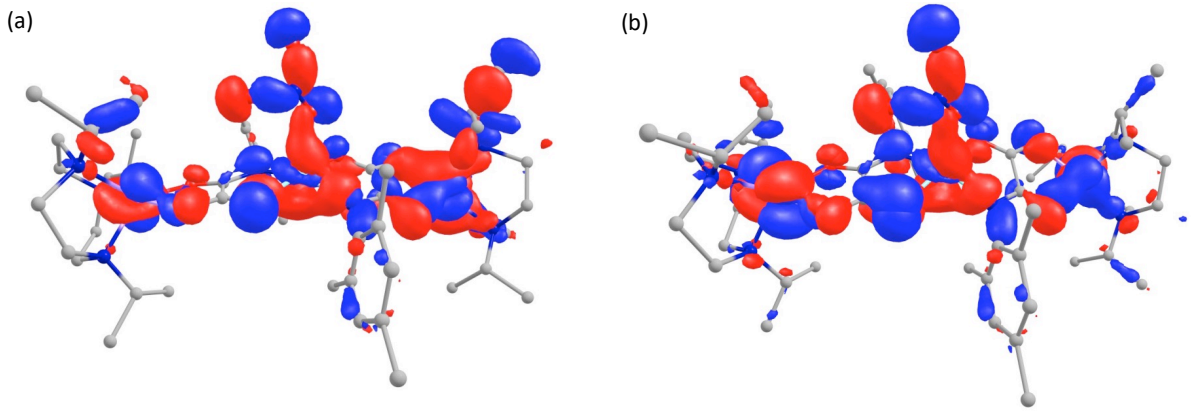


Figure S8: The overlap between (a) 273 and 291 (b) 277 and 291 SOMOs of **2**. Colour code: Cu-sky blue, Ni-violet, Cl-green, O-red, N-blue and C-grey. Hydrogens are omitted for clarity.

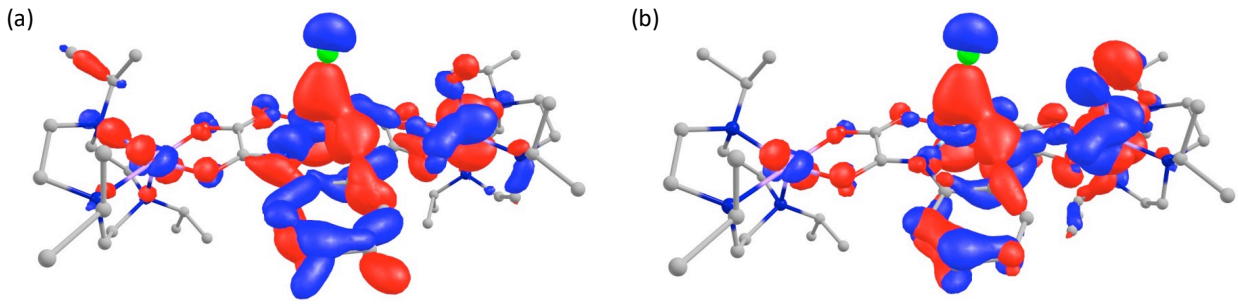


Figure S9: The overlap between (a) 238 and 243 (b) 239 and 243 SOMOs of **3**. Colour code: Cu-sky blue, Ni-violet, Cl-green, O-red, N-blue and C-grey. Hydrogens are omitted for clarity.

Table S5: The computed *g* factors of Cu(II) centre in complexes **1**-**3**.

| Complex | $g_x$ | $g_y$ | $g_z$ |
|---|---|---|---|
| **1** | 2.040 | 2.194 | 2.424 |
| **2** | 2.071 | 2.117 | 2.419 |
| **3** | 2.091 | 2.103 | 2.448 |

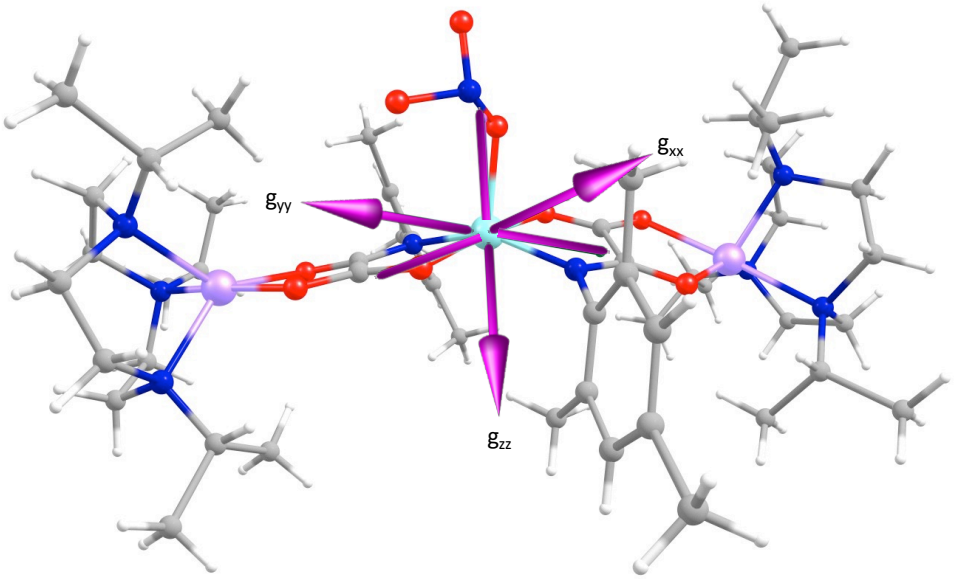


Figure S10: The *g*-anisotropy axis of the Cu(II) ion in **1**. Colour code: Cu-sky blue, Ni-violet, O-red, N-blue, Cl-green, C-grey and H-white.

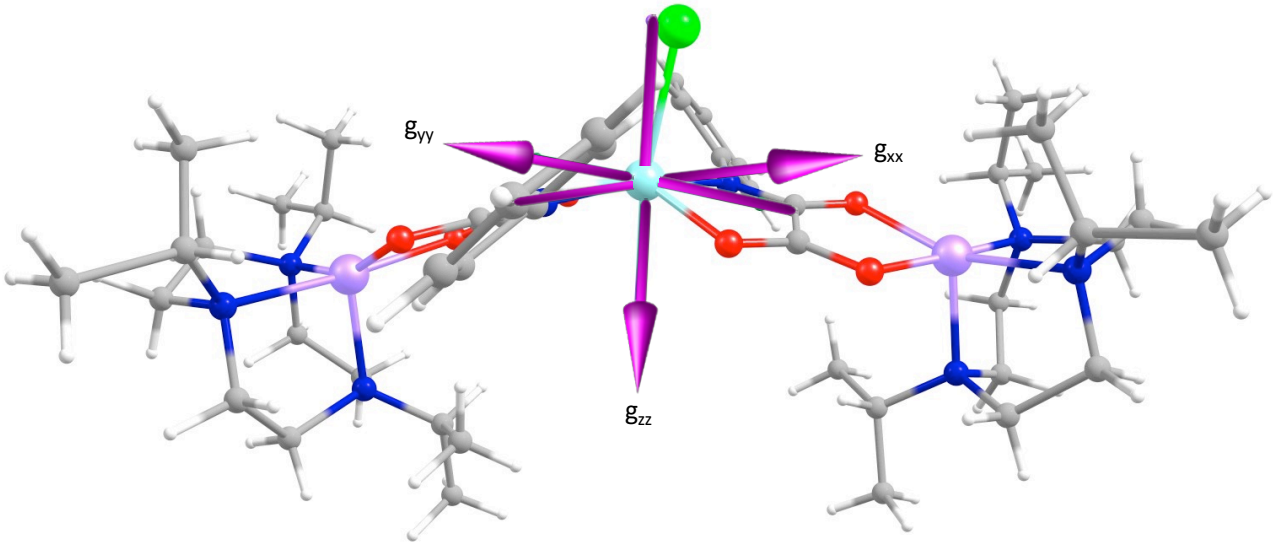


Figure S11: The *g*-anisotropy axis of the Cu(II) ion in **2**. Colour code: Cu-sky blue, Ni-violet, O-red, N-blue, Cl-green, C-grey and H-white.

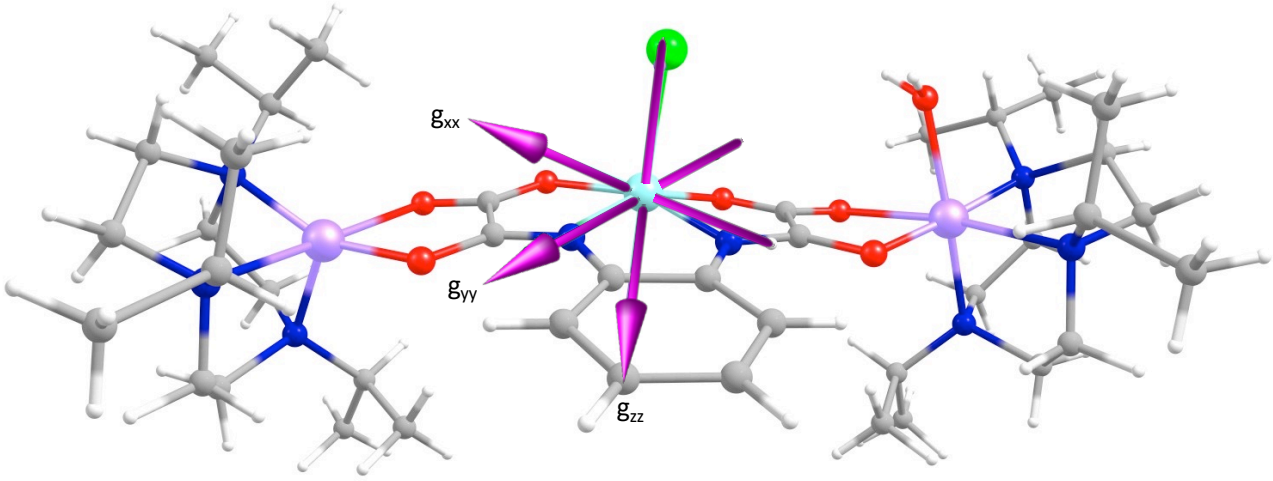


Figure S12: The *g*-anisotropy axis of the Cu(II) ion in **3**. Colour code: Cu-sky blue, Ni-violet, O-red, N-blue, Cl-green, C-grey and H-white.

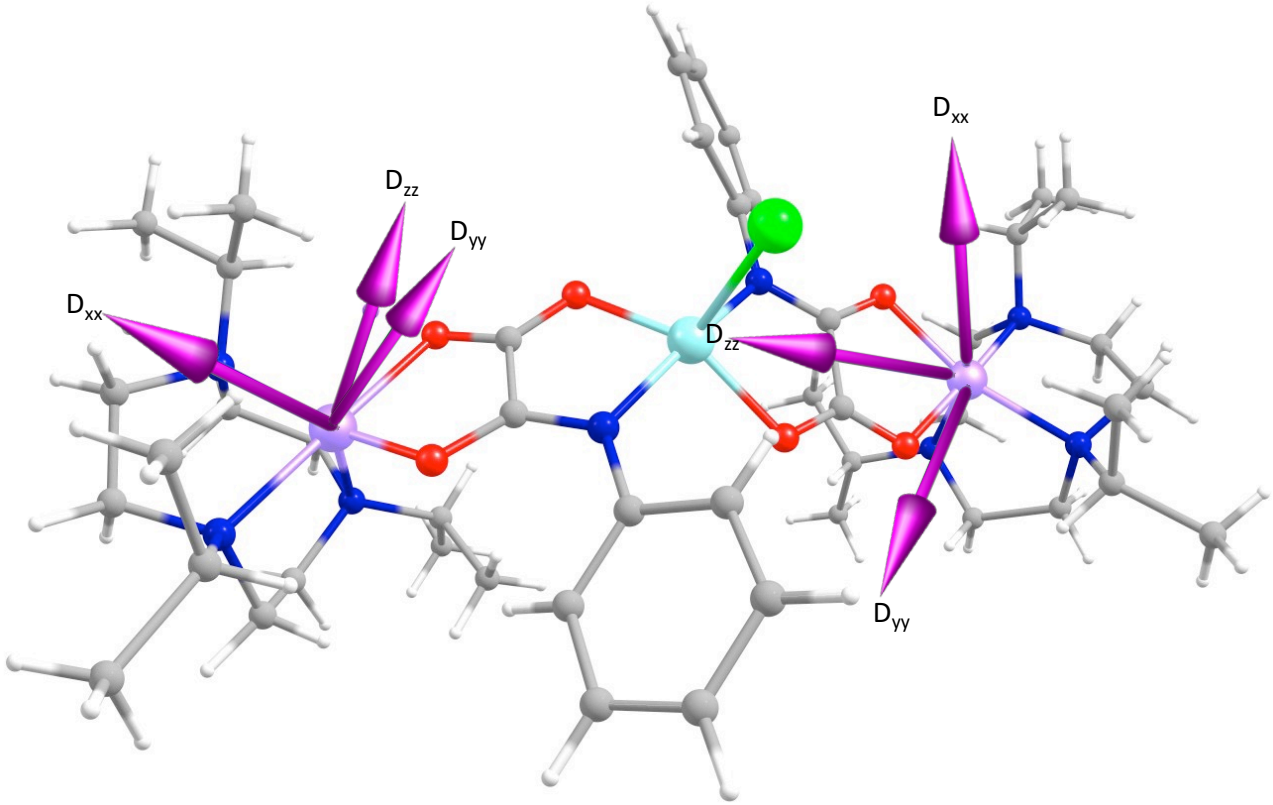


Figure S13: The *D*-anisotropy axis of the Ni(II) ions in **1**. Colour code: Cu-sky blue, Ni-violet, O-red, N-blue, Cl-green, C-grey and H-white.

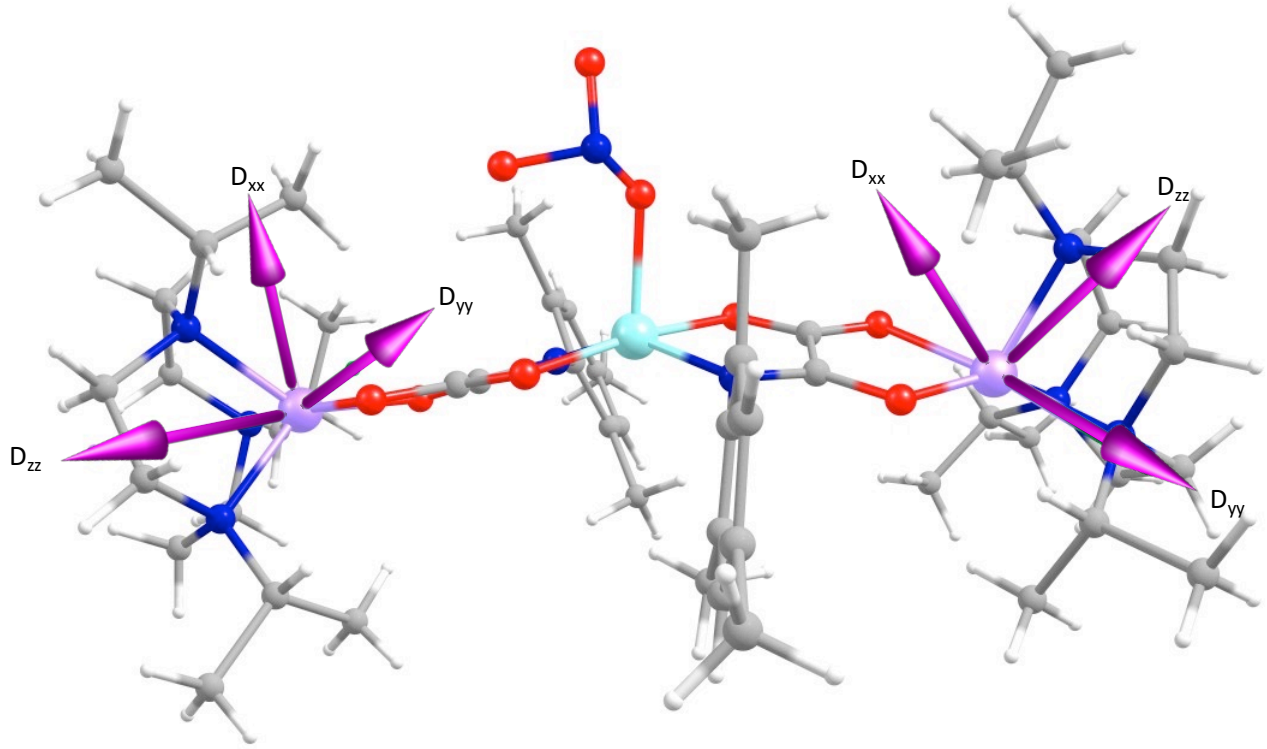


Figure S14: The *D*-anisotropy axis of the Ni(II) ions in **2**. Colour code: Cu-sky blue, Ni-violet, O-red, N-blue, Cl-green, C-grey and H-white.

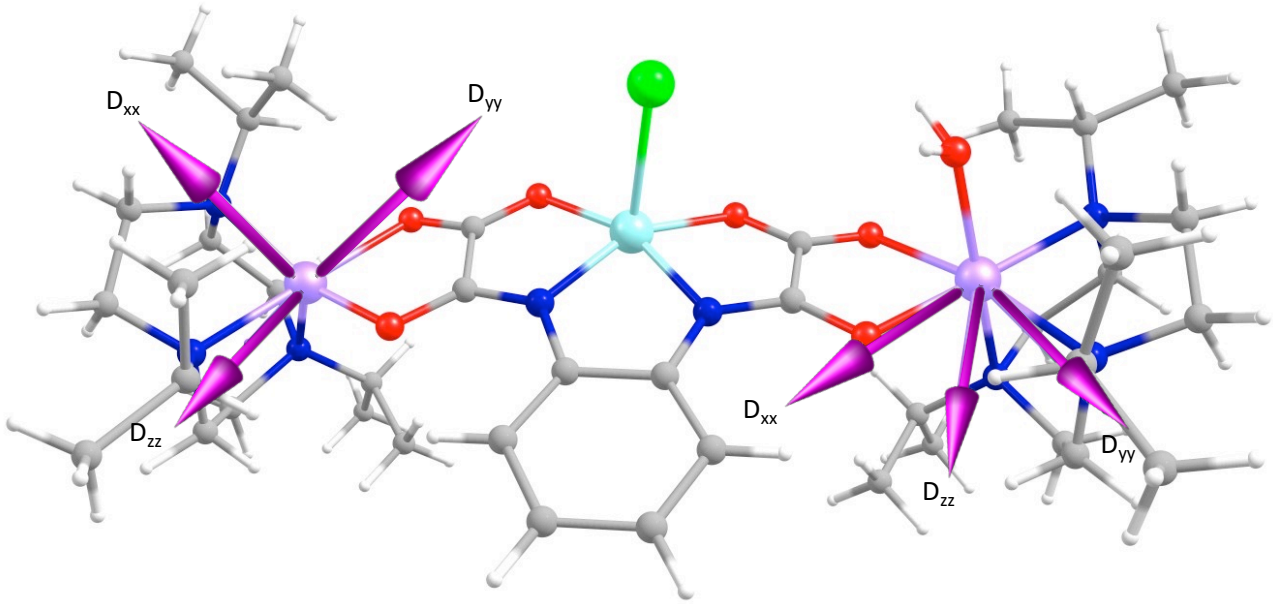


Figure S15: The *D*-anisotropy axis of the Ni(II) ions in **3**. Colour code: Cu-sky blue, Ni-violet, O-red, N-blue, Cl-green, C-grey and H-white.

Table S6: The dominant electronic configurations that contribute to the ZFS parameters of the Ni1 centre (Ni2 is similar to Ni1) in complex **1**.

| Energy ($cm^{-1}$) | Major electronic configuration | Contribution to *D* ($cm^{-1}$) | Contribution to *E* ($cm^{-1}$) |
|---|---|---|---|
| 0.0 | $d_{xz}^2d_{yz}^2d_{xy}^2d_{z^2}^1d_{x^2-y^2}^1$ | -0.00 | 0.00 |
| 6673.4 | $d_{xz}^2d_{yz}^1d_{xy}^2d_{z^2}^2d_{x^2-y^2}^1$ | 28.8 | 26.1 |
| 7972.7 | $d_{xz}^1d_{yz}^2d_{xy}^2d_{z^2}^1d_{x^2-y^2}^2$ | 20.8 | -19.3 |
| 12679.5 | $d_{xz}^2d_{yz}^2d_{xy}^1d_{z^2}^1d_{x^2-y^2}^2$ | -25.7 | -1.6 |

Table S7: The dominant electronic configurations that contribute to the ZFS parameters of the Ni1 centre (Ni2 is similar to Ni1) in complex **2**.

| Energy ($cm^{-1}$) | Major electronic configuration | Contribution to *D* ($cm^{-1}$) | Contribution to *E* ($cm^{-1}$) |
|---|---|---|---|
| 0.0 | $d_{xz}^2d_{yz}^2d_{xy}^2d_{z^2}^1d_{x^2-y^2}^1$ | -0.0 | 0.00 |
| 6998.4 | $d_{xz}^1d_{yz}^2d_{xy}^2d_{z^2}^2d_{x^2-y^2}^1$ | 27.5 | 26.0 |
| 8785.4 | $d_{xz}^2d_{yz}^1d_{xy}^2d_{z^2}^1d_{x^2-y^2}^2$ | 17.3 | -17.9 |
| 12869.8 | $d_{xz}^2d_{yz}^2d_{xy}^1d_{z^2}^1d_{x^2-y^2}^2$ | -23.3 | -1.9 |

Table S8: The dominant electronic configurations that contribute to the ZFS parameters of the Ni1 centre in complex **3**.

| Energy ($cm^{-1}$) | Major electronic configuration | Contribution to *D* ($cm^{-1}$) | Contribution to *E* ($cm^{-1}$) |
|---|---|---|---|
| 0.0 | $d_{xy}^2d_{yz}^2d_{xz}^2d_{x^2-y^2}^1d_{z^2}^1$ | -0.00 | 0.00 |
| 9799.6 | $d_{xy}^1d_{yz}^2d_{xz}^2d_{x^2-y^2}^2d_{z^2}^1$ | -31.1 | -2.1 |
| 10076.0 | $d_{xy}^2d_{yz}^1d_{xz}^2d_{x^2-y^2}^1d_{z^2}^2$ | 5.9 | -3.8 |
| 11018.1 | $d_{xy}^2d_{yz}^2d_{xz}^1d_{x^2-y^2}^1d_{z^2}^2$ | 19.1 | 4.3 |

Table S9: The dominant electronic configurations that contribute to the ZFS parameters of the Ni2 centre in complex **3**.

| Energy ($cm^{-1}$) | Major electronic configuration | Contribution to *D* ($cm^{-1}$) | Contribution to *E* ($cm^{-1}$) |
|---|---|---|---|
| 0.0 | $d_{xz}^2d_{yz}^2d_{xy}^2d_{z^2}^1d_{x^2-y^2}^1$ | -0.00 | 0.00 |
| 6580.8 | $d_{xz}^1d_{yz}^2d_{xy}^2d_{z^2}^2d_{x^2-y^2}^1$ | 29.2 | 28.1 |
| 8245.0 | $d_{xz}^2d_{yz}^1d_{xy}^2d_{z^2}^1d_{x^2-y^2}^2$ | 19.3 | -19.9 |
| 12549.1 | $d_{xz}^2d_{yz}^2d_{xy}^1d_{z^2}^1d_{x^2-y^2}^2$ | -25.2 | -1.6 |

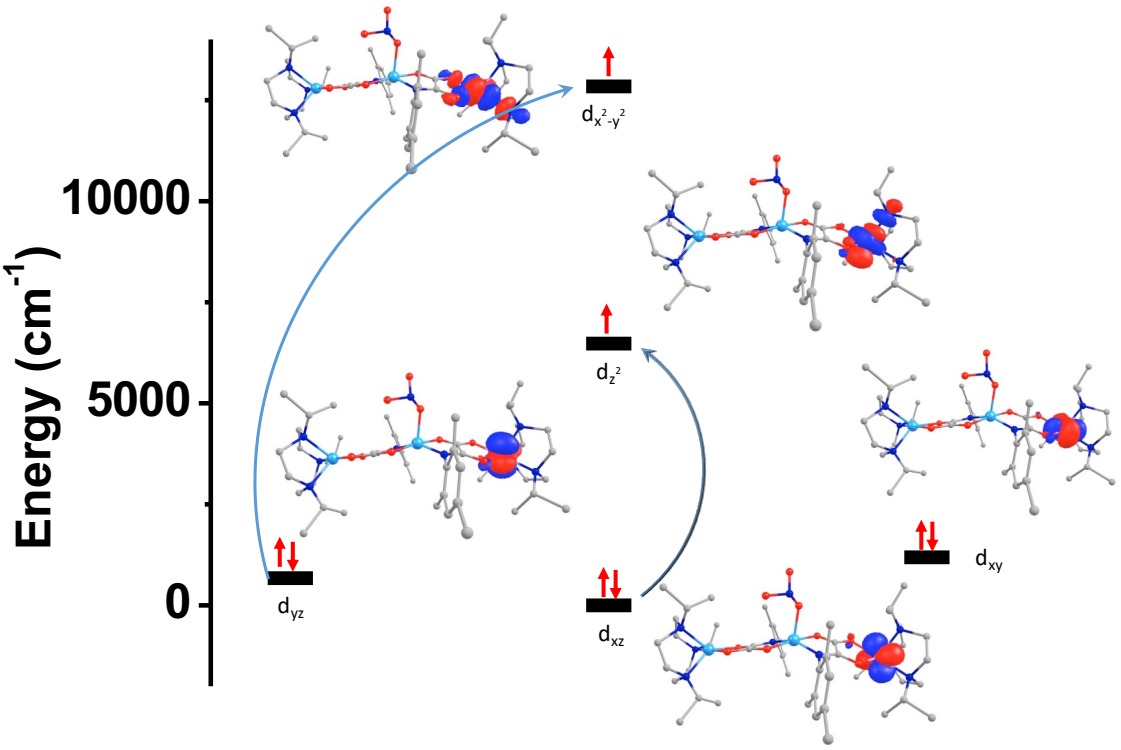


Figure S16: NEVPT2-AILFT computed d orbital energies of Ni1 centre (Ni2 is similar to Ni1) of **2** and the most important electronic transitions, which contribute to the total *D* value. Colour code: Ni-blue violet, Zn-sky blue, Cl-green, O-red, N-blue and C-grey. Hydrogens are omitted for clarity.

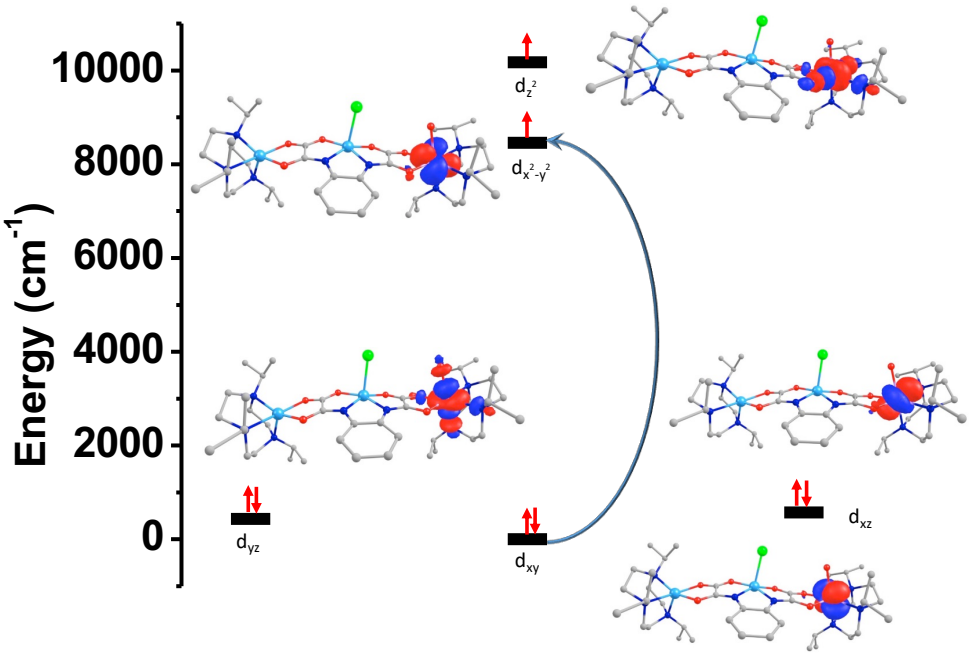


Figure S17: NEVPT2-AILFT computed d orbital energies of Ni1 centre of **3** along with the most important electronic transitions contributing to the total *D* value. Colour code: Ni-blue violet, Zn-sky blue, Cl-green, O-red, N-blue and C-grey. Hydrogens are omitted for clarity.

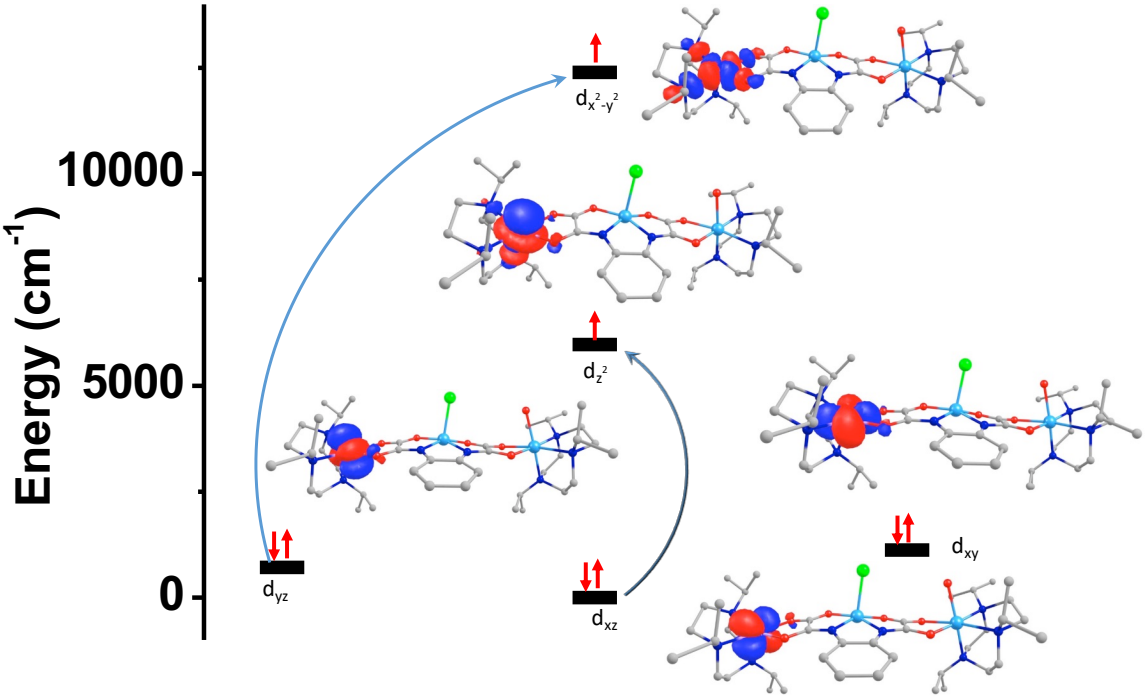


Figure S18: NEVPT2-AILFT computed d orbital energies of Ni2 centre of **3** along with the most important electronic transitions contributing to the total *D* value. Colour code: Ni-blue violet, Zn-sky blue, Cl-green, O-red, N-blue and C-grey. Hydrogens are omitted for clarity.

## IV) EPR spectra

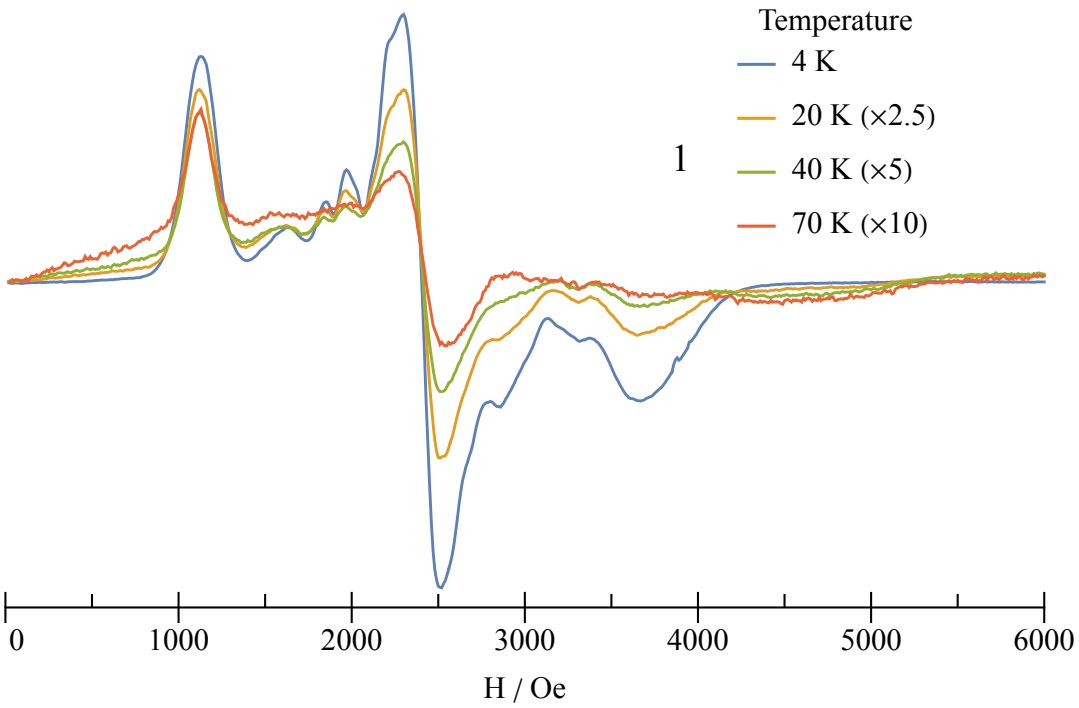


Figure S19. Evolution with the temperature of the X band EPR spectrum of **1**. The figures in brackets are the multiplicative factor applied to the spectra for better visibility

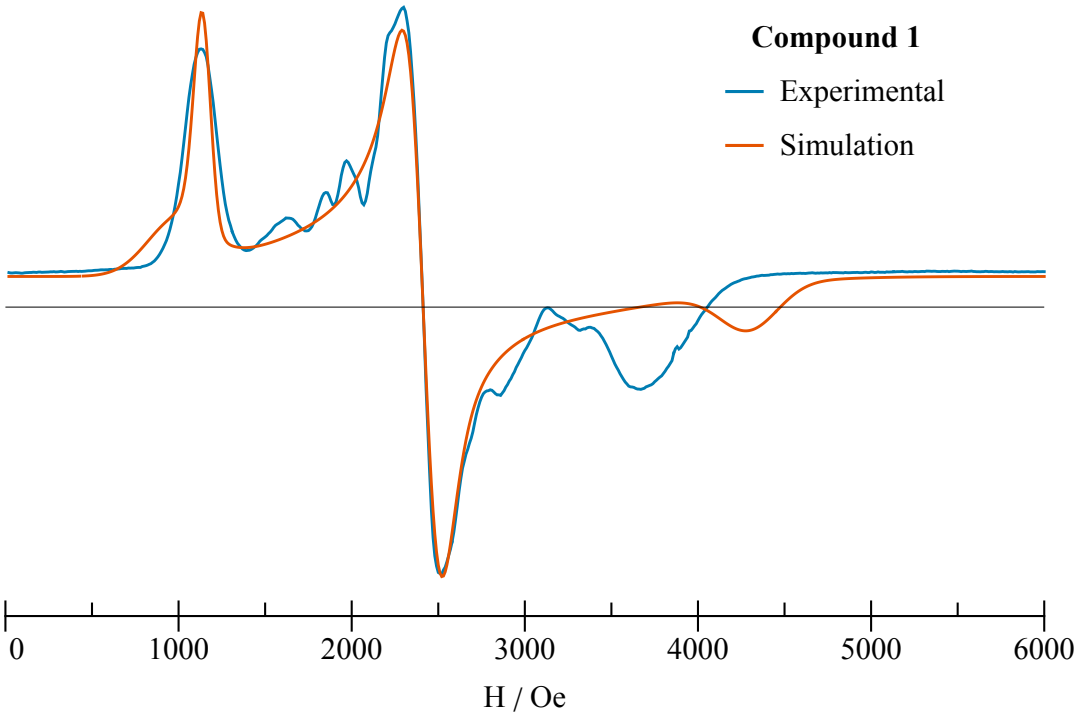


Figure S20. Experimental X band EPR spectrum of **1** at 4K and *S*=3/2 simulation obtained by least squares fitting using Easyspin Matlab toolbox (*D*= 4.6 $cm^{-1}$ fixed, best parameters $g_x$=2.75, $g_y$=2.12, $g_z$=.4823, *E*/*D*=1/3 $\Gamma_x$=747 G $\Gamma_y$=847 G, $\Gamma_z$=3827 G)

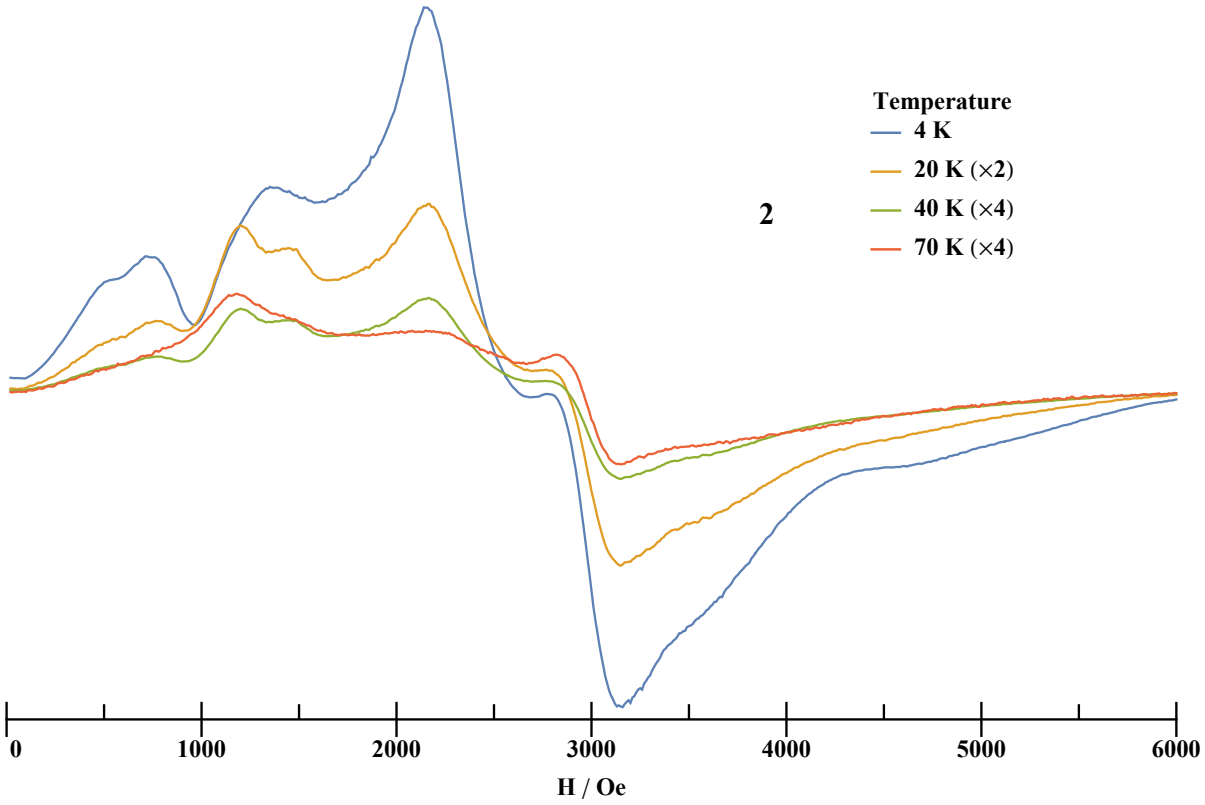


Figure S21. Evolution with the temperature of the X band EPR spectrum of **2**. The figures in brackets are the multiplicative factor applied to the spectra for better visibility

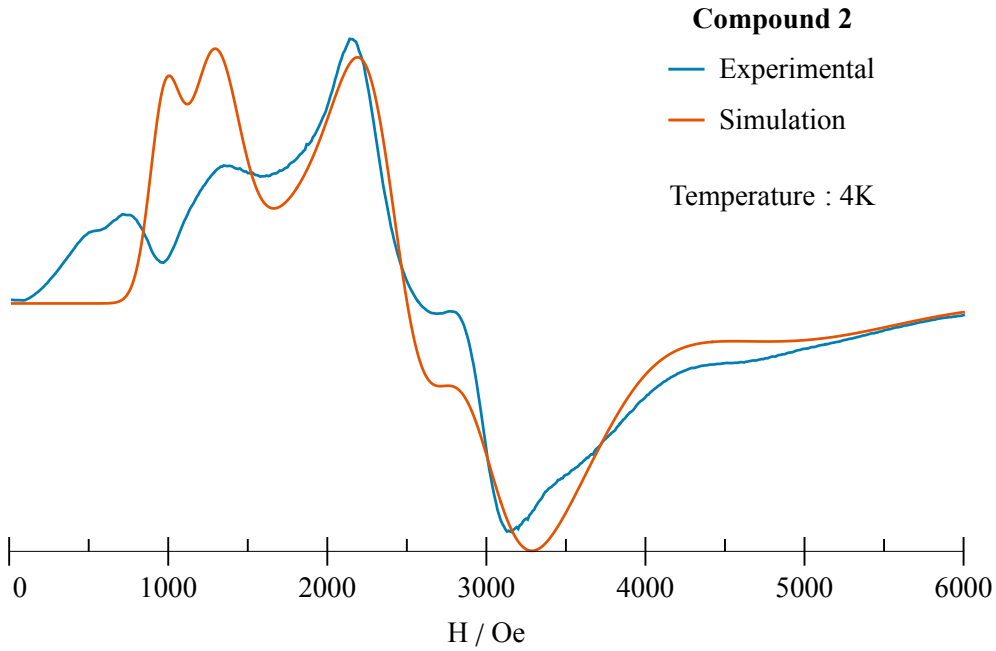


Figure S22 Experimental X band EPR spectrum of **2** at 4K and *S*=3/2 simulation obtained by least squares fitting using Easyspin Matlab toolbox ($D$= 5.98 $cm^{-1}$ fixed, best parameters $g_x$=2.75, $g_y$=2.03, $g_z$=2.33, $E/D$=0.296 )

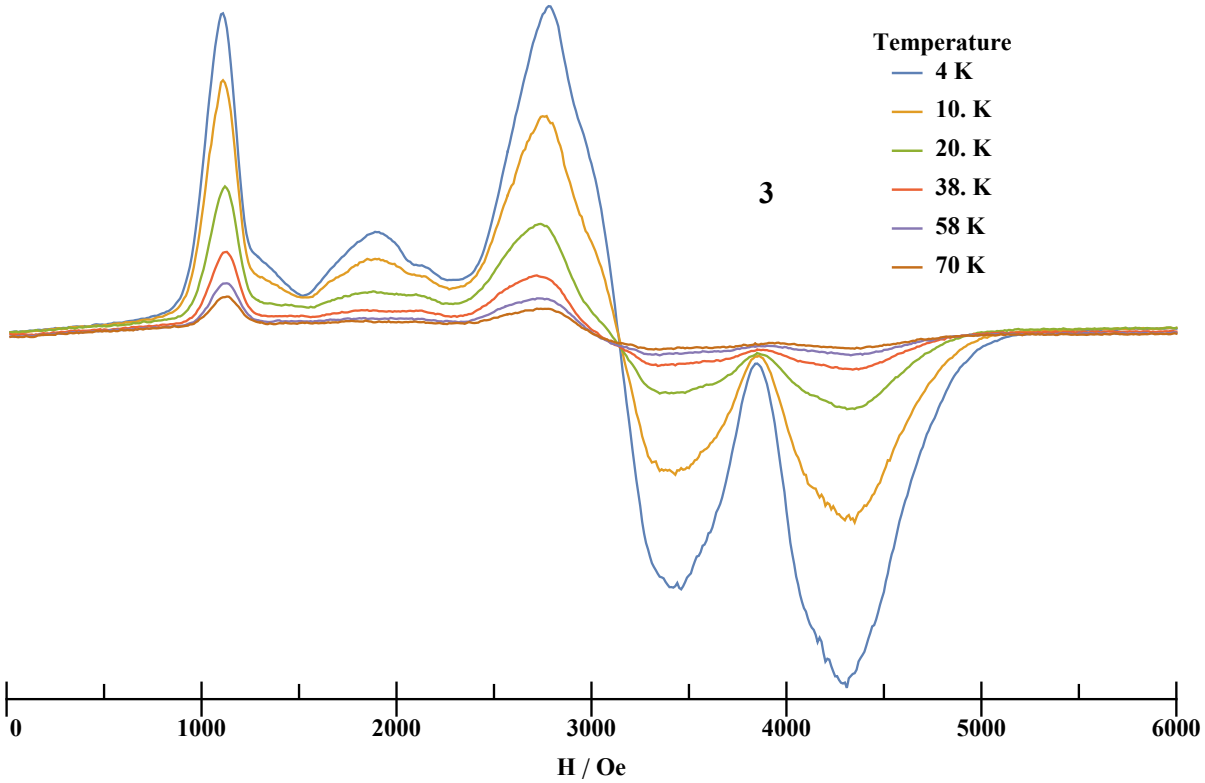


Figure S23. Evolution with the temperature of the X band EPR spectrum of **3**.

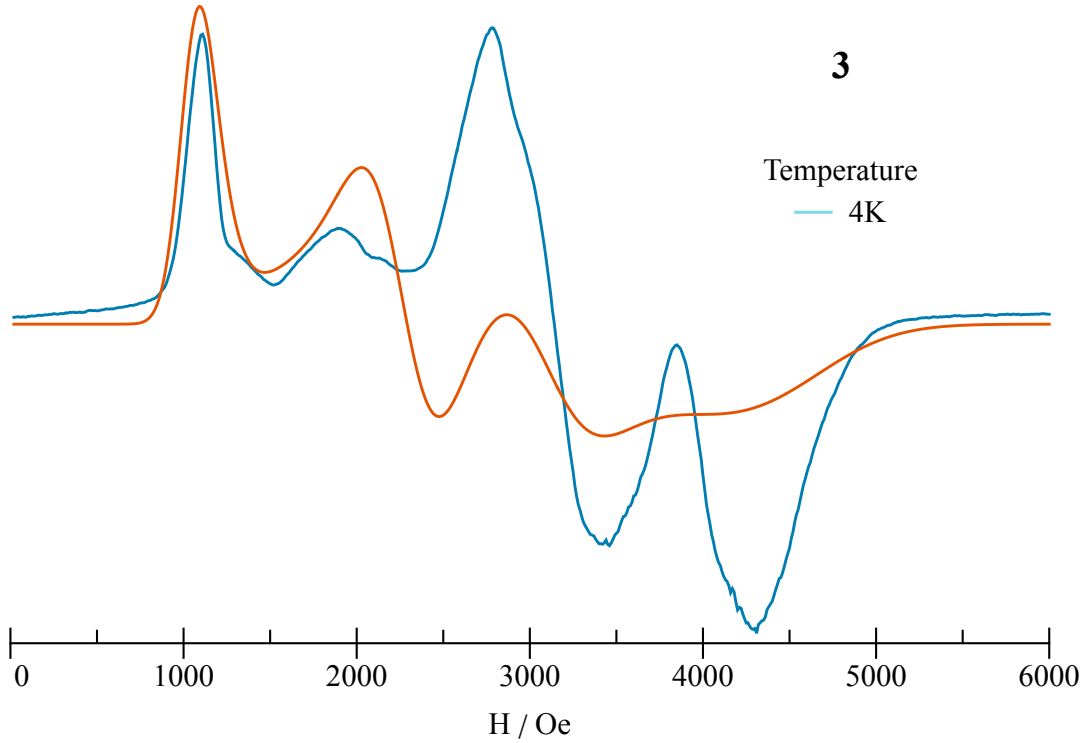


Figure S24. Experimental X band EPR spectrum of **3** at 4K and $S$=3/2 simulation obtained by least squares fitting using Easyspin Matlab toolbox ($D$= 4.08 cm$^{-1}$ fixed, best parameters $g_x$= 2.48, $g_y$=1.99 and $g_z$= 2.38, $E/D$=0.28 )

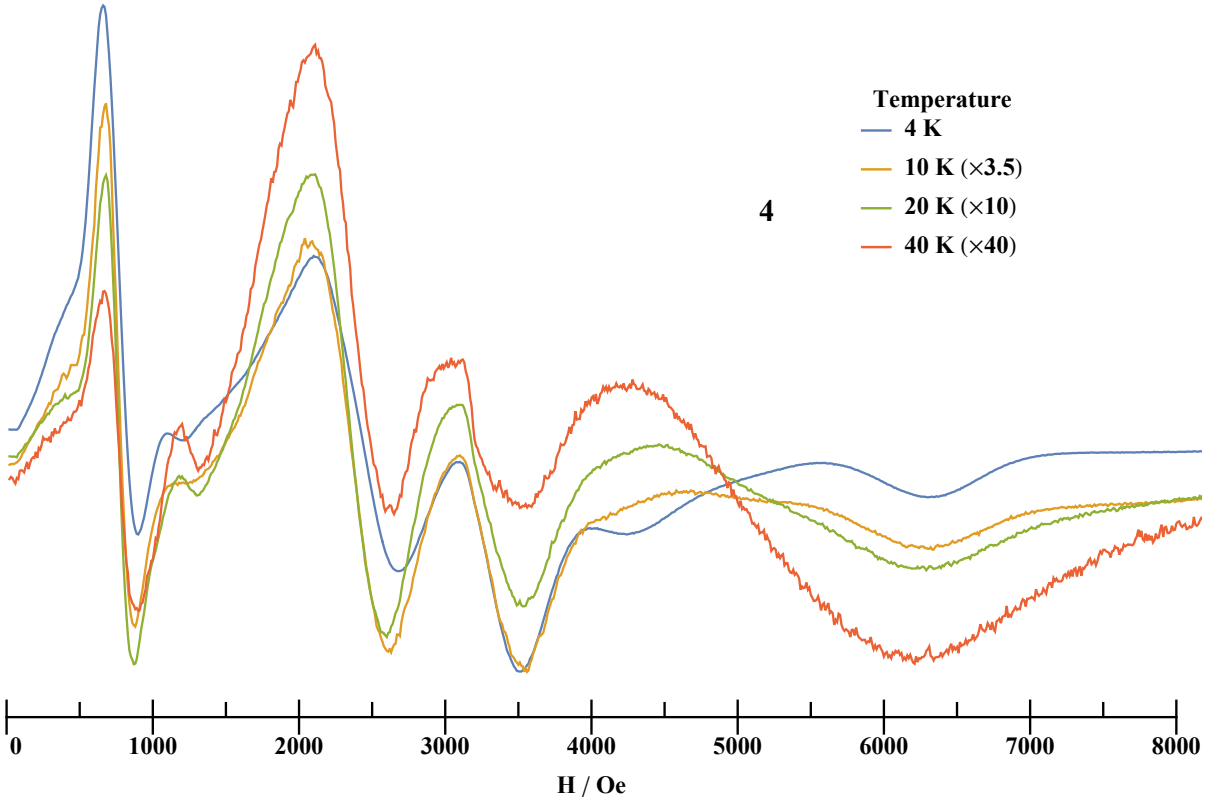


Figure S25. Evolution with the temperature of the X band EPR spectrum of **4**. The figures in brackets are the multiplicative factor applied to the spectra for better visibility

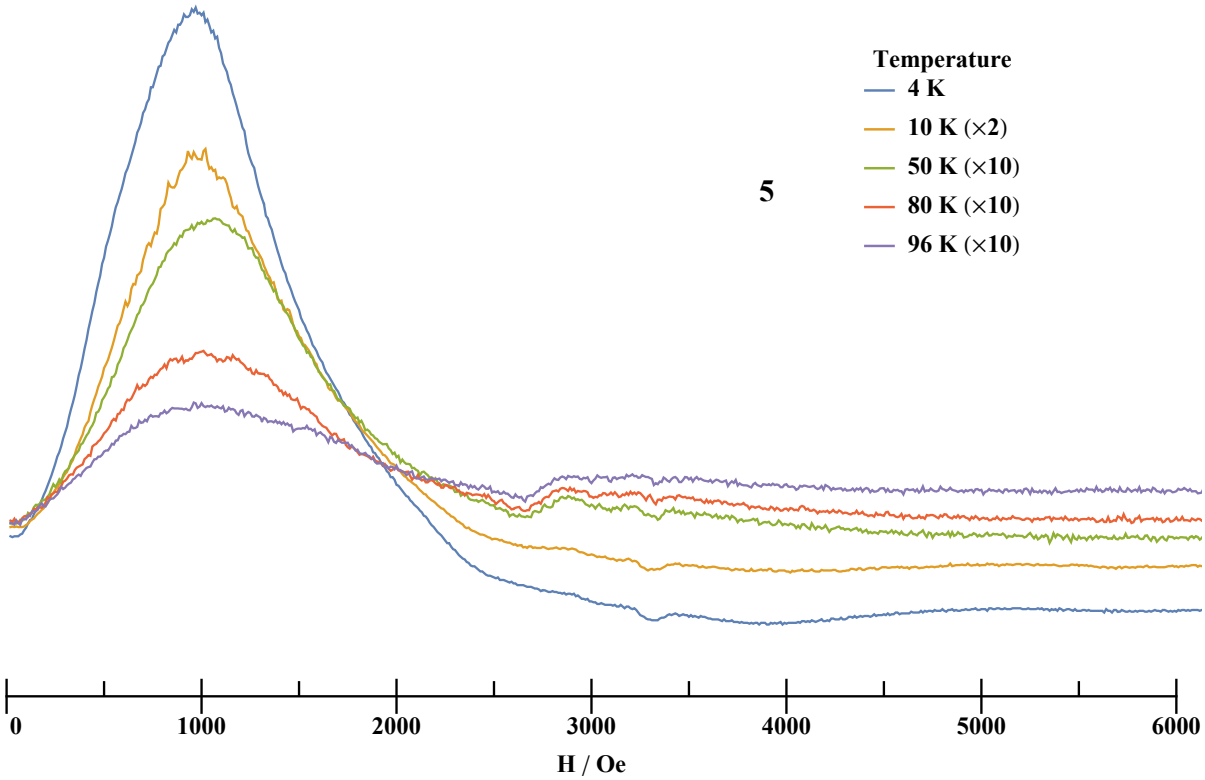


Figure S26. Evolution with the temperature of the X band EPR spectrum of **5**. The figures in brackets are the multiplicative factor applied to the spectra for better visibility

Table S10 best parameters obtained from Easyspin simulations of EPR spectra only considering the *S*=3/2 ground-state. (FWHM $g_n$ with n=x,y or z see https://easyspin.org/easyspin/documentation/broadenings.html)

| | *D*/ $cm^{-1}$ | *E*/*D* | E/ $cm^{-1}$ | $g_x$ | $g_y$ | $g_z$ | FWHM $g_x$ | FWHM $g_y$ | FWHM $g_z$ | Euler α | Euler β | Euler γ | |
|---|---|---|---|---|---|---|---|---|---|---|---|---|---|
| **1** pma | 4.62 | 1/3 | 1.54 | 2.7532 | 2.4823 | 2.1239 | 0.4536 | 0.4810 | 0.5282 | 0 | 0 | 0 | |
| **2** Me3pma | 5.98 | 0.2947 | 1.76 | 2.34 | 1.92 | 1.95 | 0.4600 | 0.5400 | 0.5400 | 0 | 0 | 0 | |
| **3** opba | 4.08 | 0.29 | 1.18 | 2.480 | 1.982 | 2.38 | 0.4600 | 0.4801 | 0.4702 | 0 | 0 | 0 | |
| | | | | | | | | | | | | | $J_{eff}$ |
| **4** mpba | 3.5 | 0.29 | | 2.4761 | 1.8221 | 2.3815 | 0.3500 | 0.4500 | 0.3500 | 0 | 0 | 0 | 0.2 |

## V) Spin Hamiltonians of compounds 1-5

### *V.1) Spin hamiltonian in trimetallic compound*

The tensorial relations between local parameters $D_{Mi}$ and $g_{Mi}$ and parameters of a spin state in a trinuclear compound are calculated using the Wigner-Eckart theorem and ITO algebra.

$$D_S = \sum_i d_i^S D_i + \sum_{i<j} d_{i,j}^S D_{i,j}$$

and

$$g_S = \sum_i c_i \; g_i$$

the $d_i$, $d_{i,j}$ and $c_i$ coeficients are calculated as the ratio of two reduced matrix elements

$$c_i = \frac{< S \left|\left|T^{(1)}(S_i)\right|\right| S' >}{< S \left|\left|T^{(1)}(S)\right|\right| S' >}$$

$$d_i = \frac{< S \left|\left|T^{(2)}(S_i)\right|\right| S' >}{< S \left|\left|T^{(2)}(S)\right|\right| S' >}$$

$$d_{ij} = \frac{< S \left|\left|T^{(2)}(S_i S_j)\right|\right| S' >}{< S \left|\left|T^{(2)}(S)\right|\right| S' >}$$

with $< S \left|\left|T^{(1)}(S)\right|\right| S' > = \delta_{S,S'} \sqrt{S(S+1)(2S+1)}$ and

$$< S \left|\left|T^{(2)}(S)\right|\right| S' > = \delta_{S,S'} \sqrt{\frac{S(S+1)(2S+1)(2S-1)(2S+3)}{6}}$$

But reduced matrix elements such as $< S \left|\left|T^{(k)}(S_i)\right|\right| S' >$ are unknown. To calculate these elements it is necessary to relate these reduced matrix elements in the coupled basis $< S \left|\left|T^{(k)}(S_i)\right|\right| S' >$ to known reduced elements $< S_i \left|\left|T^{(k)}(S_i)\right|\right| S_i >$ using ITO algebra and formula established for product of irreductible tensor operators[1,2].

All calculation made, the following results are obtained :

$$c_1^S = (-1)^{2S_{12}+S_1+S_2+S_3+S} (2S+1)(2S_{12}+1) \sqrt{\frac{(2S_1+1)S_1(S_1+1)}{(2S+1)S(S+1)}} \begin{Bmatrix} S_{12} & 1 & S_{12} \\ S & S_3 & S \end{Bmatrix} \begin{Bmatrix} S_1 & 1 & S_1 \\ S_{12} & S_2 & S_{12} \end{Bmatrix}$$

$$c_2^S = (-1)^{2S_{12}+S_1+S_2+S_3+S} (2S+1)(2S_{12}+1) \sqrt{\frac{(2S_2+1)S_2(S_2+1)}{(2S+1)S(S+1)}} \begin{Bmatrix} S_{12} & 1 & S_{12} \\ S & S_3 & S \end{Bmatrix} \begin{Bmatrix} S_2 & 1 & S_2 \\ S_{12} & S_1 & S_{12} \end{Bmatrix}$$

$$c_3^S = (-1)^{2S_1+2S_2+S_3+3S_{12}+S+1} (2S+1) \sqrt{\frac{(2S_3+1)S_3(S_3+1)}{(2S+1)S(S+1)}} \begin{Bmatrix} S_3 & 1 & S_3 \\ S & S_{12} & S \end{Bmatrix}$$

$$d_1^S = (-1)^{2S_{12}+S_1+S_2+S_3+S} (2S+1)(2S_{12}+1) \sqrt{\frac{(2S_1+3)(2S_1+1)(2S_1-1)S_1(S_1+1)}{(2S+3)(2S+1)(2S-1)S(S+1)}} \begin{Bmatrix} S_{12} & 2 & S_{12} \\ S & S_3 & S \end{Bmatrix} \begin{Bmatrix} S_1 & 2 & S'_1 \\ S'_{12} & S_2 & S_{12} \end{Bmatrix}$$

$$d_2^S = (-1)^{2S_{12}+S_1+S_2+S_3+S}\ (2S+1)(2S_{12}+1)\sqrt{\frac{(2S_2+3)(2S_2+1)(2S_2-1)S_2(S_2+1)}{(2S+3)(2S+1)(2S-1)S(S+1)}}\begin{Bmatrix} S_{12} & 2 & S_{12} \\ S & S_3 & S \end{Bmatrix}\begin{Bmatrix} S_2 & 2 & S_2 \\ S_{12} & S_1 & S_{12} \end{Bmatrix}$$

$$d_3^S = (-1)^{2S_1+2S_2+S_3+3S_{12}+S}\ (2S+1)\sqrt{\frac{(2S_3+3)(2S_3+1)(2S_3-1)S_3(S_3+1)}{(2S+3)(2S+1)(2S-1)S(S+1)}}\begin{Bmatrix} S_3 & 2 & S_3 \\ S & S_{12} & S \end{Bmatrix}$$

$$d_{13}^S = (-1)^{S_{12}+S_1+S_2+1}\ (2S+1)(2S_{12}+1)\sqrt{30}\sqrt{\frac{(2S_1+1)S_1(S_1+1)(2S_3+1)S_3(S_3+1)}{(2S+1)(2S+3)(2S-1)S(S+1)}}\begin{Bmatrix} S_1 & 1 & S_1 \\ S_{12} & S_2 & S_{12} \end{Bmatrix}\begin{Bmatrix} S_{12} & S_{12} & 1 \\ S_3 & S_3 & 1 \\ S & S & 2 \end{Bmatrix}$$

$$d_{23}^S = (-1)^{S_{12}+S_1+S_2+1}\ (2S+1)(2S_{12}+1)\sqrt{30}\sqrt{\frac{(2S_2+1)S_2(S_2+1)(2S_3+1)S_3(S_3+1)}{(2S+1)(2S+3)(2S-1)S(S+1)}}\begin{Bmatrix} S_2 & 1 & S_2 \\ S_{12} & S_1 & S_{12} \end{Bmatrix}\begin{Bmatrix} S_{12} & S_{12} & 1 \\ S_3 & S_3 & 1 \\ S & S & 2 \end{Bmatrix}$$

$$d_{12}^S = (-1)^{S+S_{12}+S_3}\ (2S+1)(2S_{12}+1)\sqrt{30}\sqrt{\frac{(2S_1+1)S_1(S_1+1)(2S_2+1)S_2(S_2+1)}{2S+1)(2S+3)(2S-1)S(S+1)}}\begin{Bmatrix} S_{12} & 2 & S_{12} \\ S' & S_3 & S \end{Bmatrix}\begin{Bmatrix} S_1 & S_1 & 1 \\ S_2 & S_2 & 1 \\ S_{12} & S_{12} & 2 \end{Bmatrix}$$

There is no contribution of the *S*=1/2 central copper ion, so $d_3^S = 0$. Anisotropic exchange is expected to be a weak contribution to the ZFS of the spin-states when compared to the large local $D_{Ni}$ values and consequently we neglect $D_{i,j}$ contributions to ZFS of the spin-states. For a {NiCuNi} trimetallic compound these relations give for the *S*=3/2 ground state.

$D_{|^3/_2>} = {}^{7D_{Ni1}}/_{30} + {}^{7D_{Ni2}}/_{30}$

$E_{|^3/_2>} = {}^{7E_{Ni1}}/_{30} + {}^{7E_{Ni2}}/_{30}$ and

$g_{|\frac{3}{2}>} = \frac{6g_{Ni}-g_{Cu}}{5}$.

### *V.2) Spin hamiltonian in hexametallic compound*

As in trinulcear unit the $c_i$ and $d_i$ coeffcients are given by the ratio of the reduced elements

$$c_i = \frac{<S\left\|T^{(1)}(S_i)\right\|S'>}{<S\left\|T^{(1)}(S)\right\|S'>} \qquad d_i = \frac{<S\left\|T^{(2)}(S_i)\right\|S'>}{<S\left\|T^{(2)}(S)\right\|S'>}$$

To calculate these coefficients it is necessary to relate the unknown reduced matrix element

$< S \left\|T^{(k)}(S_i)\right\| S' >$ to the known $< S_i \left\|T^{(k)}(S_i)\right\| S_i >$

*V.2) Spin hamiltonian in hexanuclear compound*

The correspondance between the hamiltonian [3] and the numerotation of the spin in formulas is given below

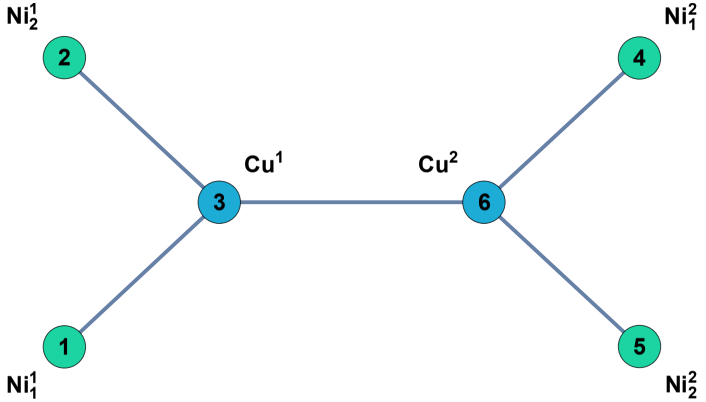


The following expressions are obtained for the hexanuclear complex

For $Ni_1^1$ ($S_1$)

$$< (S_{123}\,,\ S_{456}), S \| T^{(2)}(S_1) \| (S'_{123}, S'_{456}) S' > = \delta_{S_{12456}\, S'_{12456}} (-1)^{S'+S_{123}+S_{456}+2} \sqrt{(2S+1)(2S'+1)} \begin{Bmatrix} S_{123} & 2 & S'_{123} \\ S' & S_{456} & S \end{Bmatrix} < S_{123} \| T^{(2)}(S_1) \| S'_{123} >$$

with

$$< S_{123} \| T^{(2)}(S_1) \| S_{123} > = < (S_1, S_2) S_{12}\,,\ S_3 \| T^{(2)}(S_1) \| (S'_1, S'_2) S'_{12}\,,\ S'_3 > =$$

$$\delta_{S_3 S'_3} (-1)^{S'_{123}+S_{12}+S_3+2} \sqrt{(2S_{123}+1)(2S'_{123}+1)} \begin{Bmatrix} S_{12} & 2 & S'_{12} \\ S'_{123} & S_3 & S_{123} \end{Bmatrix} \Big( \quad \delta_{S_2 S'_2} (-1)^{S'_{12}+S_1+S_2+2} \sqrt{(2S_{12}+1)(2S'_{12}+1)} \begin{Bmatrix} S_1 & 2 & S'_1 \\ S'_{12} & S_2 & S_{12} \end{Bmatrix} < S_1 \| T^{(2)}(S_1) \| S'_1 > \Big)$$

For $Ni_2^1$ ($S_2$)

$$(S_{123},\ S_{456}),S||\ T^{(2)}(S_2)\ ||(S'_{123},S'_{456})S'>=\delta_{S_{12456}S'_{12456}}(-1)^{S'+S_{123}+S_{456}+2}\sqrt{(2S+1)(2S'+1)}\begin{Bmatrix}S_{123} & 2 & S'_{123}\\ S' & S_{456} & S\end{Bmatrix}<S_{123}||\ T^{(2)}(S_2)\ ||\ S'_{123}>$$

with

$$<\ S_{123}\ ||\ T^{(2)}(S_2)\ ||\ S_{123}'>=\ <(S_1,S_2)S_{12},\ S_3||\ T^{(2)}(S_2)\ ||(S'_1,S'_2)S'_{12},\ S'_3>=$$

$$\delta_{S_3S'_3}(-1)^{S'_{123}+S_{12}+S_3+2}\sqrt{(2S_{123}+1)\left(2S'_{123}+1\right)}\begin{Bmatrix}S_{12} & 2 & S'_{12}\\ S'_{123} & S_3 & S_{123}\end{Bmatrix}\Bigg(\qquad\delta_{S_1S'_1}(-1)^{S_{12}+S_1+S'_2+2}\sqrt{(2S_{12}+1)\left(2S'_{12}+1\right)}\begin{Bmatrix}S_2 & 2 & S'_2\\ S'_{12} & S_1 & S_{12}\end{Bmatrix}<S_1||\ T^{(2)}(S_2)\ ||S'_1>\Bigg)$$

For $Ni_1^2$ ($S_4$)

$$<(S_{123},\ S_{456}),S||\ T^{(2)}(S_4)\ ||(S'_{123},S'_{456})S'>=\delta_{S_{12456}S'_{12456}}(-1)^{S+S_{123}+S'_{456}+2}\sqrt{(2S+1)(2S'+1)}\begin{Bmatrix}S_{456} & 2 & S'_{456}\\ S' & S_{123} & S\end{Bmatrix}<S_{456}||\ T^{(2)}(S_4)\ ||\ S'_{456}>$$

with

$$<\ S_{456}\ ||\ T^{(2)}(S_4)\ ||\ S_{456}'>=\ <(S_4,S_5)S_{45},\ S_6||\ T^{(2)}(S_4)\ ||(S'_4,S'_5)S'_{45},\ S'_6>=$$

$$\delta_{S_6S'_6}(-1)^{S'_{456}+S_{45}+S_6+2}\sqrt{(2S_{456}+1)\left(2S'_{456}+1\right)}\begin{Bmatrix}S_{45} & 2 & S'_{45}\\ S'_{456} & S_6 & S_{456}\end{Bmatrix}\Bigg(\qquad\delta_{S_5S'_5}(-1)^{S'_{45}+S_5+S_4+2}\sqrt{(2S_{45}+1)\left(2S'_{45}+1\right)}\begin{Bmatrix}S_4 & 2 & S'_4\\ S'_{45} & S_5 & S_{45}\end{Bmatrix}<S_4||\ T^{(2)}(S_4)\ ||S'_4>\Bigg)$$

For $Ni_2^2$ ($S_5$)

$$<(S_{123},\ S_{456}),S||\ T^{(2)}(S_5)\ ||(S'_{123},S'_{456})S'>=$$
$$\delta_{S_{12456}S'_{12456}}(-1)^{S+S_{123}+S'_{456}+2}\sqrt{(2S+1)(2S'+1)}\begin{Bmatrix}S_{456} & 2 & S'_{456}\\ S' & S_{123} & S\end{Bmatrix}<S_{456}||\ T^{(2)}(S_5)\ ||\ S'_{456}>$$

with

$$<\ S_{456}\ ||\ T^{(2)}(S_5)\ ||\ S_{456}'>=\ <(S_4,S_5)S_{45},\ S_6||\ T^{(2)}(S_5)\ ||(S'_4,S'_5)S'_{45},\ S'_6>=$$

$$\delta_{S_6S'_6}(-1)^{S'_{456}+S_{45}+S_6+2}\sqrt{(2S_{456}+1)\left(2S'_{456}+1\right)}\begin{Bmatrix}S_{45} & 2 & S'_{45}\\ S'_{456} & S_6 & S_{456}\end{Bmatrix}\Bigg(\qquad\delta_{S_4S'_4}(-1)^{S_{45}+S_4+S'_5+2}\sqrt{(2S_{45}+1)\left(2S'_{45}+1\right)}\begin{Bmatrix}S_5 & 2 & S'_5\\ S'_{45} & S_4 & S_{45}\end{Bmatrix}<S_5||\ T^{(2)}(S_5)\ ||\ S'_5>\Bigg)$$

In this hexametallic complex calculations become rather tedious, hence Bencini and Gatteschi suggested for large system to use recurrence relations instead[2]

$c_1 = c_1(S_1, S_2, S_{12}, S_3, S_{123}).c_{123}(S_{123}, S_{456}, S)$ $\quad$ $d_1 = d_1(S_1, S_2, S_{12}, S_3, S_{123}).d_{123}(S_{123}, S_{456}, S)$

$c_2 = c_2(S_1, S_2, S_{12}, S_3, S_{123}).c_{123}(S_{123}, S_{456}, S)$ $\quad$ $d_2 = d_2(S_1, S_2, S_{12}, S_3, S_{123}).d_{123}(S_{123}, S_{456}, S)$

$c_4 = c_4(S_4, S_5, S_{45}, S_6, S_{456}).c_{456}(S_{123}, S_{456}, S)$ $\quad$ $d_4 = d_4(S_4, S_5, S_{45}, S_6, S_{456}).d_{456}(S_{123}, S_{456}, S)$

$c_5 = c_5(S_4, S_5, S_{45}, S_6, S_{456}).c_{456}(S_{123}, S_{456}, S)$ $\quad$ $d_5 = d_5(S_4, S_5, S_{45}, S_6, S_{456}).d_{456}(S_{123}, S_{456}, S)$

where $c_i$ and $d_i$ are the dilution coefficient in the trinuclear {NiCuNi} unit and $c_{ijk}$ and $d_{ijk}$ are the dilution factor in the dinuclear [$S_{123}$, $S_{456}$] unit. For **4** the dilution coefficient for the anisotropy in the {NiCuNi} subunit $d_i$ is equal to 7/30 and for $S$=3 state in the ferromagnetically coupled $S$=3/2 di-spin unit $d_{ijk}$ are equal to 1/5 leading to a dilution coefficient equal to 7/150 for individual Ni ions in the $S$=3 ground-state.

$$D_3 = \frac{7\,D_1^{Ni} + 7\,D_2^{Ni} + 7\,D_4^{Ni} + 7\,D_5^{Ni}}{150}$$

The $D_3$ tensor of the ground state can be also related to local $D_{3/2}$ tensors of {NiCuNi} subunits by:

$$D_3 = \frac{1}{5}\left(D_{3/2}^1 + D_{3/2}^2\right)$$

For the $g$ factors $c_i$ are equal to 3/5 for Ni ions and -1/5 for Cu ions and $c_{ijk}$ are equal to 1/2 leading to a contribution $3g_{Ni}/10$ for each Ni ions and $-g_{Cu}/10$ for each Cu ions in the $S$=3 ground state.

$$g_3 = \frac{3\,g_1^{Ni} + 3\,g_2^{Ni} + 3\,g_4^{Ni} + 3\,g_5^{Ni} - g_3^{Cu} - g_6^{Cu}}{10}$$

*Effective intercation between the two S=3/2 subunits*

To relate the effective interaction between the two $S$=3/2 with the real interaction between the two Cu ions the following matrix element must be calculated using ITO technique

$< n,S_{123},S_{456},S,m| - J\, S_{cu3}.S_{cu6} |n'S'_{123},S'_{456},S',m'>=$

$$-J\,\delta_{ss'}\,\delta_{mm'}(-1)^{S'_{123}+S_{456}+S}\begin{Bmatrix} S_{123} & k & S'_{123} \\ S'_{456} & S & S_{456}\end{Bmatrix} <n_{123},S_{123}||T^{(k)}(S_3)||n'_{123},S_{123}><n_{456},S_{456}||U^{(k)}(S_6)||n'_{456},S'_{456}>$$

with $T^{(1)}(S_3)$=Scu3 et $U^{(1)}(S_6)$=Scu6 and S=$S_{123\,456}$

Then we use on the right and left RMEs the relation established for the case where the left tensorial operator $V^{k1}$ in the tensorial product
$W^K = V^{k1} \otimes T^{k2}$ is equal to $V^{k1}$=1 and K=k2

$$< n,\ S_{12}\,S_3\,,S_{123}\|\,T^{(k)}(S_3)\,\|\,n',S'_{12},S'_3\,S'_{123}\ > \ =\ \delta_{n_{123}\,n_{123}'}\,\delta_{S_{12}\,S_{12}'}(-1)^{S_{123}+S_2+S_{13}+k}\sqrt{(2\,S_{123}+1)\times(2\,S'_{123}+1)}\begin{Bmatrix} S_3 & k & S'_3 \\ S'_{123} & S_{12} & S_{123}\end{Bmatrix}<n,\ S_3,\|\,T^{(k)}(S_3)\|\,n',S'_3>$$

$$< n,\ S_{45}\,S_6\,,S_{456}\|\,T^{(k)}(S_6)\,\|\,n',S'_{45},S'_6\,S'_{456}\ > \ =\ \delta_{n_{456}\,n_{456}'}\,\delta_{S_{45}\,S_{45}'}(-1)^{S_{456}+S_6+S_{46}+k}\sqrt{(2\,S_{456}+1)\times(2\,S'_{456}+1)}\begin{Bmatrix} S_6 & k & S'_6 \\ S'_{456} & S_{45} & S_{456}\end{Bmatrix}<n,\ S_6,\|\,T^{(k)}(S_6)\|\,n',S'_6>$$

That is

$$< n,S123,\ S456,S,m| - J\,Scu3.\,Scu6|n'S'123,\ S'456,3,m>= -J\,\delta_{ss'}\,\delta_{mm'}\,\delta_{n_{123}\,n_{123}'}\,\delta_{n_{456}\,n_{456}'}\,\delta_{S_{12}\,S_{12}'}\,\delta_{S_{45}\,S_{45}'}$$

$$(-1)^{S_{456}+S_6+S_{45}+k}\,(-1)^{S_{123}+S_3+S_{12}+k}\,(-1)^{S'_{123}+S_{456}+S}\begin{Bmatrix} S_{123} & k & S'_{123} \\ S'_{456} & S & S_{456}\end{Bmatrix}\begin{Bmatrix} S_2 & k & S'_3 \\ S'_{123} & S_{12} & S_{123}\end{Bmatrix}\begin{Bmatrix} S_6 & k & S'_6 \\ S'_{456} & S_{45} & S_{456}\end{Bmatrix}(2\,S_{456}+1)\,(2\,S_{123}+1)<n,\ S_3,\|\,T^{(k)}(S_3)\|\,n',S'_2><n,\ S_6,\|\,T^{(k)}(S_6)\|\,n',S'_6>$$

With avec $S$=3, $S_{123}$=$S_{456}$=3/2, $S_{12}$=$S_{45}$=2, $S_3$=$S_6$=1/2 and k=1
This gives $9J_{CuCu}/100$
which must be equalized to the matrix element $-J_{eff}<S_T,S_A,S_b|S_A.S_B|S_T,S_A,S_b>$ with $S_T$=3, $S_A$=$S_b$=3/2
this leads to :

$$\frac{9\,J_{CuCu}}{100}=\frac{9\,J_{eff}}{4}\quad \Rightarrow J_{CuCu}=25\,J_{eff}$$

*V.3) Spin hamiltonian in enneametallic compound*

The correspondance between the hamiltonian [5] and the numerotation of the spin in formulas is given below

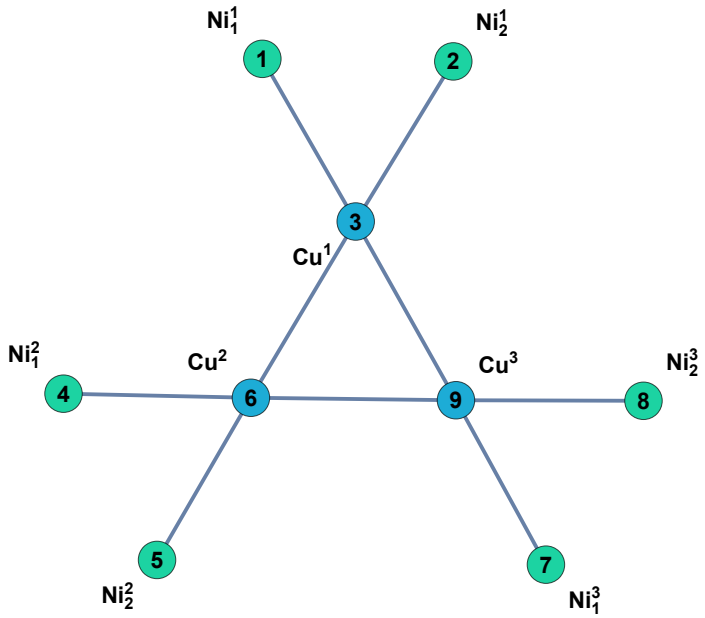


As in hexametallic complexes calculation of the relation beween $< S \left|\left|T^{(k)}(S_i)\right|\right| S' >$ and $< S_i \left|\left|T^{(k)}(S_i)\right|\right| S_i >$ in enneametallic complexes are very tedious, hence it is easier to use recurrence relations[2] :

$c_1 = c_1(S_1, S_2, S_{12}, S_3, S_{123}).c_{123}(S_{123}, S_{456}, S_{123456}, S_{789}, S)$
$c_2 = c_2(S_1, S_2, S_{12}, S_3, S_{123}).c_{123}(S_{123}, S_{456}, S_{123456}, S_{789}, S)$
$c_4 = c_4(S_4, S_5, S_{45}, S_6, S_{456}).c_{456}(S_{123}, S_{456}, S_{123456}, S_{789}, S)$
$c_5 = c_5(S_4, S_5, S_{45}, S_6, S_{456}).c_{456}(S_{123}, S_{456}, S_{123456}, S_{789}, S)$
$c_7 = c_7(S_7, S_8, S_{78}, S_9, S_{789}).c_{789}(S_{123}, S_{456}, S_{123456}, S_{789}, S)$
$c_8 = c_8(S_7, S_8, S_{78}, S_9, S_{789}).c_{789}(S_{123}, S_{456}, S_{123456}, S_{789}, S)$

$d_1 = d_1(S_1, S_2, S_{12}, S_3, S_{123}).d_{123}(S_{123}, S_{456}, S_{123456}, S_{789}, S)$
$d_2 = d_2(S_1, S_2, S_{12}, S_3, S_{123}).d_{123}(S_{123}, S_{456}, S_{123456}, S_{789}, S)$
$d_4 = d_4(S_4, S_5, S_{45}, S_6, S_{456}).d_{456}(S_{123}, S_{456}, S_{123456}, S_{789}, S)$
$d_5 = d_5(S_4, S_5, S_{45}, S_6, S_{456}).d_{456}(S_{123}, S_{456}, S_{123456}, S_{789}, S)$
$d_7 = d_7(S_7, S_8, S_{78}, S_9, S_{789}).d_{789}(S_{123}, S_{456}, S_{123456}, S_{789}, S)$
$d_8 = d_8(S_7, S_8, S_{78}, S_9, S_{789}).d_{789}(S_{123}, S_{456}, S_{123456}, S_{789}, S)$

where $c_i$ and $d_i$ are the dilution coefficient in the trinuclear {NiCuNi} unit and $c_{ijk}$ and $d_{ijk}$ are the dilution factor in the trinuclear [$S_{123}$, $S_{456}$, $S_{789}$] unit. For **5** the dilution coefficient for the

anisotropy in the {NiCuNi} subunit $d_i$ is equal to 7/30 and $d_{ijk}$ is equal to 1/12 for the $S$=9/2 state of the ferromagnetically coupled $S$=3/2 tri-spin unit leading to a dilution coefficient equal to 7/360 for individual Ni ions in the $S$=9/2 ground-state.

$$D_{9/2} = \frac{7\,D_1^{Ni} + 7\,D_2^{Ni} + 7\,D_4^{Ni} + 7\,D_5^{Ni} + 7\,D_7^{Ni} + 7\,D_8^{Ni}}{360}$$

The $D_{9/2}$ tensor of the ground state can be also related to local $D_{3/2}$ tensors of {NiCuNi} subunits by:

$$D_{9/2} = \frac{1}{12}\left(D_{3/2}^1 + D_{3/2}^2 + D_{3/2}^3\right)$$

for ideal $D_3$ symmetry, if the principal axis of the local $D_{3/2}^i$ are parallel to the $C_3$ axis which is perpendicular to the aromatic rings, the resultant $D_{9/2}$ tensor is axial with its principal axis parallel to the $C_3$ axis even if the local $D_{3/2}^i$ are rhombic. On the other hand, if the principal axis of the local $D_{3/2}^i$ tensors are perpendicular to the $C_3$ axis pointing toward the axis, the combination of the local tensors leads to an axial tensor with considerably reduced anisotropy

For the $g$ factors $c_i$ are equal to 3/5 for Ni ions and -1/5 for Cu ions and $c_{ijk}$ are equal to 1/3 leading to a contribution $3g_{Ni}/15$ for each Ni ions and $-g_{Cu}/15$ for each Cu ions in the $S$=9/2 ground state.

$$g_{9/2} = \frac{3\,g_1^{Ni} + 3\,g_2^{Ni} + 3\,g_4^{Ni} + 3\,g_5^{Ni} + 3\,g_7^{Ni} + 3\,g_8^{Ni} - g_3^{Cu} - g_6^{Cu} - g_9^{Cu}}{15}$$

The relation between the effective interaction between the $S$=3/2 ground state of the trinuclear subunits and the real Cu-Cu interaction is given by

$$J_{\mathrm{CuCu}} = \frac{(\mathrm{s1}\,(\mathrm{s1}+1) + \mathrm{s123}\,(\mathrm{s123}+1) - \mathrm{s2}\,(\mathrm{s2}+1) - \mathrm{s3}\,(\mathrm{s3}+1))\,(\mathrm{s4}\,(\mathrm{s4}+1) + \mathrm{s456}\,(\mathrm{s456}+1) - \mathrm{s5}\,(\mathrm{s5}+1) - \mathrm{s6}\,(\mathrm{s6}+1))}{4\,\mathrm{s123}\,(\mathrm{s123}+1)\,\mathrm{s456}\,(\mathrm{s456}+1)} J_{\mathrm{eff}}$$

*References*

(8) Bencini, A.; Gatteschi, D.; Chemistry. *Epr of Exchange Coupled Systems*; Dover Publications, 2012.

(95) Zare, R. N. *Angular Momentum: Understanding Spatial Aspects in Chemistry and Physics*; Wiley: New York, 1988.